



TECH BRIEFS

NATIONAL AERONAUTICS AND SPACE ADMINISTRATION

-  **Technology Focus**
-  **Electronics/Computers**
-  **Software**
-  **Materials**
-  **Mechanics/Machinery**
-  **Manufacturing**
-  **Bio-Medical**
-  **Physical Sciences**
-  **Information Sciences**
-  **Books and Reports**

INTRODUCTION

Tech Briefs are short announcements of innovations originating from research and development activities of the National Aeronautics and Space Administration. They emphasize information considered likely to be transferable across industrial, regional, or disciplinary lines and are issued to encourage commercial application.

Availability of NASA Tech Briefs and TSPs

Requests for individual Tech Briefs or for Technical Support Packages (TSPs) announced herein should be addressed to

National Technology Transfer Center

Telephone No. (800) 678-6882 or via World Wide Web at www2.nttc.edu/leads/

Please reference the control numbers appearing at the end of each Tech Brief. Information on NASA's Innovative Partnerships Program (IPP), its documents, and services is also available at the same facility or on the World Wide Web at <http://ipp.nasa.gov>.

Innovative Partnerships Offices are located at NASA field centers to provide technology-transfer access to industrial users. Inquiries can be made by contacting NASA field centers listed below.

NASA Field Centers and Program Offices

Ames Research Center

Lisa L. Lockyer
(650) 604-1754
lisa.l.lockyer@nasa.gov

Dryden Flight Research Center

Gregory Poteat
(661) 276-3872
greg.poteat@dfrc.nasa.gov

Glenn Research Center

Kathy Needham
(216) 433-2802
kathleen.k.needham@nasa.gov

Goddard Space Flight Center

Nona Cheeks
(301) 286-5810
nona.k.cheeks@nasa.gov

Jet Propulsion Laboratory

Andrew Gray
(818) 354-3821
gray@jpl.nasa.gov

Johnson Space Center

information
(281) 483-3809
jsc.techtran@mail.nasa.gov

Kennedy Space Center

David R. Makufka
(321) 867-6227
david.r.makufka@nasa.gov

Langley Research Center

Brian Beaton
(757) 864-2192
brian.f.beaton@nasa.gov

Marshall Space Flight Center

Jim Dowdy
(256) 544-7604
jim.dowdy@msfc.nasa.gov

Stennis Space Center

Ramona Travis
(228) 688-3832
ramona.e.travis@nasa.gov

Carl Ray, Program Executive

Small Business Innovation
Research (SBIR) & Small
Business Technology
Transfer (STTR) Programs
(202) 358-4652
carl.g.ray@nasa.gov

Doug Comstock, Director

Innovative Partnerships
Program Office
(202) 358-2560
doug.comstock@nasa.gov



TECH BRIEFS

NATIONAL AERONAUTICS AND SPACE ADMINISTRATION



5 Technology Focus: Wireless

- 5 Valve-"Health"-Monitoring System
- 6 Microstrip Antenna for Remote Sensing of Soil Moisture and Sea Surface Salinity
- 7 Biomedical Wireless Ambulatory Crew Monitor
- 7 Wireless Avionics Packet To Support Fault Tolerance for Flight Applications
- 8 Aerobot Autonomy Architecture



9 Electronics/Computers

- 9. Submillimeter Confocal Imaging Active Module
- 10 Traveling-Wave Maser for 32 GHz
- 11 System Synchronizes Recordings From Separated Video Cameras
- 12 Piecewise-Planar Parabolic Reflectarray Antenna
- 13 Reducing Interference in ATC Voice Communication



15 Software

- 15 EOS MLS Level 1B Data Processing, Version 2.2
- 15 Auto-Generated Semantic Processing Services
- 15 Geospatial Authentication
- 15 Maneuver Automation Software
- 16 Event Driven Messaging With Role-Based Subscriptions
- 16 Estimating Relative Positions of Outer-Space Structures



17 Manufacturing & Prototyping

- 17 Fabricating PFPE Membranes for Capillary Electrophoresis
- 17 Linear Actuator Has Long Stroke and high Resolution
- 18 Installing a Test Tap on a Metal Battery Case
- 18 Fabricating PFPE Membranes for Microfluidic Valves and Pumps



21 Materials

- 21 Room-Temperature-Cured Copolymers for Lithium Battery Gel Electrolytes
- 22 Catalysts for Efficient Production of Carbon Nanotubes

- 22 Amorphous Silk Fibroin Membranes for Separation of CO₂



23 Mechanics/Machinery

- 23 "Zero-Mass" Noninvasive Pressure Transducers
- 24 Radial-Electric-Field Piezoelectric Diaphragm Pumps
- 25 Ejector-Enhanced, Pulsed, Pressure-Gain Combustor



27 Physical Science

- 27 Suppressing Ghost Diffraction in E-Beam-Written Gratings
- 28 Target-Tracking Camera for a Metrology System
- 29 Polarimetric Imaging Using Two Photoelastic Modulators
- 30 Miniature Wide-Angle Lens for Small-Pixel Electronic Camera
- 30 Modal Filters for Infrared Interferometry
- 31 Mo₃Sb_{7-x}Te_x for Thermoelectric Power Generation
- 32 Two-Dimensional Quantum Model of a Nanotransistor
- 33 Scanning Miniature Microscopes Without Lenses
- 34 Manipulating Neutral Atoms in Chip-Based Magnetic Traps
- 35 Expansion Compression Contacts for Thermoelectric Legs



37 Information Sciences

- 37 Processing Electromyographic Signals To Recognize Words
- 38 Physical Principle for Generation of Randomness
- 38 DSN Beowulf Cluster-Based VLBI Correlator
- 39 Hybrid NN/SVM Computational System for Optimizing Designs



41 Books & Reports

- 41 Criteria for Modeling in LES of Multicomponent Fuel Flow
- 41 Computerized Machine for Cutting Space Shuttle Thermal Tiles

- 41 Orbiting Depot and Reusable Lander for Lunar Transportation
- 41 FPGA-Based Networked Phasemeter for a Heterodyne Interferometer
- 42 Aquarius Digital Processing Unit



43 Bio-Medical

- 43 Three-Dimensional Optical Coherence Tomography
- 44 Benchtop Antigen Detection Technique Using Nanofiltration and Fluorescent Dyes
- 45 Isolation of Precursor Cells From Waste Solid Fat Tissue
- 45 Identification of Bacteria and Determination of Biological Indicators
- 46 Further Development of Scaffolds for Regeneration of Nerves
- 47 Chemically Assisted Photocatalytic Oxidation System
- 47 Use of Atomic Oxygen for Increased Water Contact Angles of Various Polymers for Biomedical Applications
- 48 Crashworthy Seats Would Afford Superior Protection
- 49 Open-Access, Low-Magnetic-Field MRI System for Lung Research
- 49 Microfluidic Mixing Technology for a Universal Health Sensor
- 50 Microfluidic Extraction of Biomarkers Using Water as Solvent
- 51 Microwell Arrays for Studying Many Individual Cells
- 51 Droplet-Based Production of Liposomes
- 51 Identifying and Inactivating Bacterial Spores

This document was prepared under the sponsorship of the National Aeronautics and Space Administration. Neither the United States Government nor any person acting on behalf of the United States Government assumes any liability resulting from the use of the information contained in this document, or warrants that such use will be free from privately owned rights.



Technology Focus: Wireless

Valve-“Health”-Monitoring System

This system is adaptable to diverse long-term sensor-data-monitoring applications.

Stennis Space Center, Mississippi

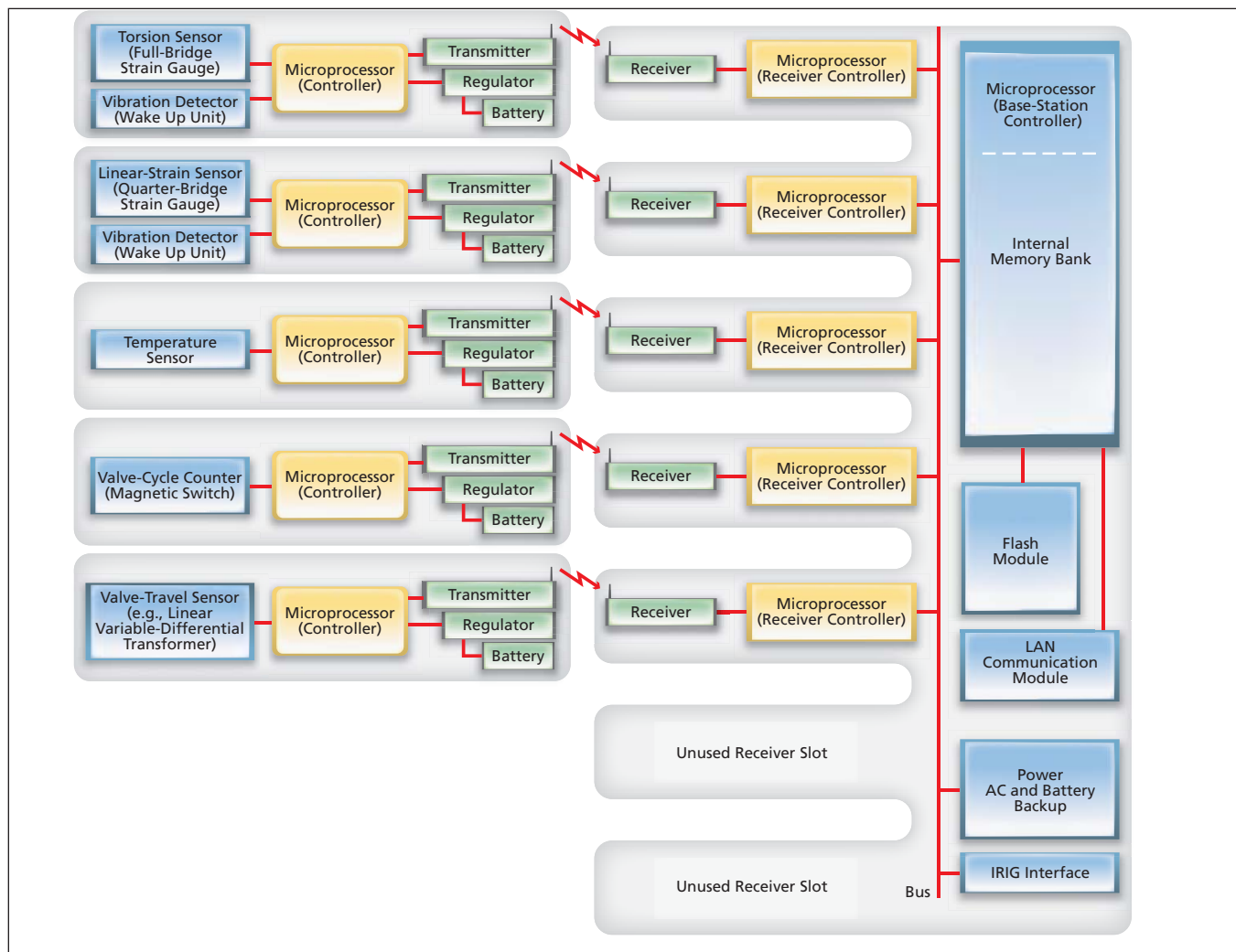
A system that includes sensors and data-acquisition, wireless data-communication, and data-processing subsystems has been developed as a means of both real-time and historical tracking of information indicative of deterioration in the mechanical integrity and performance of a high-geared ball valve or a linearly actuated valve that operates at a temperature between cryogenic and ambient.

In the original application for which the system is specifically designed, the valve is of a type used in controlling the flow of a propellant fluid (e.g., liquid hydrogen)

during testing of a rocket engine. The data collected by use of this system are used to build a knowledge base of operational characteristics of valves, for the purpose of obtaining insight into operational lifetime and enabling prediction of valve operational lifetimes. This system can stand alone or can be incorporated into a network that is part of a higher-level “health”-management system. This system is also readily adaptable to commercial applications in which there are requirements for long-term monitoring of events associated with quantities that may include, but

are not limited to, torsional strain, biaxial strain, linear strain, cryogenic temperatures, ambient temperatures, tripping of limit switches, current signals ranging from 4 to 20 mA, potential signals ranging from 0 to 10 V, and/or magnetic fields.

The data collected in the original application include the number of cryogenic valve cycles, the total number of all valve cycles, inlet temperature, outlet temperature, valve-body temperature, torsional strain, linear strain, valve preload position, total rotational or linear valve travel, and total number of directional changes.



The **Sensor Units** and a **Base Station** together constitute an instrumentation and data-acquisition system that can function alone or can be connected into a network that is part of a higher-level “health”-management system.

Events associated with the aforementioned data are recorded and are time-stamped with sufficient precision to enable synchronization within a time increment of 1 ms. The data are then organized into a text file and stored in a compact flash memory card, from whence the data can be uploaded.

The system (see figure) includes a base station and several self-contained, microprocessor-controlled sensor units that (1) can be mounted remotely from the base station and (2) transmit data to the base station via low-power, short-range [≤ 35 ft (up to about 10 m)] digital radio communication links in the frequency band from 902 to 928 MHz. Each sensor unit has overall dimensions of 3 by 2½ by 2 in. (about 7.6 by 6.4 by 5.1 cm) — small enough to be mounted in the confined spaces typically available for mounting on valves of the type used in the original rocket-engine-testing application. Each sensor unit is potted in a flame-retardant epoxy and designed to draw a current of no more than 0.25 A at a supply potential of 9 V, as required for safe operation in an atmosphere that may contain hydrogen. The base station is not potted; instead, it is mounted in an enclosure that is purged with nitrogen.

Each sensor unit contains two changeable battery packs and a voltage regulator that enables bumpless transfer of the load from one battery pack to the other. The temperatures of the battery packs and the microprocessor are monitored to safeguard against operation outside temperature limits. Each sensor unit includes a display-and-control panel through which a human technician can effect setup and can receive a low-battery indication. An interface port for on-board programming and serial communication is also provided. In the case of a strain-sensor unit, to minimize time-average power demand and thereby prolong battery life, the microprocessor is designed to spend most of the time in a low-power sleep mode, from which it is awakened when any valve movement is detected by a highly sensitive piezoelectric vibration-detection subunit.

The base station includes a receiver module, for each sensor unit, comprising a radio receiver and an associated microprocessor. The base station also includes another microprocessor that serves as the base-station controller, a compact flash module comprising the aforementioned flash memory card and its controller, a local-area-network (LAN)

communication module, a power supply with battery backup, and an interface to a source of time-stamp signals that conform to an Inter Range Instrumentation Group (IRIG) standard. The base-station controller correlates related data from the sensor units and generates data-event log entries, which are transferred to the compact flash module. In addition, if the system is connected into a network, these log entries can be transferred to the LAN communication module for broadcasting over the network. The compact flash module can be manually removed to obtain access to the data stored therein.

Each receiver module maintains communications and time synchronization. It relays, to the base-station controller, information on events correlated with sensory and diagnostic information from its sensor unit. Each receiver module includes an interface port for on-board programming and serial communication with a mobile computer.

This work was done by Scott L. Jensen of Stennis Space Center and George J. Drouant of Jacobs Technology.

Inquiries concerning this technology should be addressed to the Intellectual Property Manager at Stennis Space Center (228) 688-1929. SSC-00247-1

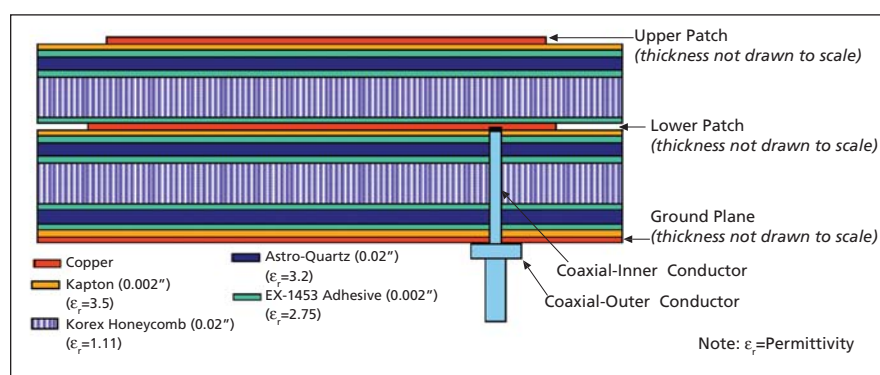
Microstrip Antenna for Remote Sensing of Soil Moisture and Sea Surface Salinity

The microstrip array design enables combined radar and radiometer instrumentation for satellite or airborne remote sensing.

NASA's Jet Propulsion Laboratory, Pasadena, California

This compact, lightweight, dual-frequency antenna feed developed for future soil moisture and sea surface salinity (SSS) missions can benefit future soil and ocean studies by lowering mass, volume, and cost of the antenna system. It also allows for airborne soil moisture and salinity remote sensors operating on small aircraft. While microstrip antenna technology has been developed for radio communications, it has yet to be applied to combined radar and radiometer for Earth remote sensing.

The antenna feed provides a key instrument element enabling high-resolution radiometric observations with large, deployable antennas. The design is based on the microstrip stacked-patch array (MSPA) used to feed a large, lightweight, deployable, rotating mesh antenna for spaceborne L-band (≈ 1 GHz) passive and active



The **Microstrip Stacked-Patch Array** incorporates three layers that function as the upper patch, lower patch, and ground plane. The lower radar patches sit on a honeycomb structure above the ground plane. The lower radar patches are fed through the ground plane, while the upper patch acts as a parasitic patch.

sensing systems. The array consists of stacked patches to provide dual-frequency capability and suitable radiation patterns. The stacked-patch microstrip element was

designed to cover the required L-band center frequencies at 1.26 GHz (lower patch) and 1.413 GHz (upper patch), with dual-linear polarization capabilities. The

dimension of patches produces the required frequencies.

To achieve excellent polarization isolation and control of antenna sidelobes for the MSPA, the orientation of each stacked-patch element within the array is optimized to reduce the cross-polarization. A specialized feed-distribution network was designed to achieve the required excitation amplitude and phase for each stacked-patch element.

The patches are thin copper/Kapton layers bonded to Astro-Quartz layers. As illustrated in the figure, three copper/Kapton/Astro-Quartz layers are

built to function as the upper patch, lower patch, and ground plane. The lower radar patches sit on a honeycomb dielectric structure above the conducting ground plane. The honeycomb is filled mostly with air and, therefore, introduces only a small loss at L-band frequencies. On the top of the radar patches sits another honeycomb dielectric structure to support the radiometer patches. All of the layers and the honeycombs are drilled to allow attachment to the feed wires to the lower patch (radar). The lower patch is fed through the ground plane, while the upper patch acts as a par-

asitic patch to introduce the 1.413 GHz.

A seven-element stacked patch array with elements forming a hexagonal pattern is the most suitable for space applications; however, a 16-element array with a 4x4 rectangular configuration is better for airborne and ground applications.

This work was done by Yahya Ramhat-Samii, Keerti Kona, and Majid Manteghi of the University of California at Los Angeles (UCLA); and Steven Dinardo, Don Hunter, Eni Njoku, William Wilson, and Simon Yueh of Caltech for NASA's Jet Propulsion Laboratory. For more information, contact iaoffice@jpl.nasa.gov. NPO-44470

🔗 Biomedical Wireless Ambulatory Crew Monitor

John H. Glenn Research Center, Cleveland, Ohio

A compact, ambulatory biometric data acquisition system has been developed for space and commercial terrestrial use. BioWATCH (Biomedical Wireless and Ambulatory Telemetry for Crew Health) acquires signals from biomedical sensors using acquisition modules attached to a common data and power bus. Several slots allow the user to configure the unit by inserting sensor-specific modules. The data are then sent real-time from the unit over any com-

mercially implemented wireless network including 802.11b/g, WCDMA, 3G.

This system has a distributed computing hierarchy and has a common data controller on each sensor module. This allows for the modularity of the device along with the tailored ability to control the cards using a relatively small master processor. The distributed nature of this system affords the modularity, size, and power consumption that better the current state of the art in medical ambulatory data acquisition.

A new company was created to market this technology.

This work was done by Alan Chmiel and Brad Humphreys of ZIN Technologies for Glenn Research Center. Further information is contained in a TSP (see page 1).

Inquiries concerning rights for the commercial use of this invention should be addressed to NASA Glenn Research Center, Innovative Partnerships Office, Attn: Steve Fedor, Mail Stop 4-8, 21000 Brookpark Road, Cleveland, Ohio 44135. Refer to LEW-18357-1.

🔗 Wireless Avionics Packet To Support Fault Tolerance for Flight Applications

A simple network interface supports fault detection and autonomous fault recovery.

NASA's Jet Propulsion Laboratory, Pasadena, California

In this protocol and packet format, data traffic is monitored by all network interfaces to determine the health of transmitter and subsystems. When failures are detected, the network interface applies its recovery policies to provide continued service despite the presence of faults. The protocol, packet format, and interface are independent of the data link technology used. The current demonstration system supports both commercial off-the-shelf wireless connections and wired Ethernet connections. Other technologies such as 1553 or serial data links can be used for the network backbone.

The Wireless Avionics packet is divided into three parts: a header, a data payload, and a checksum. The header

has the following components: magic number, version, quality of service, time to live, sending transceiver, function code, payload length, source Application Data Interface (ADI) address, destination ADI address, sending node address, target node address, and a sequence number.

The magic number is used to identify WAV packets, and allows the packet format to be updated in the future. The quality of service field allows routing decisions to be made based on this value and can be used to route critical management data over a dedicated channel. The time to live value is used to discard misrouted packets while the source transceiver is updated at each hop. This information is used to moni-

tor the health of each transceiver in the network.

To identify the packet type, the function code is used. Besides having a regular data packet, the system supports diagnostic packets for fault detection and isolation. The payload length specifies the number of data bytes in the payload, and this supports variable-length packets in the network. The source ADI is the address of the originating interface. This can be used by the destination application to identify the originating source of the packet where the address consists of a subnet, subsystem class within the subnet, a subsystem unit, and the local ADI number. The destination ADI is used to route the packet to its ultimate destination. At each hop, the sending interface uses the

destination address to determine the next node for the data.

The sending node is the node address of the interface that is broadcasting the packet. This field is used to determine the health of the subsystem that is sending the packet. In the case of a packet that traverses several intermediate nodes, it may be the node address of the intermediate node. The target node is the node address of the next hop for the packet. It may be an intermediate node, or the final destination for the packet.

The sequence number is used to identify duplicate packets. Because each in-

terface has multiple transceivers, the same packet will appear at both receivers. The sequence number allows the interface to correlate the reception and forward a single, unique packet for additional processing. The subnet field allows data traffic to be partitioned into segregated local networks to support large networks while keeping each subnet at a manageable size. This also keeps the routing table small enough so routing can be done by a simple table lookup in an FPGA device.

The subsystem class identifies members of a set of redundant subsystems,

and, in a hot standby configuration, all members of the subsystem class will receive the data packets. Only the active subsystem will generate data traffic. Specific units in a class of redundant units can be identified and, if the hot standby configuration is not used, packets will be directed to a specific subsystem unit.

This work was done by Gary L. Block, William D. Whitaker, James W. Dillon, James P. Lux, and Mohammad Ahmad of Caltech for NASA's Jet Propulsion Laboratory. For more information, contact iaoffice@jpl.nasa.gov. NPO-46327

Aerobot Autonomy Architecture

Potential applications include scientific exploration, military surveillance, and radio relay.

NASA's Jet Propulsion Laboratory, Pasadena, California

An architecture for autonomous operation of an aerobot (i.e., a robotic blimp) to be used in scientific exploration of planets and moons in the Solar system with an atmosphere (such as Titan and Venus) is undergoing development. This architecture is also applicable to autonomous airships that could be flown in the terrestrial atmosphere for scientific exploration, military reconnaissance and surveillance, and as radio-communication relay stations in disaster areas. The architecture was conceived to satisfy requirements to perform the following functions:

- Vehicle safing, that is, ensuring the integrity of the aerobot during its entire mission, including during extended communication blackouts.
- Accurate and robust autonomous flight control during operation in diverse modes, including launch, deployment of scientific instruments, long traverses, hovering or station-keeping, and maneuvers for touch-and-go surface sampling.
- Mapping and self-localization in the absence of a global positioning system.
- Advanced recognition of hazards and targets in conjunction with tracking of,



Testing of a Prototype Aerobot is an essential part of the continuing effort to develop an architecture for autonomous operation of aerial vehicles in the atmosphere of Earth as well as of remote planets. These photos show the JPL aerobot during autonomous flight tests conducted at the El Mirage dry lake in the Mojave Desert. The top image shows vehicle liftoff, and the bottom image shows the aerobot in autonomous flight mode.

and visual servoing toward, targets, all to enable the aerobot to detect and avoid atmospheric and topographic hazards and to identify, home in on, and hover over predefined terrain features or other targets of scientific interest.

The architecture is an integrated combination of systems for accurate and robust vehicle and flight trajectory control; estimation of the state of the aerobot; perception-based detection and avoidance of hazards; monitoring of the integrity and functionality ("health") of the aerobot; reflexive safing actions; multi-modal localization and mapping; autonomous planning and execution of scientific observations; and long-range planning and monitoring of the mission of the aerobot. The prototype JPL aerobot (see figure) has been tested extensively in various areas in the California Mojave desert.

This work was done by Alberto Elfes, Jeffery L. Hall, Eric A. Kulczycki, Jonathan M. Cameron, Arin C. Morfopoulos, Daniel S. Clouse, James F. Montgomery, Adnan I. Ansar, and Richard J. Machuzak of JPL for NASA's Jet Propulsion Laboratory. For more information, contact iaoffice@jpl.nasa.gov. NPO-45837



Submillimeter Confocal Imaging Active Module

This system could be used to image shorter objects between taller ones.

NASA's Jet Propulsion Laboratory, Pasadena, California

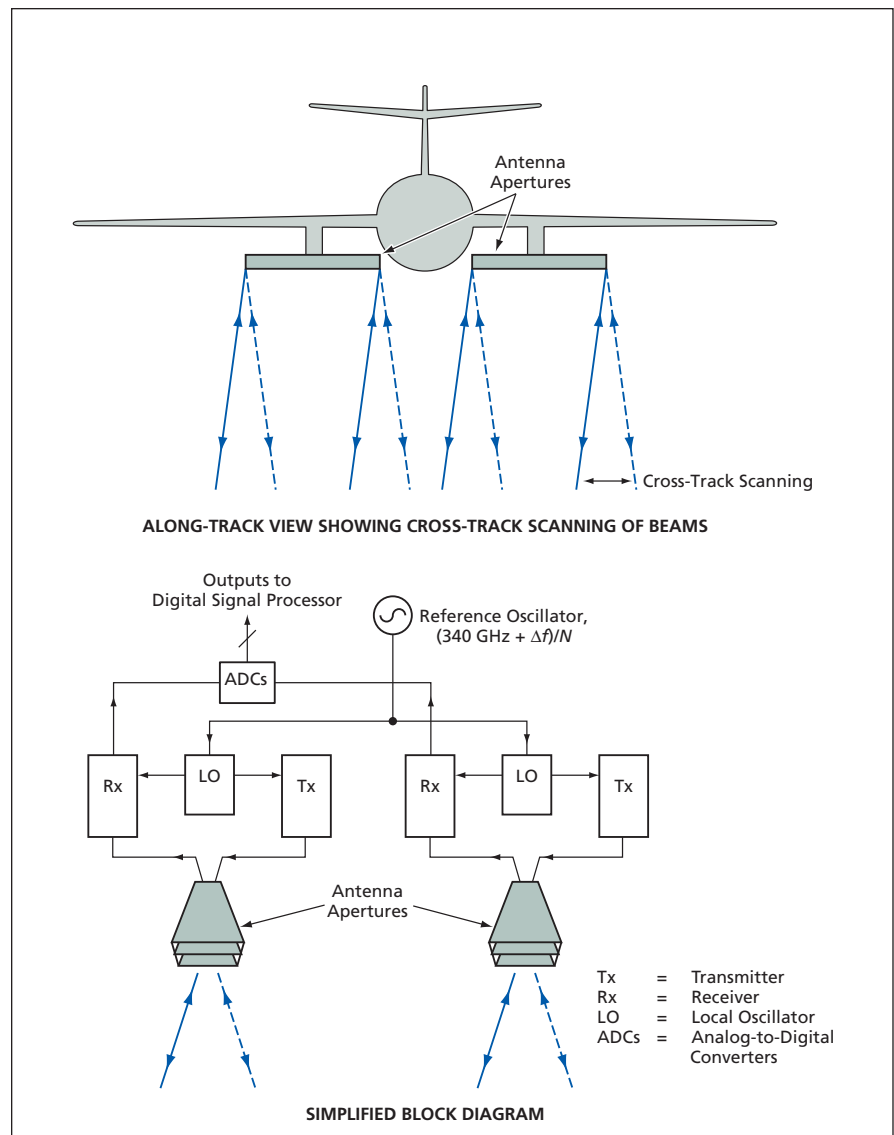
The term “submillimeter confocal imaging active module” (SCIAM) denotes a proposed airborne coherent imaging radar system that would be suitable for use in reconnaissance, surveillance, and navigation. The development of the SCIAM would include utilization and extension of recent achievements in monolithic microwave integrated circuits capable of operating at frequencies up to and beyond a nominal radio frequency of 340 GHz. Because the SCIAM would be primarily down-looking (in contradistinction to primarily side-looking), it could be useful for imaging shorter objects located between taller ones (for example, objects on streets between buildings). The SCIAM would utilize a confocal geometry to obtain high cross-track resolution, and would be amenable to synthetic-aperture processing of its output to obtain high along-track resolution.

The SCIAM (see figure) would include multiple (two in the initial version) antenna apertures, separated from each other by a cross-track baseline of suitable length (e.g., 1.6 m). These apertures would both transmit the illuminating radar pulses and receive the returns. A common reference oscillator would generate a signal at a controllable frequency of $(340 \text{ GHz} + \Delta f)/N$, where Δf is an instantaneous swept frequency difference and N is an integer. The output of this oscillator would be fed to a frequency-multiplier-and-power-amplifier module to obtain a signal, at $340 \text{ GHz} + \Delta f$, that would serve as both the carrier signal for generating the transmitted pulses and a local-oscillator (LO) signal for a receiver associated with each antenna aperture.

Because duplexers in the form of circulators or transmit/receive (T/R) switches would be lossy and extremely difficult to implement, the antenna apertures would be designed according to a spatial-duplexing scheme, in which signals would be coupled in and out via separate, adjacent transmitting and receiving feed horns. This scheme would cause the transmitted and re-

ceived beams to be aimed in slightly different directions, and, hence, to not overlap fully on the targets on the ground. However, a preliminary analysis has shown that the loss of overlap would be small enough that the resulting loss in signal-to-noise ratio (SNR) would be much less than the SNR loss associated with the use of a 340-GHz T/R switch.

In each antenna aperture, the receiving and transmitting feed horns would face a reflector structure that would be designed partly according to both a Fresnel-lens principle to minimize antenna volume and partly according to a diffraction-grating principle so that the beam direction in the cross-track plane would become dependent on the signal frequency. The Fresnel surfaces would



The SCIAM would initially include two antenna apertures, through each of which radar signals would be both transmitted and received. The antenna structures in each aperture would be frequency-dispersive so that frequency scanning could be used to effect cross-track scanning.

be confocal paraboloids having focal-length increments of a half wavelength, and the sizes of the Fresnel steps would be chosen to obtain a desired amount of angular deviation for a given amount of frequency tuning. For example, according to one tentative design, sweeping the radio frequency from 335 to 345 GHz would cause the beam to scan a cross-track ground swath 30 m wide

from a height of 1 km. Through post-detection processing of the return signals received via the two apertures, a cross-track image resolution of 27 cm would be obtained; in effect, the 30-m cross-track swath could be divided into 111 pixels of 27-cm width. Comparable along-track resolution would be obtained through synthetic-aperture post-processing.

*This work was done by John Hong, Imran Mehdi, Peter Siegel, Goutam Chattopadhyay, and Thomas Cwik of Caltech; Mark Rowell of the University of California, Santa Barbara; and John Hacker of Rockwell Scientific Company LLC for NASA's Jet Propulsion Laboratory. Further information is contained in a TSP (see page 1).
NPO-42924*

Traveling-Wave Maser for 32 GHz

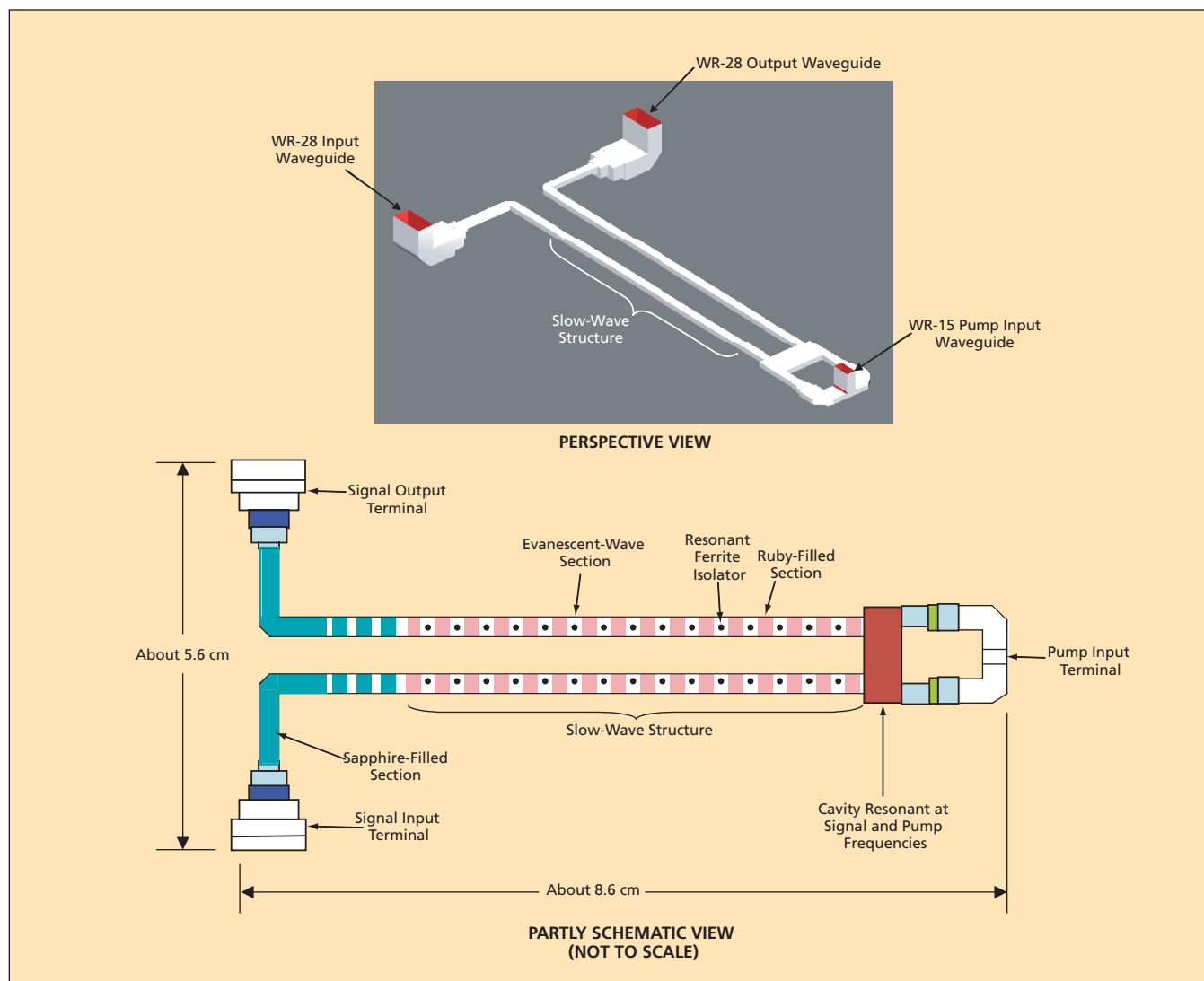
Significant improvements over prior 32-GHz low-noise amplifiers are anticipated.

NASA's Jet Propulsion Laboratory, Pasadena, California

The figure depicts a traveling-wave ruby maser that has been designed (though not yet implemented in hardware) to serve as a low-noise amplifier for reception of weak radio signals in

the frequency band of 31.8 to 32.3 GHz. The design offers significant improvements over previous designs of 32-GHz traveling-wave masers. In addition, relative to prior designs of 32-GHz ampli-

fiers based on high-electron-mobility transistors, this design affords higher immunity to radio-frequency interference and lower equivalent input noise temperature.



This 32-GHz Maser would include an improved slow-wave structure containing alternating ruby-filled and evanescent-wave sections.

In addition to the basic frequency-band and low-noise requirements, the initial design problem included a requirement for capability of operation in a closed-cycle helium refrigerator at a temperature ≤ 4 K and a requirement that the design be mechanically simplified, relative to prior designs, in order to minimize the cost of fabrication and assembly. Previous attempts to build 32-GHz traveling-wave masers involved the use of metallic slow-wave structures comprising coupled transverse electromagnetic (TEM)-mode resonators that were subject to very tight tolerances and, hence, were expensive to fabricate and assemble. Impedance matching for coupling signals into and out of these earlier masers was very difficult.

A key feature of the design is a slow-wave structure, the metallic portions of which would be mechanically relatively simple in that, unlike in prior slow-wave structures, there would be no internal metal steps, irises, or posts. The metallic portions of the slow-wave structure would consist only of two rectangular metal waveguide arms. The arms would contain

sections filled with the active material (ruby) alternating with evanescent-wave sections. This structure would be transparent in both the signal-frequency band (the aforementioned range of 31.8 to 32.3 GHz) and the pump-frequency band (65.75 to 66.75 GHz), and would impose large slowing factors in both frequency bands. Resonant ferrite isolators would be placed in the evanescent-wave sections to provide reverse loss needed to suppress reverse propagation of power at the signal frequency.

This design is expected to afford a large gain-bandwidth product at the signal frequency and efficient coupling of the pump power into the paramagnetic spin resonances of the ruby sections. The more efficiently the pump power could be thus coupled, the more efficiently it could be utilized and the heat load on the refrigerator correspondingly reduced. To satisfy the requirement for operation over the 0.5-GHz-wide signal-frequency band, the paramagnetic spin resonances would be broadened by applying a magnetic field having a linear gradient along the slow-wave structure.

The gradients in the two arms are offset in order to compensate for the gaps of the evanescent sections.

The two arms of the slow-wave structure would be connected into a U-shaped assembly. At the base of the U (at the right end in the figure) there would be a cavity that would be simultaneously resonant in the TE_{301} mode at the signal frequency and in the TE_{403} mode at the pump frequency. The pump power would be injected into this cavity that would be beyond cut-off at the signal frequency. The dielectric-filled waveguides would be excited from the two output arms of an electric-field-plane T junction. The signal power would enter and leave via WR-28 waveguides connected to opposite ends of the U-shaped assembly. Impedance matching would be effected by means of dielectric-filled (sapphire) sections of the waveguide arms near their input and output ends.

This work was done by James Shell and Robert Clauss of Caltech for NASA's Jet Propulsion Laboratory. Further information is contained in a TSP (see page 1). NPO-41273

System Synchronizes Recordings From Separated Video Cameras

A large, immobile timing infrastructure is not needed.

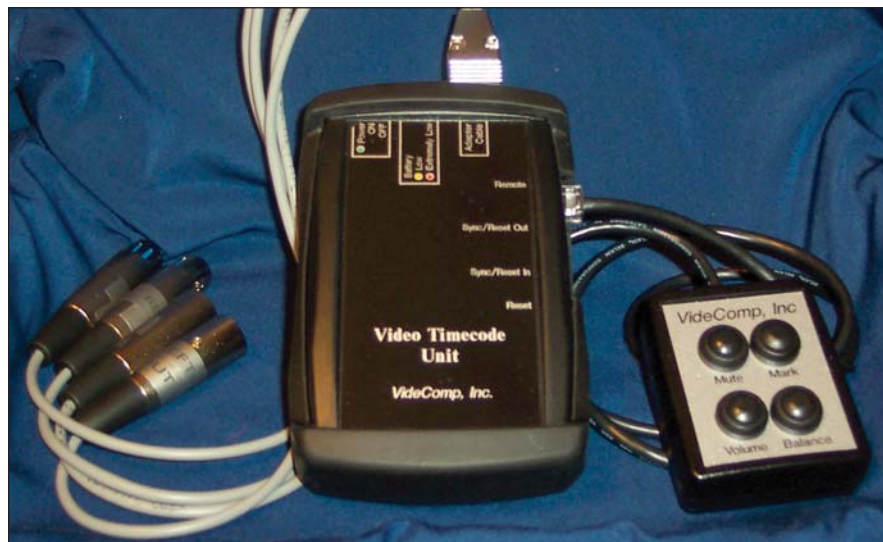
Stennis Space Center, Mississippi

A system of electronic hardware and software for synchronizing recordings from multiple, physically separated video cameras is being developed, primarily for use in multiple-look-angle video production. The system, the time code used in the system, and the underlying method of synchronization upon which the design of the system is based are denoted generally by the term "Geo-TimeCode™." The system is embodied mostly in compact, lightweight, portable units (see figure) denoted video time-code units (VTUs) — one VTU for each video camera. The system is scalable in that any number of camera recordings can be synchronized. The estimated retail price per unit would be about \$350 (in 2006 dollars).

The need for this or another synchronization system external to video cameras arises because most video cameras do not include internal means for maintaining synchronization with other video cameras. Unlike prior video-camera-synchronization systems, this system does not depend on continuous cable or

radio links between cameras (however, it does depend on occasional cable links lasting a few seconds). Also, whereas the time codes used in prior video-camera-synchronization systems typically repeat

after 24 hours, the time code used in this system does not repeat for slightly more than 136 years; hence, this system is much better suited for long-term deployment of multiple cameras.



This **Mockup** of a VTU is based on a prototype VTU circuit powered by a standard 9-volt battery. To the extent possible, production VTUs would be made of low-power, precision electronic components that are already commercially available.

Each VTU contains a free-running, extremely stable clock, based on a 32,768-Hz (2^{15} -Hz) quartz-crystal oscillator. The clock begins a binary count up from zero when reset and continues counting up until reset again (or until it automatically restarts from zero when the time code repeats after more than 136 years). Each VTU also contains digital and analog audio circuitry required for synchronization of video recording.

The GeoTimeCode is a variant of the Inter Range Instrumentation Group B (IRIG-B) time code, which is widely used in the aerospace industry. The GeoTimeCode can easily be converted to other standard time codes, including the Society of Motion Picture and Television Engineers (SMPTE) time code. The GeoTimeCode is similar enough to the IRIG-B time code that software can easily be adapted to read either code.

A VTU can be synchronized to a Universal Time source (e.g., an Internet

time server or a radio time signal) or to other, possibly distant VTUs by use of a computer equipped with the appropriate software and ancillary electronic hardware. Optionally, without using a computer, multiple VTUs can be synchronized with each other by temporarily connecting them together via standard patch cables and pressing a reset button. At the instant when synchronization is performed, the synchronization is accurate to within less than a millisecond. Synchronization can be done either before or after a video recording is made; the clock in a VTU is stable and accurate enough that as long as synchronization is performed within about 8 hours of recording, timing is accurate to within 0.033 second (a typical video frame period).

A portion of the time code is reserved for a serial number that identifies each VTU and, hence, the camera from which each recording is taken. Another

portion of the time code is reserved for event markers, which can be added manually during recording by means of a pushbutton switch. Each event marker includes an event number from a counter that is incremented for each event. The serial numbers and event markers can be used to identify specific image sequences during post processing of video images by editing software.

This work was done by William "Bud" Nail, William L. Nail, Jasper M. Nail, and Duong T. Le of Technological Services Co. for Stennis Space Center.

Inquiries concerning rights for the commercial use of this invention should be addressed to:

*Technological Services Company
100 Street A, Suite B
Picayune, MS 39466
(601) 799-2403*

E-mail: budnail@videcomp.com

Refer to SSC-00253, volume and number of this NASA Tech Briefs issue, and the page number

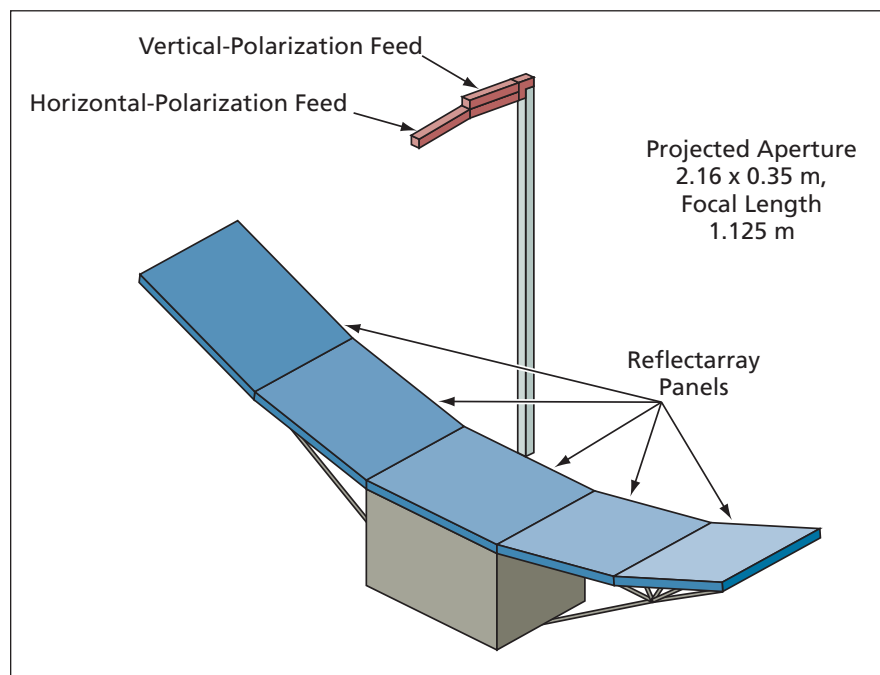
Piecewise-Planar Parabolic Reflectarray Antenna

Performance is equalized in horizontal and vertical polarizations.

NASA's Jet Propulsion Laboratory, Pasadena, California

The figure shows a dual-beam, dual-polarization Ku-band antenna, the reflector of which comprises an assembly of small reflectarrays arranged in a piecewise-planar approximation of a parabolic reflector surface. The specific antenna design is intended to satisfy requirements for a wide-swath spaceborne radar altimeter, but the general principle of piecewise-planar reflectarray approximation of a parabolic reflector also offers advantages for other applications in which there are requirements for wide-swath antennas that can be stowed compactly and that perform equally in both horizontal and vertical polarizations.

The main advantages of using flat (e.g., reflectarray) antenna surfaces instead of paraboloidal or parabolic surfaces is that the flat ones can be fabricated at lower cost and can be stowed and deployed more easily. Heretofore, reflectarray antennas have typically been designed to reside on single planar surfaces and to emulate the focusing properties of, variously, paraboloidal (dish) or parabolic antennas. In the present case, one approximates the nominal parabolic shape by concatenating several flat pieces, while still exploiting the principles of the planar reflectarray for each piece.



Five Flat Panels are arranged in a piecewise-planar approximation of a parabolic reflector surface. Each panel is a reflectarray designed to emulate the corresponding part of the parabolic reflector.

Prior to the conception of the present design, the use of a single large reflectarray was considered, but then abandoned when it was found that the directional

and gain properties of the antenna would be noticeably different for the horizontal and vertical polarizations. The reason for this difference in per-

formance is related to strong spatial variations in phase, including phase wraps (phase variations in excess of 360°).

By arranging small reflectarrays in a piecewise-planar approximation of a parabola, instead of constructing one large reflectarray on a single planar

surface, one minimizes the number of phase wraps per panel and reduces the angle of incidence at each reflectarray patch. This makes it possible to simultaneously maximize the vertical- and horizontal-polarization gains, to improve the radiation pattern, and re-

duce sensitivity to fabrication and adjustment errors.

This work was done by Richard Hodges and Mark Zawadzki of Caltech for NASA's Jet Propulsion Laboratory. For more information, contact iaoffice@jpl.nasa.gov. NPO-40889

Reducing Interference in ATC Voice Communication

Digital signal processing would be used to suppress unwanted signals.

NASA's Jet Propulsion Laboratory, Pasadena, California

Three methods have been proposed to be developed to enable reduction of the types of interference that often occur among voice-communication radio signals involved in air-traffic control (ATC). For historical reasons and for compatibility with some navigation systems, control towers and aircraft use amplitude modulation (AM) for voice communication. In the presence of two simultaneous AM transmissions in the same frequency channel, what is heard through a receiver includes not only the audio portions of both transmissions but also an audio heterodyne signal at the difference between the carrier frequencies of the transmissions (as a practical matter, the carrier frequencies almost always differ somewhat). The situation is further complicated by multiple heterodyne signals in the presence of more than two simultaneous transmissions. Even if one of the transmissions does not include AM because of a transmitter malfunction or because a transmitter was inadvertently turned on or left on, the heterodyne signal makes it difficult to understand the audio of the other transmission. The proposed methods would utilize digital signal processing to counteract this type of interference.

In the first of the three methods, a post-detection audio digital signal processor (DSP) in a receiver would re-

duce the level of the heterodyne signal significantly. The DSP would be a self-contained unit that would be connected between (1) the output terminal of the ATC receiver audio circuitry and (2) a loudspeaker and/or headphones. The DSP would use a well-understood least-mean-square (LMS) algorithm to automatically adjust the coefficients of a finite-impulse-response filter in order to minimize the amplitude of such highly correlated signals as sine waves (including audio heterodyne signals). The DSP would operate without intervention by the human operator.

In the event that the first method as described thus far did not reduce interference sufficiently, it could be supplanted or augmented by a variant in which a DSP would be added to the last intermediate-frequency (IF) stage of the receiver, where it would be possible to effect improvements through increased dynamic range and linearity and the opportunity to shape the IF pass band for optimum rejection of other types of interference.

The second method, involving independent sideband reception, could be used alone or in combination with the first method. This method would exploit the fact that (1) the two simultaneously transmitted signals would not have the same carrier frequency and (2) the upper sideband would yield a higher

signal-to-noise ratio (SNR) for the higher-carrier-frequency signal while the lower sideband would yield a higher SNR for the lower-carrier-frequency signal. Some development would be necessary to determine the best way to make use of the two signals.

In the third method, multiple antennas would be used for reception and their outputs would be combined by an adaptive beam former that would use the same LMS algorithm as that of the first method. In this case, the weighting between the antennas would be adjusted to minimize the coherent component of the received signal. A method equivalent to this one has been used in microwave data communication.

This work was done by John O. Battle of Caltech for NASA's Jet Propulsion Laboratory.

In accordance with Public Law 96-517, the contractor has elected to retain title to this invention. Inquiries concerning rights for its commercial use should be addressed to:

*Innovative Technology Assets Management
JPL*

*Mail Stop 202-233
4800 Oak Grove Drive
Pasadena, CA 91109-8099*

*(818) 354-2240
E-mail: iaoffice@jpl.nasa.gov*

Refer to NPO-43950, volume and number of this NASA Tech Briefs issue, and the page number.



EOS MLS Level 1B Data Processing, Version 2.2

A computer program performs level-1B processing (the term "1B" is explained below) of data from observations of the limb of the Earth by the Earth Observing System (EOS) Microwave Limb Sounder (MLS), which is an instrument aboard the Aura spacecraft. This software accepts, as input, the raw EOS MLS scientific and engineering data and the Aura spacecraft ephemeris and attitude data. Its output consists of calibrated instrument radiances and associated engineering and diagnostic data. [This software is one of several computer programs, denoted product generation executives (PGEs), for processing EOS MLS data. Starting from level 0 (representing the aforementioned raw data, the PGEs and their data products are denoted by alphanumeric labels (e.g., 1B and 2) that signify the successive stages of processing.]

At the time of this reporting, this software is at version 2.2 and incorporates improvements over a prior version that make the code more robust, improve calibration, provide more diagnostic outputs, improve the interface with the Level 2 PGE, and effect a 15-percent reduction in file sizes by use of data compression.

This program was written by Vincent Perun, Robert Jarnot, Herbert Pickett, Richard Cofield, Michael Schwartz, and Paul Wagner for Caltech for NASA's Jet Propulsion Laboratory.

This software is available for commercial licensing. Please contact Karina Edmonds of the California Institute of Technology at (626) 395-2322. Refer to NPO-44841.

Auto-Generated Semantic Processing Services

Auto-Generated Semantic Processing (AGSP) Services is a suite of software tools for automated generation of other computer programs, denoted cross-platform semantic adapters, that support interoperability of computer-based communication systems that utilize a variety of both new and legacy communication software running in a variety of operating-system/computer-hardware combinations. AGSP has numerous potential uses in military, space-exploration, and other government applications as well as

in commercial telecommunications. The cross-platform semantic adapters take advantage of common features of computer-based communication systems to enforce semantics, messaging protocols, and standards of processing of streams of binary data to ensure integrity of data and consistency of meaning among interoperating systems.

The auto-generation aspect of AGSP Services reduces development time and effort by emphasizing specification and minimizing implementation: In effect, the design, building, and debugging of software for effecting conversions among complex communication protocols, custom device mappings, and unique data-manipulation algorithms is replaced with metadata specifications that map to an abstract platform-independent communications model. AGSP Services is modular and has been shown to be easily integrable into new and legacy NASA flight and ground communication systems.

This program was written by Rodney Davis and Greg Huff of Command and Control Technologies Corp. for Kennedy Space Center. For further information, contact:

*Command and Control Technologies Corp.
Rodney Davis
1425 Chaffee Drive, Suite 1
Titusville, FL 32780-7900
Phone No.: (321) 264-1193
davisrd@cctcorp.com*

Inquiries concerning rights for the commercial use of this invention should be addressed to the Kennedy Innovative Partnerships Office at (321) 861-7158. Refer to KSC-13072.

Geospatial Authentication

A software package that has been designed to allow authentication for determining if the rover(s) is/are within a set of boundaries or a specific area to access critical geospatial information by using GPS signal structures as a means to authenticate mobile devices into a network wirelessly and in real-time has been developed. The advantage lies in that the system only allows those with designated geospatial boundaries or areas into the server.

The Geospatial Authentication software has two parts — Server and Client. The server software is a virtual private network (VPN) developed in Linux operating system using Perl programming language. The server can be a stand-alone

VPN server or can be combined with other applications and services. The client software is a GUI Windows CE software, or Mobile Graphical Software, that allows users to authenticate into a network. The purpose of the client software is to pass the needed satellite information to the server for authentication.

This work was done by Stacey D. Lyle of Geospatial Research Innovation Design for NASA's Stennis Space Center.

Inquiries concerning rights for its commercial use should be addressed to:

*Dr. Stacey D. Lyle, RLPS
Conrad Blucher Institute of Surveying and Science
6300 Ocean Drive
Texas A&M University
Corpus Christi, TX 78412
Phone No. : (361) 825-3712
Fax: (361) 825-5848
E-mail: stacey.lyle@tamucc.edu*

Refer to SSC-00282, volume and number of this NASA Tech Briefs issue, and the page number

Maneuver Automation Software

The Maneuver Automation Software (MAS) automates the process of generating commands for maneuvers to keep the spacecraft of the Cassini-Huygens mission on a predetermined prime mission trajectory. Before MAS became available, a team of approximately 10 members had to work about two weeks to design, test, and implement each maneuver in a process that involved running many maneuver-related application programs and then serially handing off data products to other parts of the team. MAS enables a three-member team to design, test, and implement a maneuver in about one-half hour after Navigation has process-tracking data. MAS accepts more than 60 parameters and 22 files as input directly from users.

MAS consists of Practical Extraction and Reporting Language (PERL) scripts that link, sequence, and execute the maneuver-related application programs: "Pushing a single button" on a graphical user interface causes MAS to run navigation programs that design a maneuver; programs that create sequences of commands to execute the maneuver on the spacecraft; and a program that generates predictions about maneuver performance and generates reports and other files that enable users to quickly review and verify

the maneuver design. MAS can also generate presentation materials, initiate electronic command request forms, and archive all data products for future reference.

This program was written by Hal Uffelmann, Troy Goodson, Michael Pellegrin, Lynn Stavert, Thomas Burk, David Beach, Joel Signorelli, Jeremy Jones, Yungsun Hahn, Ahlam Attiyah, and Jeannette Illsley of Caltech for NASA's Jet Propulsion Laboratory.

This software is available for commercial licensing. Please contact Karina Edmonds of the California Institute of Technology at (626) 395-2322. Refer to NPO-42137.

Event Driven Messaging With Role-Based Subscriptions

Event Driven Messaging with Role-Based Subscriptions (EDM-RBS) is a framework integrated into the Service Management Database (SMDB) to allow for role-based and subscription-based delivery of synchronous and asynchronous messages over JMS (Java Messaging Service), SMTP (Simple Mail Transfer Protocol), or SMS (Short Messaging Service). This allows for 24/7 operation with users in all parts of the world. The software classifies messages by triggering data type, application source, owner of data triggering event (mission), classification, sub-classification and various other secondary classifying tags. Messages are routed to applications or users based on subscription rules using a combination of the above message attributes.

This program provides a framework for identifying connected users and their applications for targeted delivery of messages over JMS to the client appli-

cations the user is logged into. EDM-RBS provides the ability to send notifications over e-mail or pager rather than having to rely on a live human to do it. It is implemented as an Oracle application that uses Oracle relational database management system intrinsic functions. It is configurable to use Oracle AQ JMS API or an external JMS provider for messaging. It fully integrates into the event-logging framework of SMDB (Subnet Management Database).

EDM-RBS is currently integrated into the SMDB component of the Service Preparation Subsystem of the DSN (Deep Space Network). Users worldwide rely on this service for notification confirming acceptance or denial of submitted products in support of mission tracking activities. DSN operations rely on this service for asynchronous notifications of problems needing human intervention. This innovation is a core service supporting the concept of lights-out operations and operations with human intervention by exception, a plan to improve the level of service while reducing operations costs.

This work was done by Tung Bui, Bach Bui, Shantanu Malhotra, Fannie Chen, Rachel Kim, Christopher Allen, Ivy Luong, George Chang, and Silvino Zendejas of Caltech and Syed Sadaqathulla of Raytheon for NASA's Jet Propulsion Laboratory.

In accordance with Public Law 96-517, the contractor has elected to retain title to this invention. Inquiries concerning rights for its commercial use should be addressed to:

*Innovative Technology Assets Management
JPL*

*Mail Stop 202-233
4800 Oak Grove Drive
Pasadena, CA 91109-8099
E-mail: iaoffice@jpl.nasa.gov*

Refer to NPO-45015, volume and number of this NASA Tech Briefs issue, and the page number.

Estimating Relative Positions of Outer-Space Structures

A computer program estimates the relative position and orientation of two structures from measurements, made by use of electronic cameras and laser range finders on one structure, of distances and angular positions of fiducial objects on the other structure. The program was written specifically for use in determining errors in the alignment of large structures deployed in outer space from a space shuttle.

The program is based partly on equations for transformations among the various coordinate systems involved in the measurements and on equations that account for errors in the transformation operators. It computes a least-squares estimate of the relative position and orientation. Sequential least-squares estimates, acquired at a measurement rate of 4 Hz, are averaged by passing them through a fourth-order Butterworth filter. The program is executed in a computer aboard the space shuttle, and its position and orientation estimates are displayed to astronauts on a graphical user interface.

This program was written by Harry Balian, William Breckenridge, and Paul Brugarolas of Caltech for NASA's Jet Propulsion Laboratory.

This software is available for commercial licensing. Please contact Karina Edmonds of the California Institute of Technology at (626) 395-2322. Refer to NPO-45071.



Fabricating PFPE Membranes for Capillary Electrophoresis

Precisely sized and positioned holes are defined by photomasks.

NASA's Jet Propulsion Laboratory, Pasadena, California

A process has been developed for fabricating perfluoropolyether (PFPE) membranes that contain microscopic holes of precise sizes at precise locations. The membranes are to be incorporated into "laboratory-on-a-chip" microfluidic devices to be used in performing capillary electrophoresis.

The present process is a modified version of part of the process, described in the immediately preceding article, that includes a step in which a liquid PFPE layer is cured into solid (membrane) form by use of ultraviolet light. In the present process, one exploits the fact that by masking some locations to prevent exposure to ultraviolet light, one

can prevent curing of the PFPE in those locations. The uncured PFPE can be washed away from those locations in the subsequent release and cleaning steps. Thus, holes are formed in the membrane in those locations.

The most straightforward way to implement the modification is to use, during the ultraviolet-curing step, an ultraviolet photomask similar to the photomasks used in fabricating microelectronic devices. In lieu of such a photomask, one could use a mask made of any patternable ultraviolet-absorbing material (for example, an ink or a photoresist).

This work was done by Michael C. Lee, Peter A. Willis, and Frank Greer of Caltech

and Jason Rolland of Liquidia Technologies Inc. for NASA's Jet Propulsion Laboratory.

In accordance with Public Law 96-517, the contractor has elected to retain title to this invention. Inquiries concerning rights for its commercial use should be addressed to:

Innovative Technology Assets Management
JPL

Mail Stop 202-233
4800 Oak Grove Drive
Pasadena, CA 91109-8099

E-mail: iaoffice@jpl.nasa.gov

Refer to NPO-45782, volume and number of this NASA Tech Briefs issue, and the page number.

Linear Actuator Has Long Stroke and High Resolution

There are potential applications in precise measurement and precise fabrication.

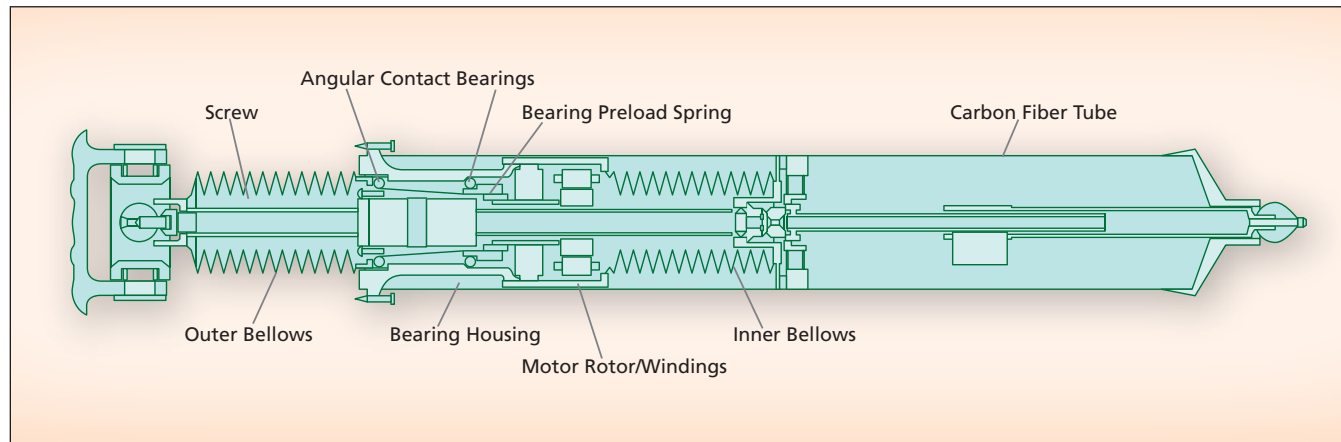
NASA's Jet Propulsion Laboratory, Pasadena, California

The term "precision linear actuator, direct drive" ("PLADD") refers to a robust linear actuator designed to be capable of repeatedly performing, over a lifetime of the order of 5 to 10 years, positioning maneuvers that include, variously, submicron increments or slews of the order of a centimeter. The PLADD is capable of both long stroke (120 mm) and high resolution (repeatable incre-

ments of 20 nm). Unlike precise linear actuators of prior design, the PLADD contains no gears, levers, or hydraulic converters. The PLADD, now at the prototype stage of development, is intended for original use as a coarse-positioning actuator in a spaceborne interferometer. The PLADD could also be adapted to terrestrial applications in which there are requirements for long stroke and

high resolution: potential applications include medical imaging and fabrication of semiconductor devices.

The PLADD (see figure) includes a commercially available ball-screw actuator driven directly by a commercially available three-phase brushless DC motor. The ball-screw actuator comprises a spring-preloaded ball nut on a ball screw that is restrained against rota-



This Partly Schematic Cross Section depicts some of the components of the PLADD.

tion as described below. The motor is coupled directly (that is, without an intervening gear train) to a drive link that, in turn, is coupled to the ball nut. By eliminating the gear train, the direct-drive design eliminates the complexity, backlash, and potential for misalignment associated with a gear train.

To prevent inadvertent movement, there is a brake that includes flexured levers compressed against the drive link by preload springs. This is a power-off brake: There are also piezoelectric stacks that can be activated to oppose the springs and push the levers away from the drive link. Hence, power must be applied to the piezoelectric stacks to release the drive link from braking.

To help ensure long operational life, all of the mechanical drive components are immersed in an oil bath within hermetically sealed bellows. The outer end of the bellows holds the outer end of the ball screw, thereby preventing rotation of the ball screw.

Positioning is controlled by an electronic control system that includes digital and analog subsystems that interact with the motor and brake and with two sensor/encoder units: a Hall-effect-sensor rotation encoder and a linear glass-scale encoder. This system implements a proportional + integral + derivative control algorithm that results in variation of voltage commands to each of the three pairs of windings of the brushless DC motor. In one of two alter-

native control modes, the voltages are applied to the windings in a trapezoidal commutation scheme on the basis of timing signals obtained from the Hall-effect sensors; this scheme yields relatively coarse positioning — 24 steps per motor revolution. The second control mode involves a sinusoidal commutation scheme in which the output of the linear glass-scale encoder is transposed to rotational increments to yield much finer position feedback — more than 400,000 steps per revolution.

This work was done by Brant T. Cook, Donald M. Moore, David F. Braun, John S. Koenig, and Steve M. Hankins of Caltech for NASA's Jet Propulsion Laboratory. For more information, contact iaoffice@jpl.nasa.gov. NPO-45692

Installing a Test Tap on a Metal Battery Case

Lyndon B. Johnson Space Center, Houston, Texas

A mechanical fitting and relatively simple and safe method of installing it on the metal case of a battery have been devised to provide access to the interior of the battery to perform inspection and/or to measure such internal conditions as temperature and pressure. A metal boss or stud having an exterior thread is attached to the case by capacitor-discharge stud welding (CDSW), which takes only 3 to 6 milliseconds and in which the metallur-

gical bond (weld) and the heat-affected zone are limited to a depth of a few thousandths of an inch (a few hundredths of a millimeter).

These characteristics of CDSW prevent distortion of the case and localized internal heating that could damage the chemical components inside of the battery. An access hole is then drilled through the stud and case, into the interior of the battery. A mechanical fitting having a matching thread is in-

stalled on the stud and the interior end of the fitting is sealed with a pressure-sealing washer/gasket. The exterior end of the fitting is configured for attachment of whatever instrumentation is required for the selected inspection or measurement.

This work was done by Daniel R. Mayes of Johnson Space Center and Daniel J. Rybicki of Lockheed Martin Corp. Further information is contained in a TSP (see page 1). MSC-23827-1

Fabricating PFPE Membranes for Microfluidic Valves and Pumps

This process contributes to development of “laboratory-on-a-chip” devices.

NASA's Jet Propulsion Laboratory, Pasadena, California

A process has been developed for fabricating membranes of a perfluoropolyether (PFPE) and integrating them into valves and pumps in “laboratory-on-a-chip” microfluidic devices. Membranes of poly(tetrafluoroethylene) [PTFE] and poly(dimethylsilane) [PDMS] have been considered for this purpose and found wanting. By making it possible to use PFPE instead of PTFE or PDMS, the present process expands the array of options for further development of microfluidic devices for diverse applications that could include detection of biochemicals of interest, detection of toxins and biowarfare agents, synthesis

and analysis of proteins, medical diagnosis, and synthesis of fuels.

To be most useful, a membrane material for a microfluidic valve or pump should be a chemically inert elastomer. PTFE is highly chemically inert and is a thermoplastic and, therefore, subject to cold flow and creep. Also, procedures for fabricating PTFE membranes are excessively complex. PDMS is an elastomer that has been used in prior microfluidic devices but, undesirably, reacts chemically with some liquids (acetonitrile, acids, and fuels) that might be required to be handled by microfluidic devices in some applications. On the other hand,

the PFPE in question has elastomeric properties similar to those of PDMS and a degree of chemical inertness similar to that of PTFE.

The specific membrane material to which the present process applies is a commercially available, ultraviolet-curable PFPE. A microfluidic device of the type to which the process applies consists mainly of this PFPE sandwiched between two plates of a highly chemically resistant, low-thermal-expansion borosilicate glass manufactured by the float method. Heretofore, there have been two obstacles to fabrication of microfluidic devices from this combination of

materials: (1) The lack of chemical reactivity between the PFPE and the glass makes it impossible to form a lasting bond between them; and (2) such conventional membrane-fabrication techniques as spin coating yield membranes that are not sufficiently flat and not sufficiently resistant to curling upon themselves. The present process overcomes these obstacles.

The process consists mainly of the following steps:

1. A fluorocarbon-based polymer is formed on the glass plates by means of a plasma deposition subprocess.
2. The polymer is patterned by use of a photoresist and conventional photolithography.
3. The polymer is removed in the pattern by use of an O₂/Ar plasma.
4. The remaining polymer surface areas are cleaned and modified by use of a low-energy O₂ plasma.
5. The glass plates are spin-coated with a lift-off material, which is then cured by heating to a temperature of 150 °C for 5 minutes.
6. The liquid (uncured) PFPE material is pressed between the two lift-off-layer-coated glass plates, along with 250- μ m-thick shims to define the desired thickness of the PFPE membrane.
7. The liquid PFPE is cured to a solid by exposure to ultraviolet light for 5 minutes.
8. The PFPE membrane is released from the glass plates by submersion in a developer solution and/or acetone.
9. The glass plates and the PFPE membrane are cleaned and activated for bonding by exposure to an O₂ plasma.
10. The glass plates and the membrane are aligned and sandwiched together at a temperature \leq 100 °C and a pressure of 3 bar (0.3 MPa) for one hour. This combination of pressure

and temperature is sufficient to cause a chemical reaction that results in bonding of the PFPE membrane to the polymer coats on the glass plates.

This work was done by Frank Greer, Victor E. White, Michael C. Lee, Peter A. Willis, and Frank J. Grunthaner of Caltech and Jason Rolland and Jake Sprague of Liquidia Technologies Inc. for NASA's Jet Propulsion Laboratory.

In accordance with Public Law 96-517, the contractor has elected to retain title to this invention. Inquiries concerning rights for its commercial use should be addressed to:

*Innovative Technology Assets Management
JPL*

Mail Stop 202-233

4800 Oak Grove Drive

Pasadena, CA 91109-8099

E-mail: iaoffice@jpl.nasa.gov

Refer to NPO-45725, volume and number of this NASA Tech Briefs issue, and the page number.



Room-Temperature-Cured Copolymers for Lithium Battery Gel Electrolytes

Room-temperature curing offers an important advantage in room-temperature functionality.

John H. Glenn Research Center, Cleveland, Ohio

Polyimide-PEO copolymers ("PEO" signifies polyethylene oxide) that have branched rod-coil molecular structures and that can be cured into film form at room temperature have been invented for use as gel electrolytes for lithium-ion electric-power cells. These copolymers offer an alternative to previously patented branched rod-coil polyimides that have been considered for use as polymer electrolytes and that must be cured at a temperature of 200 °C. In order to obtain sufficient conductivity

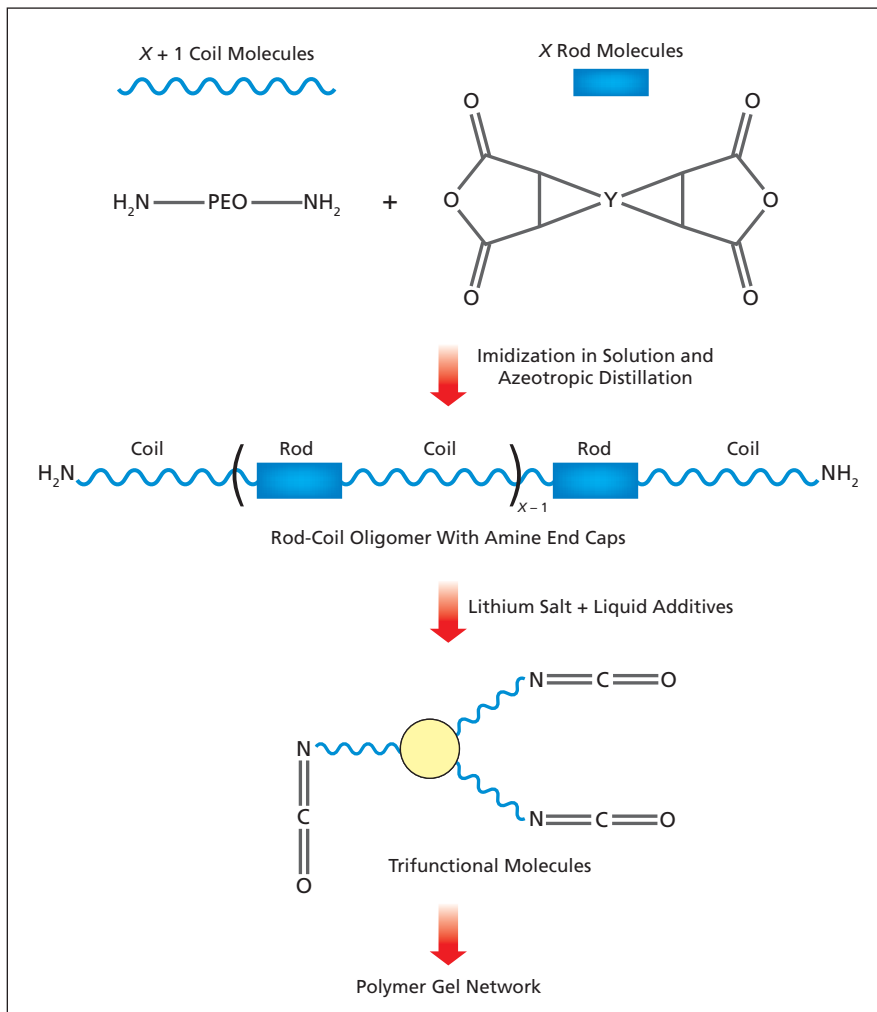
for lithium ions in practical applications at and below room temperature, it is necessary to imbibe such a polymer with a suitable carbonate solvent or ionic liquid, but the high-temperature cure makes it impossible to incorporate and retain such a liquid within the polymer molecular framework. By eliminating the high-temperature cure, the present invention makes it possible to incorporate the required liquid.

The curing of a polyimide-PEO copolymer according to the invention

results in formation of a gel network that is capable of conducting lithium ions. The PEO molecular segments provide the lithium-ion conductivity, while the imide segments and branching provide dimensional stability. The network can hold as much as four times its own weight of liquid while maintaining a high degree of dimensional stability. The liquid can aid significantly in the conduction of lithium ions, and in some circumstances, can increase cell cycle life. Electrolytes have been prepared that contain no volatile components, have a potential stability window of >4.5 V, and have exhibited stable Galvanic cycling between lithium metal electrodes in a coin cell for over 1,000 hours at 60 °C and 0.25 mA/cm² current density.

The copolymer is synthesized in the following process (see figure):

1. A PEO oligomer that is terminated with primary aliphatic amines on both ends is reacted with a dianhydride to make a polyamide-acid prepolymer. The reaction takes place in a solvent, and the stoichiometry of the oligomer and the dianhydride is adjusted so that the resulting prepolymer is a linear polymer capped with amines on both ends. The solvent must be carefully chosen to solubilize the prepolymer, have a boiling temperature preferably between 150 and 200 °C, and to be inert to lithium metal and other cell ingredients.
2. The polyamide-acid prepolymer is imidized in solution. The water generated in the imidization reaction is removed by azeotropic distillation.
3. The appropriate additives (e.g., a lithium salt and a carbonate solvent) are dissolved in the polymer solution. A trifunctional molecule that reacts with the amine end caps at ambient temperatures to form a gel is then added to the solution. The gelation time and the properties of the resulting film can be adjusted by changing the length of the polymer chains. The properties of the film can also be ad-



A Polymer Gel Network based on a branched rod-coil polyimide-PEO copolymer is synthesized in a relatively simple process that can be adapted to tailoring the properties of the final product.

justed through choice of the dianhydride, the length of the starting PEO oligomer molecules, and partial replacement of the trifunctional molecule with a difunctional molecule.

4. The film can be packaged once gelation has occurred. Because the reaction solvent is inert toward all cell ingredients, it is not necessary to

remove this solvent. Optionally, because the reaction solvent boils at a temperature $\approx 100\text{ }^\circ\text{C}$ lower than does a typical cyclic carbonate solvent, the reaction solvent can be preferentially evaporated before packaging.

This work was done by Mary Ann B. Meador of Glenn Research Center and Dean M. Tigelaar of Ohio Aerospace Institute. Fur-

ther information is contained in a TSP (see page 1).

Inquiries concerning rights for the commercial use of this invention should be addressed to NASA Glenn Research Center, Innovative Partnerships Office, Attn: Steve Fedor, Mail Stop 4-8, 21000 Brookpark Road, Cleveland, Ohio 44135. Refer to LEW-18205-1.

Catalysts for Efficient Production of Carbon Nanotubes

Some alloys have been found to work at lower temperatures.

Lyndon B. Johnson Space Center, Houston, Texas

Several metal alloys have shown promise as improved catalysts for catalytic thermal decomposition of hydrocarbon gases to produce carbon nanotubes (CNTs). Heretofore almost every experiment on the production of carbon nanotubes by this method has involved the use of iron, nickel, or cobalt as the catalyst. However, the catalytic-conversion efficiencies of these metals have been observed to be limited. The identification of better catalysts is part of a continuing program to develop means of mass production of high-quality carbon nanotubes at costs lower than those achieved thus far (as much as \$100/g for purified multi-wall CNTs or \$1,000/g for single-wall CNTs in year 2002).

The main effort thus far in this program has been the design and implementation of a process tailored specifically for high-throughput screening of

alloys for catalyzing the growth of CNTs. The process includes an integral combination of (1) formulation of libraries of catalysts, (2) synthesis of CNTs from decomposition of ethylene on powders of the alloys in a pyrolytic chemical-vapor-decomposition reactor, and (3) scanning-electron-microscope screening of the CNTs thus synthesized to evaluate the catalytic efficiencies of the alloys. Information gained in this process is put into a database and analyzed to identify promising alloy compositions, which are to be subjected to further evaluation in a subsequent round of testing.

The promising alloys identified thus far have been the following (compositions in atomic percentages): 90 Co, 10 Ti; 20 Co, 70 Ni, 5 Ti, 5 Ta; 90 Co, 10 Mo; 20 Co, 75 Ni, 5 Mo; 80 Co, 10 Ti, 10 Al; 70 Co, 15 Ni, 15 Ti; 80 Co, 10 Ni, 10 Ti; 70 Co, 5 Ta, 5 Mo, 20 Mn; 80 Ni, 10 Mo, 10

A; 80 Co, 12 Ni, 8 Al; and 80 Co, 20 Cr.

Some of these alloys have been found to catalyze the formation of carbon nanotubes from ethylene at temperatures as low as 350 to 400 $^\circ\text{C}$. In contrast, the temperatures typically required for prior catalysts range from 550 to 750 $^\circ\text{C}$.

This work was done by Ted X. Sun and Yi Dong of Intermetrix Corp. for Johnson Space Center. Further information is contained in a TSP (see page 1).

In accordance with Public Law 96-517, the contractor has elected to retain title to this invention. Inquiries concerning rights for its commercial use should be addressed to:

Intermetrix Corp.

351 Rheem Blvd.

Moraga, CA 94556

Refer to MSC-23477-1, volume and number of this NASA Tech Briefs issue, and the page number.

Amorphous Silk Fibroin Membranes for Separation of CO₂

Lyndon B. Johnson Space Center, Houston, Texas

Amorphous silk fibroin has shown promise as a polymeric material derivable from natural sources for making membranes for use in removing CO₂ from mixed-gas streams. For most applications of silk fibroin, for purposes other than gas separation, this material is used in its highly crystalline, nearly natural form because this form has uncommonly high tensile strength. However, the crystalline phase of silk fibroin is impermeable, making it necessary to convert the material to amorphous form to obtain the high permeability needed for gas separation.

Accordingly, one aspect of the present development is a process for generating amorphous silk fibroin by treating native silk fibroin in an aqueous methanol/salt solution. The resulting material remains self-standing and can be prepared as thin film suitable for permeation testing. The permeability of this material by pure CO₂ has been found to be highly improved, and its mixed-gas permeability has been found to exceed the mixed-gas permeabilities of several ultrahigh-CO₂-permeable synthetic polymers. Only one of the synthetic polymers — poly(trimethylsilyl-

propyne) [PTMSP] — may be more highly permeable by CO₂. PTMSP becomes unstable with time, whereas amorphous silk should not, although at the time of this reporting this has not been conclusively proven.

This work was done by Christopher M. Aberg, Anand K. Patel, Eun Seok Gil, and Richard J. Spontak of North Carolina State University and May-Britt Hagg of Norwegian University of Science and Technology for Johnson Space Center.

For further information, contact the JSC Innovation Partnerships Office at (281) 483-3809. MSC-24032-1



“Zero-Mass” Noninvasive Pressure Transducers

High-performance strain gauges are formed in sputtered thin films.

NASA's Jet Propulsion Laboratory, Pasadena, California

Extremely lightweight, compact, non-invasive, rugged, relatively inexpensive strain-gauge transducers have been developed for use in measuring pressures of fluids in tubes. These gauges were originally intended for measuring pressures of spacecraft-propulsion fluids, but they are also attractive for use in numerous terrestrial applications — especially those involving fluids that are extremely chemically reactive, fluids that must be isolated for hygienic purposes, fluids that must be allowed to flow without obstruction, and fluid-containing tubes exposed to severe environments.

A basic pressure transducer of this type comprises one or more pair(s) of thin-film strain gauges integral with a tube that contains the fluid of interest. Following established strain-gauge practice, the gauges in each pair are connected into opposite arms of a Wheatstone bridge (see figure). Typically, each pressure transducer includes one pair (the active pair) of strain gauges for measuring the hoop stress proportional to the pressure of the fluid in the tube and another pair (the dummy pair) of strain gauges that are nominally un-

strained: The dummy gauges are mounted on a substrate that is made of the same material as that of the tube. The substrate is welded to the tube at only one spot so that stresses and strains are not coupled from the tube into the substrate. The dummy strain gauges measure neutral strains (basically, strains associated with thermal expansion), so that the neutral-strain contribution can be subtracted out of the final gauge reading.

The active strain gauges are oriented to obtain an adequate response to hoop strain while minimizing the response to torsional and bending strains, which can be induced by mechanical coupling between the tube and other components of the fluid-handling system. The precise optimum orientation for this purpose depends on the Poisson's ratios of the materials used; a representative approximate optimum orientation is specified as an angle of 61.3° between the gauge axis and the tube axis.

The strain gauges are formed by sputter deposition of a dielectric film directly on the tube, followed by sputter deposition of a film of a suitable piezore-

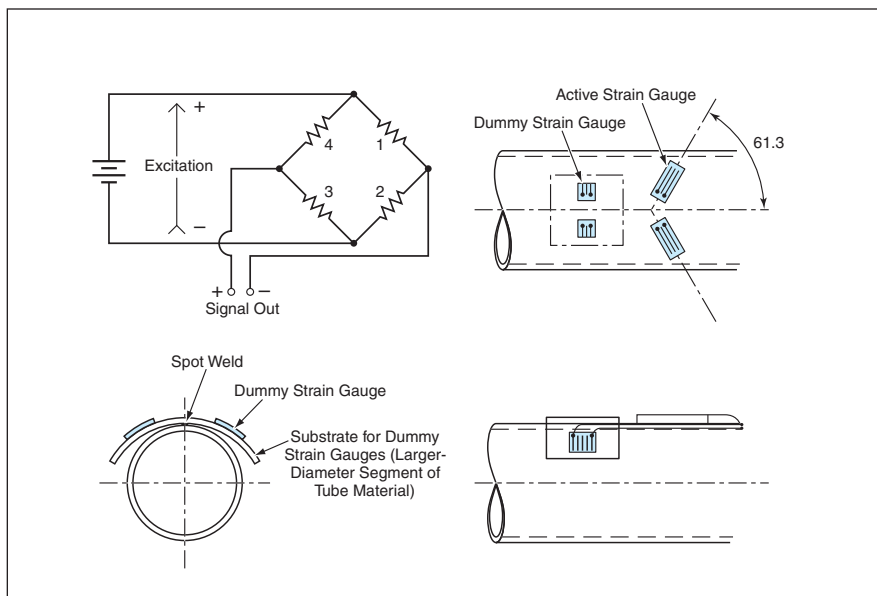
sistive material (typically, a nickel-chromium alloy), followed by laser cutting of strain-gauge grid lines into the piezoresistive film. These gauges have been characterized by the term “zero-mass,” which is not entirely an exaggeration: the sputtered layers are so thin that when one accounts for tube material removed by polishing in preparation for sputtering, one could find that the net mass of the tube plus pressure transducer is equal to or less than that of the plain tube.

The connections between the strain gauges and the external parts of the Wheatstone bridge are made with thin-film flexible electrical leads. A thin film of dielectric material can be sputtered over the strain gauges and bridge wiring to protect the gauge circuitry, to prevent outgassing, and/or to prevent chemical reactions between the strain gauges and the environment.

In addition to the advantages already mentioned, these pressure transducers offer several advantages over prior pressure transducers, including those based on strain gauges bonded to tubes by use of adhesives:

- The intimate coupling between strain gauges and tubes increases the magnitudes and speeds of gauge responses, simplifies accounting for thermal coefficients, reduces thermal-response times, and diminishes long-term drifts and zero shifts.
- A pressure transducer of this type is essentially part of the tube on which it is mounted, with little or no protuberances or additional mass, with high resilience in the face of shock and vibrational loads.
- The high dissociation temperatures of the dielectric and piezoresistive films enables operation at high temperatures, while the thin-film, intimate-coupling nature of the gauge structures extends the lower operating-temperature limit down to the cryogenic range.

This work was done by Frank T. Hartley of Caltech for NASA's Jet Propulsion Laboratory. Further information is contained in a TSP (see page 1). NPO-21194



The Active and Dummy Strain Gauges are used to measure hoop strain and neutral strain, respectively, in a tube that contains a pressurized fluid. The active gauges are oriented to minimize their response to bending and torsional strains.

Radial-Electric-Field Piezoelectric Diaphragm Pumps

Displacements are increased in a departure from traditional electrode configurations.

Langley Research Center, Hampton, Virginia

In a recently invented class of piezoelectric diaphragm pumps, the electrode patterns on the piezoelectric diaphragms are configured so that the electric fields in the diaphragms have symmetrical radial (along-the-surface) components in addition to through-the-thickness components. Previously, it was accepted in the piezoelectric-transducer art that in order to produce the out-of-plane bending displacement of a diaphragm needed for pumping, one must make the electric field asymmetrical through the thickness, typically by means of electrodes placed on only one side of the piezoelectric material. In the present invention, electrodes are placed on both sides and patterned so as to produce substantial radial as well as through-the-thickness components. Moreover, unlike in the prior art, the electric field can be symmetrical through the thickness. Tests have shown in a given diaphragm that an electrode configuration according to this invention produces more displacement than does a conventional one-sided electrode pattern.

The invention admits of numerous variations characterized by various degrees of complexity. Figure 1 is a simplified depiction of a basic version. As in other piezoelectric diaphragm pumps of similar basic design, the prime mover is a piezoelectric diaphragm. Application of a suitable voltage to the electrodes on the diaphragm causes it to undergo out-of-plane bending. The bending displacement pushes a fluid out of, or pulls the fluid into, a chamber bounded partly by the diaphragm. Also as in other diaphragm pumps in general, check valves ensure that the fluid flows only in through one port and only out through another port.

Figure 2 shows the diaphragm in more detail. In this case, the diaphragm is circular. The central region of the diaphragm contains the piezoelectric material. There are two centrally located, intercirculating spiral electrodes on the top side of the piezoelectric material and two mirror-image replicas of them on the bottom side. The polarities of the voltages applied to the electrodes are chosen to produce a nearly symmetrical, substantially radial electric field. The piezoelectric material and elec-

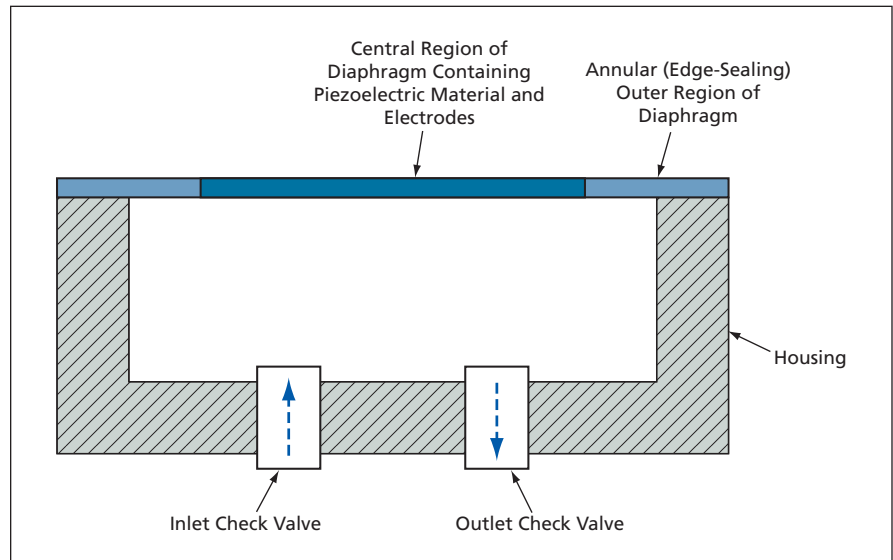


Figure 1. This Piezoelectric Diaphragm Pump is similar to other piezoelectric diaphragm pumps, except for the advanced design of the diaphragm.

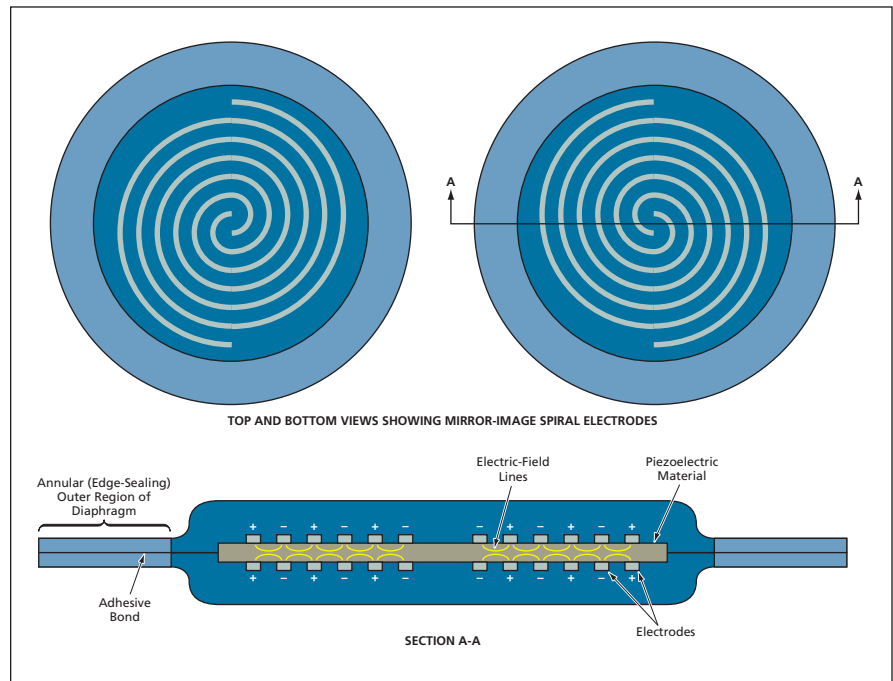


Figure 2. The Diaphragm features a central region containing a piezoelectric actuator and an annular outer region for sealing to the housing. The electrode pattern is chosen to ensure that the electric field has a substantial radial component.

trodes are adhesively bonded together and sandwiched between adhesive-coated sheets of a flexible dielectric material, which extends radially outward to form an outer annular region for sealing the diaphragm to the pump housing.

This work was done by Robert G. Bryant and Dennis C. Working of Langley Research Center and Karla Mossi, Nicholas D. Castro, and Poorna Mane of Virginia Commonwealth University. Further information is contained in a TSP (see page 1). LAR-16363-1

⚙️ Ejector-Enhanced, Pulsed, Pressure-Gain Combustor

Specific fuel consumption of a gas turbine engine could be reduced by a few percent.

John H. Glenn Research Center, Cleveland, Ohio

An experimental combination of an off-the-shelf valved pulsejet combustor and an aerodynamically optimized ejector has shown promise as a prototype of improved combustors for gas turbine engines. Despite their name, the “constant pressure” combustors heretofore used in gas turbine engines exhibit typical pressure losses ranging from 4 to 8 percent of the total pressures delivered by upstream compressors. In contrast, the present ejector-enhanced pulsejet combustor exhibits a pressure rise of about 3.5 percent at overall enthalpy and temperature ratios compatible with those of modern turbomachines. The modest pressure rise translates to a comparable increase in overall engine efficiency and, consequently, a comparable decrease in specific fuel consumption. The ejector-enhanced pulsejet combustor may also offer potential for reducing the emission of harmful exhaust compounds by making it practical to employ a low-loss rich-burn/quench/lean-burn sequence.

Like all prior concepts for pressure-gain combustion, the present concept involves an approximation of constant-volume combustion, which is inherently unsteady (in this case, more specifically, cyclic). The consequent

unsteadiness in combustor exit flow is generally regarded as detrimental to the performance of downstream turbomachinery. Among other adverse effects, this unsteadiness tends to detract from the thermodynamic benefits of pressure gain. Therefore, it is desirable in any intermittent combustion process to minimize unsteadiness in the exhaust path.

One of the easiest ways of approximating constant-volume combustion is to use a process similar to that used in commercially available pulsejets. Unfortunately, the pulsed combustion effluent is far too hot for any turbine and must, therefore, be mixed with some cooler bypass flow. The mixing process introduces losses that substantially degrade overall engine performance.

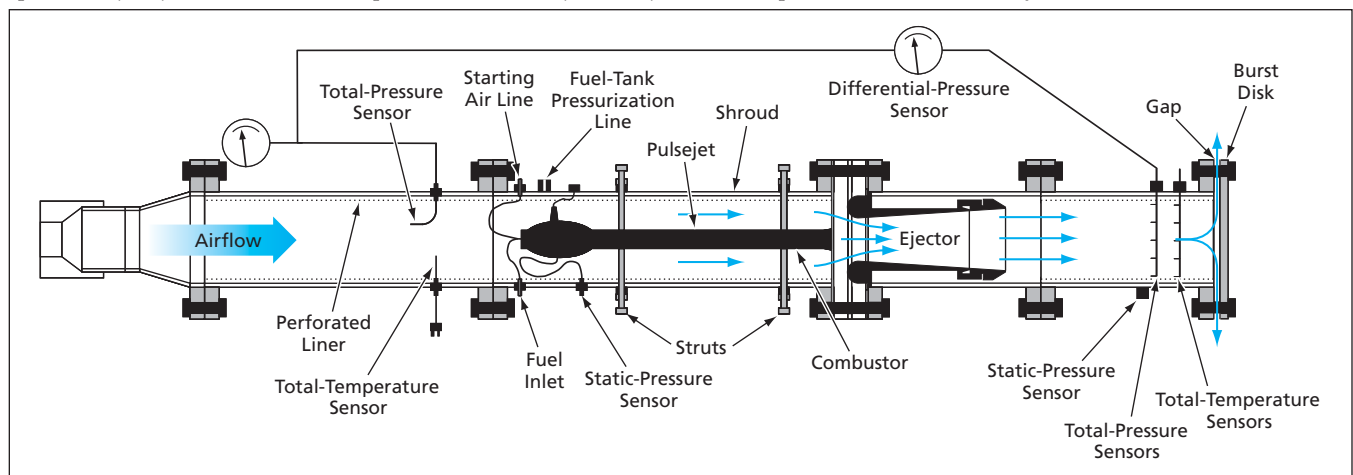
The present concept of the ejector-enhanced pulsejet combustor utilizes the demonstrated ability of properly designed, unsteady-flow ejectors (augmentors) to efficiently entrain, mix, and smooth secondary flows. The aerodynamically optimized ejector is placed aft of the pulsejet combustor. The pulsejet combustor and the ejector are encased in a shroud (see figure). The ejector is essentially an axisymmetric, tapered duct

with an aerodynamic inlet. The ejector entrains the cool secondary flow to produce an exhaust flow in a temperature range that can be tolerated by turbomachinery. Acting in combination with the shroud, the ejector also reduces spatial and temporal nonuniformities in the flow, thereby mitigating the detrimental effects of the pulsed combustion process. Finally, the relatively high momentum-transfer efficiency of the ejector ensures that taken as a whole, the ejector-enhanced pulsejet combustor yields a modest, time-averaged pressure rise.

In tests, the root-mean-square value of exit pressure fluctuations was found to be about 4.5 percent of the mean total pressure. This value is near the limit above which pressure fluctuations are considered to adversely affect the performance of downstream turbomachinery.

This work was done by Daniel E. Paxson of Glenn Research Center and Kevin T. Dougherty of QSS Group, Inc. Further information is contained in a TSP (see page 1).

Inquiries concerning rights for the commercial use of this invention should be addressed to NASA Glenn Research Center, Innovative Partnerships Office, Attn: Steve Fedor, Mail Stop 4-8, 21000 Brookpark Road, Cleveland, Ohio 44135. Refer to LEW-18096-1.



The Ejector-Enhanced Pulsejet Combustor mounted in a test rig is depicted here in cross section, approximately to scale.



Suppressing Ghost Diffraction in E-Beam-Written Gratings

The degree of periodicity of stitching errors is reduced.

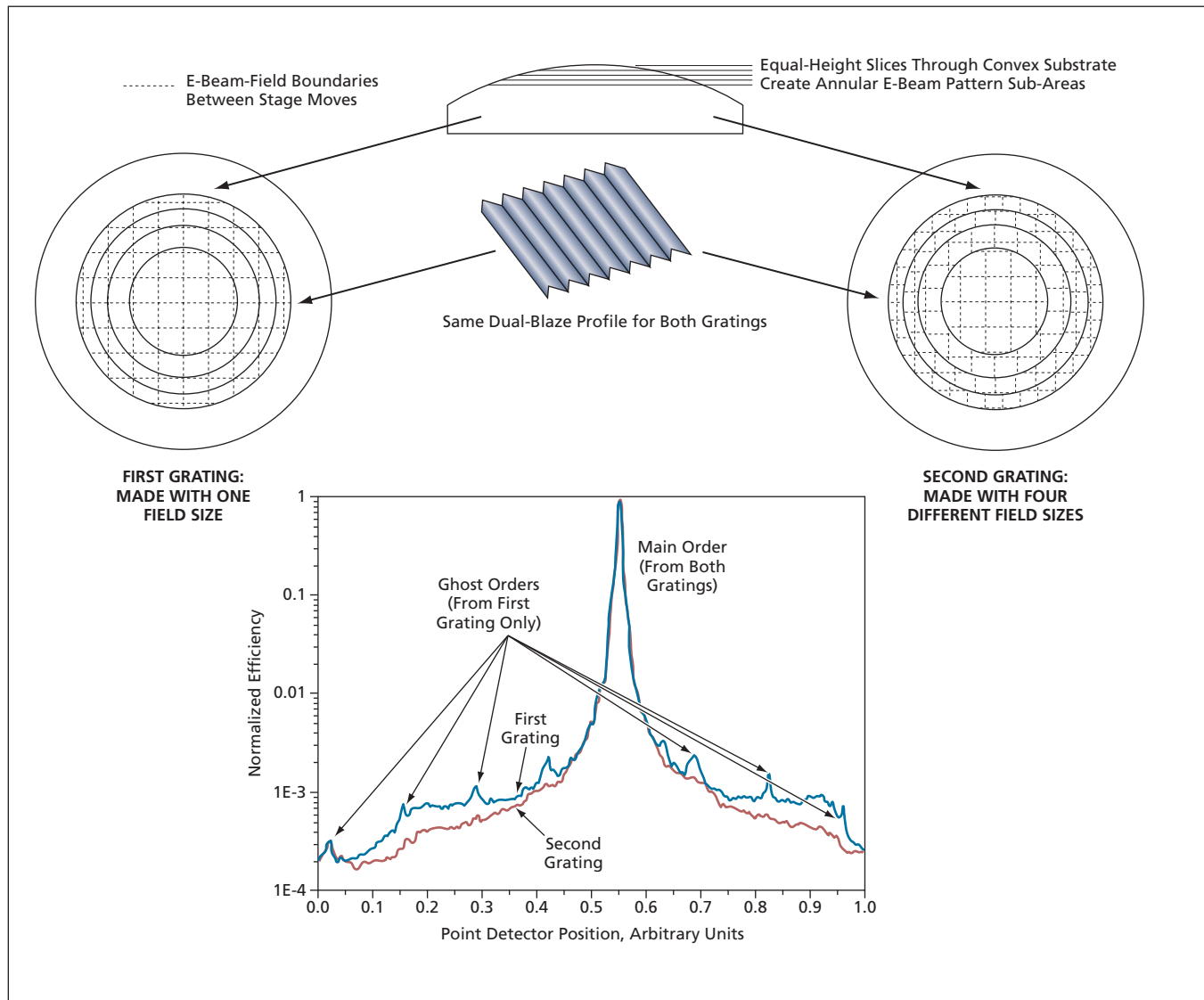
NASA's Jet Propulsion Laboratory, Pasadena, California

A modified scheme for electron-beam (E-beam) writing used in the fabrication of convex or concave diffraction gratings makes it possible to suppress the ghost diffraction heretofore exhibited by such gratings. Ghost diffraction is a spurious component of diffraction caused by a spurious component of grating periodicity as described below. The ghost diffraction orders appear between the main diffraction orders and are typi-

cally more intense than is the diffuse scattering from the grating. At such high intensity, ghost diffraction is the dominant source of degradation of grating performance.

The pattern of a convex or concave grating is established by electron-beam writing in a resist material coating a substrate that has the desired convex or concave shape. Unfortunately, as a result of the characteristics of electrostatic de-

flectors used to control the electron beam, it is possible to expose only a small field — typically between 0.5 and 1.0 mm wide — at a given fixed position of the electron gun relative to the substrate. To make a grating larger than the field size, it is necessary to move the substrate to make it possible to write fields centered at different positions, so that the larger area is synthesized by “stitching” the exposed fields.



The **Second of Two Convex Gratings** was divided into four annuli, within which the grating patterns were written with different field sizes. As a result, the second grating exhibited significantly less ghost diffraction.

Even though the mechanical stage used to position the substrate can be very accurate (positioning error of ≈ 20 nm or less), field-stitching errors occur, causing underexposures or overexposures that manifest themselves, after development of the resist, as increases or decreases in grating thickness along the field boundaries. Because all the fields are of the same size, the stitching errors form another grating that has a period equal to the field size. Hence, the light scattered from the field boundaries adds coherently: this is ghost diffraction.

The modified scheme for electron-beam writing is based on the concept of reducing the degree of periodicity of the stitching errors. In this scheme, the overall grating area is divided into sub-areas within which the grating patterns are written in differently sized fields. For a typical convex or concave grating, the

sub-areas are most easily defined as annular areas that correspond to equal-height slices through the substrate (see figure). Hence, the grating pattern in each annulus is written with a different field size.

The ghost order intensities are proportional to the square of the scattering amplitudes. Hence, if N different field sizes are used, the intensity of ghost diffraction can be expected to be reduced to approximately N^{-2} times the intensity obtained with a single field size.

To test this concept, two nominally identical gratings were fabricated. The pattern of the first grating was written by stitching together fields of the same size over its entire area, while the pattern of the second grating was established by use of four different field sizes. Whereas the ghost diffraction from the first grating was clearly noticeable, the

intensity of ghost diffraction from the second grating was so low as to be undetectable against the diffuse-scattering background.

This work was done by Daniel Wilson and Johan Backlund of Caltech for NASA's Jet Propulsion Laboratory. Further information is contained in a TSP (see page 1).

In accordance with Public Law 96-517, the contractor has elected to retain title to this invention. Inquiries concerning rights for its commercial use should be addressed to:

*Innovative Technology Assets Management
JPL*

*Mail Stop 202-233
4800 Oak Grove Drive
Pasadena, CA 91109-8099
(818) 354-2240*

E-mail: iaoffice@jpl.nasa.gov

Refer to NPO-41302, volume and number of this NASA Tech Briefs issue, and the page number.

Target-Tracking Camera for a Metrology System

Angular measurements are updated at a rate of hundreds of hertz.

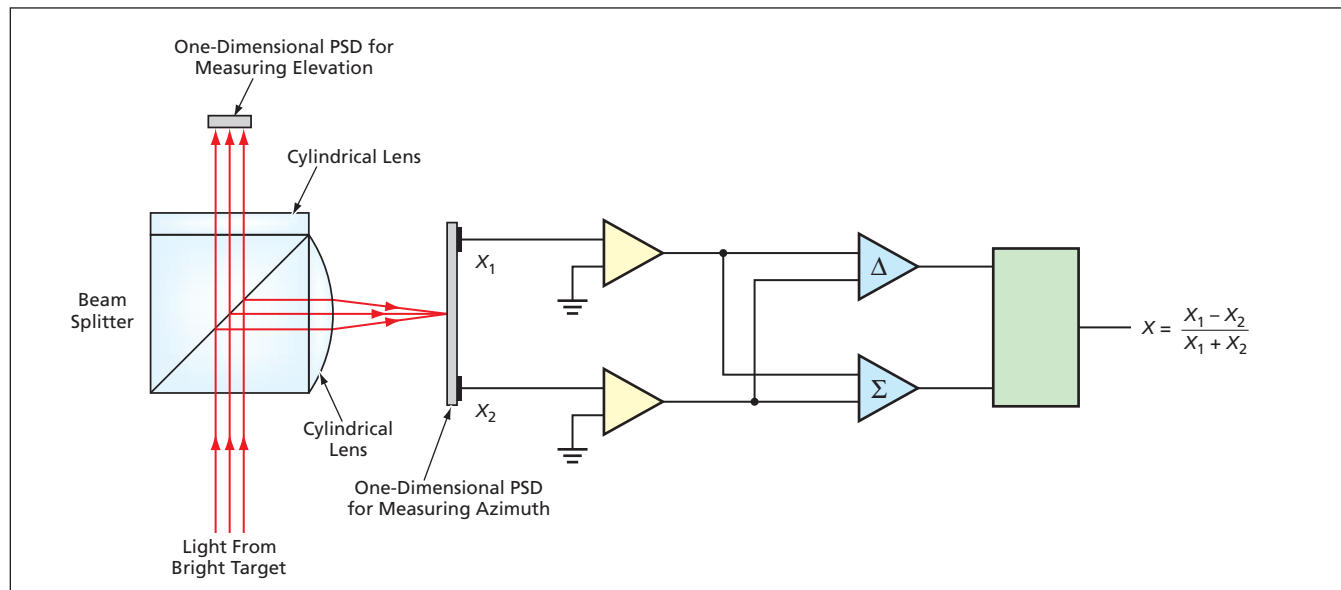
NASA's Jet Propulsion Laboratory, Pasadena, California

An analog electronic camera that is part of a metrology system measures the varying direction to a light-emitting diode that serves as a bright point target. In the original application for which the camera was developed, the metrological system is used to determine the varying relative positions of radiating elements of an airborne synthetic-aperture-radar (SAR) antenna as

the airplane flexes during flight; precise knowledge of the relative positions as a function of time is needed for processing SAR readings.

It has been common metrology system practice to measure the varying direction to a bright target by use of an electronic camera of the charge-coupled-device or active-pixel-sensor type. A major disadvantage of this practice arises from the

necessity of reading out and digitizing the outputs from a large number of pixels and processing the resulting digital values in a computer to determine the centroid of a target: Because of the time taken by the readout, digitization, and computation, the update rate is limited to tens of hertz. In contrast, the analog nature of the present camera makes it possible to achieve an update rate of



The **Optics and Electronic Circuitry** of the camera, shown here in simplified schematic form, provide two analog signals proportional to the horizontal and vertical angular displacements of the bright target.

hundreds of hertz, and no computer is needed to determine the centroid.

The camera is based on a position-sensitive detector (PSD), which is a rectangular photodiode with output contacts at opposite ends. PSDs are usually used in triangulation for measuring small distances. PSDs are manufactured in both one- and two-dimensional versions.

Because it is very difficult to calibrate two-dimensional PSDs accurately, the focal-plane sensors used in this camera

are two orthogonally mounted one-dimensional PSDs. The camera also includes a beam splitter and two cylindrical lenses to focus line images of the target onto the PSDs — more specifically, to form a horizontal line image on the vertically oriented PSD and a vertical line image on the horizontally oriented PSD. The outputs from both ends of each PSD are processed by analog circuitry (see figure) to obtain an analog signal proportional to the displacement

of the image centroid from the mid-length position along the PSD. The direction-measuring error of the readout has been found to be no more than $1/2,700$ of the angular width of the field of view.

This work was done by Carl Liebe, Randall Bartman, Jacob Chapsky, Alexander Abramovici, and David Brown of Caltech for NASA's Jet Propulsion Laboratory. Further information is contained in a TSP (see page 1). NPO-41466

Polarimetric Imaging Using Two Photoelastic Modulators

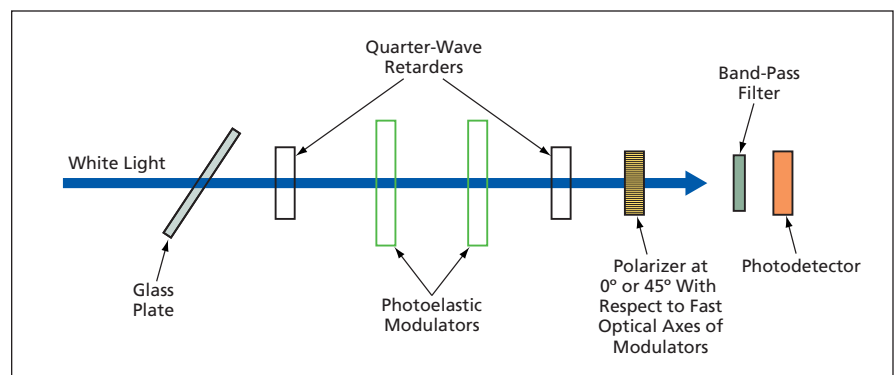
The frame rate is the difference between the resonance frequencies of the modulators.

NASA's Jet Propulsion Laboratory, Pasadena, California

A method of polarimetric imaging, now undergoing development, involves the use of two photoelastic modulators in series, driven at equal amplitude but at different frequencies. The net effect on a beam of light is to cause (1) the direction of its polarization to rotate at the average of two excitation frequencies and (2) the amplitude of its polarization to be modulated at the beat frequency (the difference between the two excitation frequencies). The resulting modulated optical light beam is made to pass through a polarizing filter and is detected at the beat frequency, which can be chosen to equal the frame rate of an electronic camera or the rate of sampling the outputs of photodetectors in an array.

The method was conceived to satisfy a need to perform highly accurate polarimetric imaging, without cross-talk between polarization channels, at frame rates of the order of tens of hertz. The use of electro-optical modulators is necessitated by a need to obtain accuracy greater than that attainable by use of static polarizing filters over separate fixed detectors. For imaging, photoelastic modulators are preferable to such other electro-optical modulators as Kerr cells and Pockels cells in that photoelastic modulators operate at lower voltages, have greater angular acceptances, and are easier to use. Prior to the conception of the present method, polarimetric imaging at frame rates of tens of hertz using photoelastic modulators was not possible because the resonance frequencies of photoelastic modulators usually lie in the range from about 20 to about 100 kHz.

It is conventional to characterize the polarimetric state of incident light in



Two Photoelastic Modulators driven at different frequencies were sandwiched between quarter-wave retarders, causing the polarization of the light to rotate at the average frequency at an amplitude that oscillated at the difference frequency.

terms of the Stokes vector (I, Q, U, V), where I represents the total intensity; Q represents the excess of intensity of light polarized at an angle designated as 0° over that of light polarized at a relative angle of 90° , U represents similarly the excess of intensity at 45° over that 135° , and V represents the excess of intensity of right circular polarization over left circular polarization. It has been shown theoretically that in the present method, there should be no cross-talk between the Q and U channels and that it should be possible to obtain the ratio U/I from two readings of a single photodetector taken when the polarizer is in two orientations that differ by 45° .

The figure schematically depicts a laboratory setup that was used to demonstrate the feasibility of the method. A collimated beam of white light was partially polarized by a glass plate at an oblique angle. The degree of polarization could be changed by rotating the glass plate. The light then passed through a circular-polarization subsys-

tem that included (1) two photoelastic modulators having their fast axes at an angle of 0° , sandwiched between (2) two quarter-wave retarders oriented at angles of 45° and 135° , respectively. The two photoelastic modulators had resonance frequencies of about 42 kHz, differing by a beat frequency of about 9 Hz. The modulated light was then made to pass through a 0° or 45° polarizer on the way to a photodetector. A band-pass filter having a nominal pass wavelength of 672 nm with 20-nm bandwidth was mounted between the polarizer and the photodetector. Results of several experiments at various degrees of linear polarization were found to agree substantially with theoretical predictions.

This work was done by Yu Wang, Thomas Cunningham, David Diner, Edgar Davis, Chao Sun, Bruce Hancock, Gary Gutt, Jason Zan, and Nasrat Raouf of Caltech for NASA's Jet Propulsion Laboratory. Further information is contained in a TSP (see page 1). NPO-43806

Miniature Wide-Angle Lens for Small-Pixel Electronic Camera

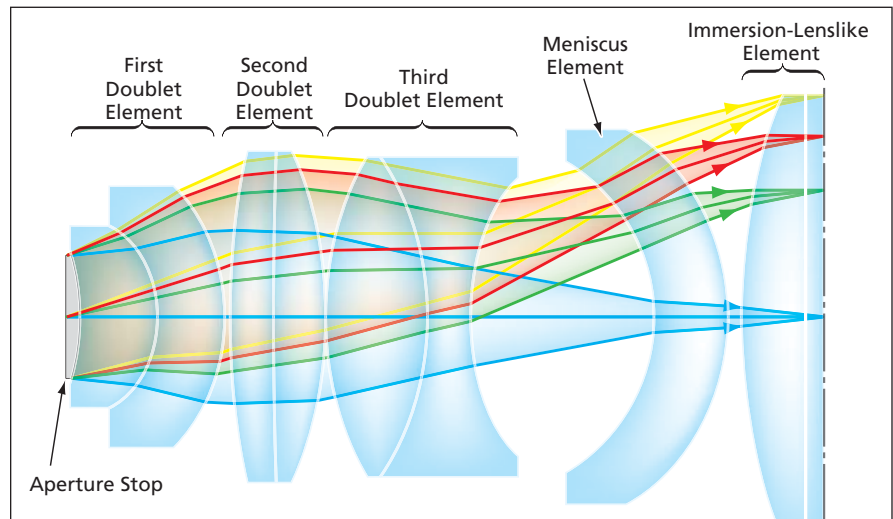
The lens design addresses issues peculiar to small-pixel image sensors.

NASA's Jet Propulsion Laboratory, Pasadena, California

The figure depicts a proposed wide-angle lens that would be especially well suited for an electronic camera in which the focal plane is occupied by an image sensor that has small pixels. The design of the lens is intended to satisfy requirements for compactness, high image quality, and reasonably low cost, while addressing issues peculiar to the operation of small-pixel image sensors. Hence, this design is expected to enable the development of a new generation of compact, high-performance electronic cameras. The lens example shown has a 60° field of view and a relative aperture (f -number) of 3.2.

The main issues affecting the design are the following:

- The response of a small-pixel image sensor is sensitive to the angle of incidence of the light. At large angles of incidence, the response includes excessive crosstalk among pixels.
- When a lens of typical prior design images a wide field, rays from the edge of the field are typically incident on the image sensor at large angles. This effect can be mitigated by use of a so-called image-space telecentric lens, for which the angle of incidence is constant. However, such a lens is typically much larger than is a comparable non-telecentric lens.
- In the original intended application, in which the lens would be used to focus light on a back-side-illuminated image sensor, there are requirements to minimize the size of the lens while making its optical behavior nearly telecentric, to obtain nearly diffraction-limited image quality while limiting distortion. The following are some key characteristics of the lens design:



This **Optical Layout** shows the main features of the lens design. The total length of the lens from aperture stop to the image plane is less than two times its focal length.

- The lens would include an element that would function like an immersion lens. The image sensor would be mounted in direct contact with this element. The incorporation of this element would enable maximization of the degree of telecentricity by bending rays from the edge of the field proportionately more than those from the middle, while otherwise exerting little effect on performance.
- A first doublet element, comprising two subelements made of glasses characterized by a large difference between their indices of refraction, would be placed immediately after an aperture stop. This doublet would control the field curvature and the color correction.
- A second doublet element made from two glasses that have similar, high indices of refraction but very different dispersion values. This element would

control the chromatic correction and provide most of the positive lens power necessary for imaging.

- An “air lens” between a third doublet element and a meniscus element would be used to balance the positive power while affording some correction for aberrations.
- The aperture stop would be located at the front of the lens.
- All of the lens elements and subelements are designed to have spherical surfaces and to be made of commonly used glasses. Hence, the lens could likely be produced at lower cost than would be possible if aspherical shapes or unusual glasses were required.

This work was done by Pantazis Mouroulis and Edward Blazejewski of Caltech for NASA's Jet Propulsion Laboratory. Further information is contained in a TSP (see page 1). NPO-44404

Modal Filters for Infrared Interferometry

NASA's Jet Propulsion Laboratory, Pasadena, California

vModal filters in the $\approx 10\text{-}\mu\text{m}$ spectral range have been implemented as planar dielectric waveguides in infrared interferometric applications such as searching for Earth-like planets. When looking for a small, dim object

(“Earth”) in close proximity to a large, bright object (“Sun”), the interferometric technique uses beams from two telescopes combined with a 180° phase shift in order to cancel the light from a brighter object. The interferometer

baseline can be adjusted so that, at the same time, the light from the dimmer object arrives at the combiner in phase. This light can be detected and its infrared (IR) optical spectra can be studied. The cancellation of light from the

“Sun” to $\approx 10^6$ is required; this is not possible without special devices — modal filters — that equalize the wavefronts arriving from the two telescopes.

Currently, modal filters in the $\approx 10\text{-}\mu\text{m}$ spectral range are implemented as single-mode fibers. Using semiconductor technology, single-mode waveguides for

use as modal filters were fabricated. Two designs were implemented: one using an InGaAs waveguide layer matched to an InP substrate, and one using InAlAs matched to an InP substrate. Photon Design software was used to design the waveguides, with the main feature all designs being single-mode operation in the

10.5- to 17- μm spectral range. Preliminary results show that the filter’s rejection ratio is 26 dB

This work was done by Alexander Ksendzov, Daniel R MacDonald, and Alexander Soibel of Caltech for NASA’s Jet Propulsion Laboratory. For more information, contact iaoffice@jpl.nasa.gov. NPO-44457

Mo₃Sb_{7-x}Te_x for Thermoelectric Power Generation

These materials could be segmented with lower-temperature thermoelectric materials.

NASA’s Jet Propulsion Laboratory, Pasadena, California

Compounds having compositions of Mo₃Sb_{7-x}Te_x (where $x = 1.5$ or 1.6) have been investigated as candidate thermoelectric materials. These compounds are members of a class of semiconductors that includes previously known thermoelectric materials. All of these compounds have complex crystalline and electronic structures. Through selection of chemical compositions and processing conditions, it may be possible to alter the structures to enhance or optimize thermoelectric properties.

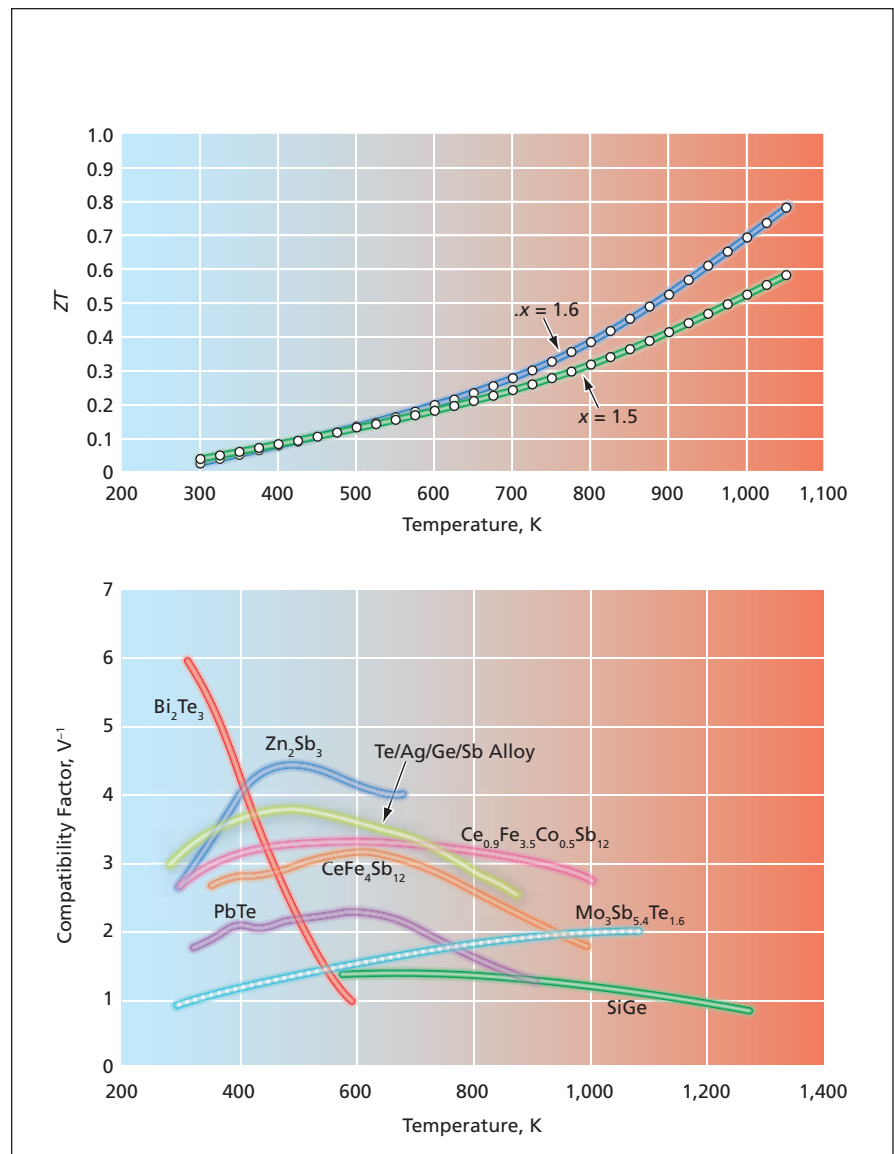
For the investigation, each specimen of Mo₃Sb_{7-x}Te_x was synthesized as follows:

1. A mixture of specified proportions of Mo, Sb, and Te powders was heated for 7 days at a temperature of 750 °C in a covered boron nitride crucible in an evacuated, sealed fused silica ampule.
2. The chemical reactions were quenched in cold water.
3. In an argon atmosphere, the crucible was opened and the reacted powder mixture was ground in an agate mortar.
4. The powder was annealed by again heating it as in step 1.
5. The powder was formed into a dense cylindrical specimen by uniaxial pressing in a high-density graphite die for 1 hour at a pressure of about 20 kpsi (≈ 138 MPa) and temperature of 873 °C in an argon atmosphere.

The traditional thermoelectric figure of merit, Z , is defined by the equation $Z = \alpha^2 / \rho \kappa$, where α is the Seebeck coefficient, ρ is the electrical resistivity, and κ is the thermal conductivity. Often, in current usage, the term “thermoelectric figure of merit” signifies the dimensionless product ZT , where T is the absolute temperature. The thermoelectric compatibility factor, s , is defined by the equation $s = [(1 + ZT)^{1/2} - 1] / \alpha T$. For maximum efficiency, s should not change with temper-

ature, both within a single material, and throughout a segmented thermoelectric-generator leg, the segments of which are made of different materials.

Values of ZT and s were calculated from measurements of the pertinent physical properties of Mo₃Sb_{7-x}Te_x specimens as functions at various tem-



Thermoelectric Figures of Merit and compatibility factors of Mo₃Sb_{7-x}Te_x and other compounds were determined as functions of temperature.

peratures, and the s values of $\text{Mo}_3\text{Sb}_{5.4}\text{Te}_{1.6}$ were compared with those of other state-of-the-art thermoelectric materials (see figure). The ZT values of both $\text{Mo}_3\text{Sb}_{5.5}\text{Te}_{1.5}$ and $\text{Mo}_3\text{Sb}_{5.4}\text{Te}_{1.6}$ were found to increase with temperature up to 1,050 K, which is just below the decomposition temperature. The fact that ZT for $x = 1.6$ exceeds that for $x = 1.5$ might be taken as a hint that one could increase ZT by increasing x , except for the observation

that attempts to synthesize $\text{Mo}_3\text{Sb}_{7-x}\text{Te}_x$ having $x > 1.6$ resulted in specimens that appeared to be multiphase. Hence, other approaches to doping may be more promising.

The s value of $\text{Mo}_3\text{Sb}_{5.4}\text{Te}_{1.6}$ was found to increase from about 1 V^{-1} at 300 K (room temperature) to about 2 V^{-1} at 1,000 K. This doubling of s indicates poor self-compatibility of $\text{Mo}_3\text{Sb}_{5.4}\text{Te}_{1.6}$ over the affected temperature range. However, $\text{Mo}_3\text{Sb}_{5.4}\text{Te}_{1.6}$

could be suitable for segmentation: for example, a $\text{Mo}_3\text{Sb}_{5.4}\text{Te}_{1.6}$ segment (which can withstand a temperature $> 800 \text{ K}$) could be joined to a lower-temperature PbTe segment at an interface temperature at or slightly below 800 K, where their s values are equal.

This work was done by G. Jeffrey Snyder, Frank S. Gascoin, and Julia Rasmussen of Caltech for NASA's Jet Propulsion Laboratory. For more information, contact iaoffice@jpl.nasa.gov. NPO-43862

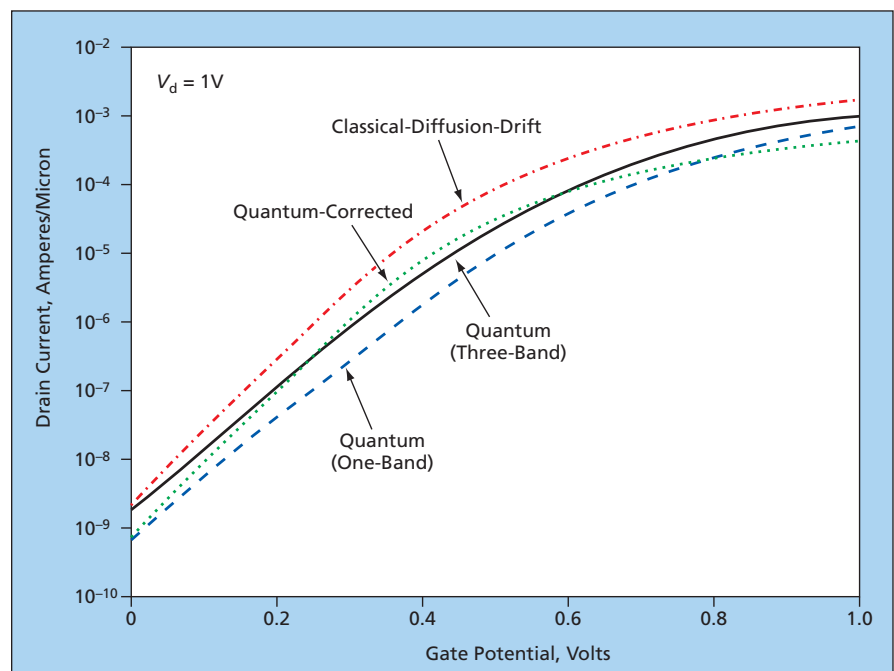
Two-Dimensional Quantum Model of a Nanotransistor

Quantum effects that become important at the nanoscale are taken into account.

Ames Research Center, Moffett Field, California

A mathematical model, and software to implement the model, have been devised to enable numerical simulation of the transport of electric charge in, and the resulting electrical performance characteristics of, a nanotransistor [in particular, a metal oxide/semiconductor field-effect transistor (MOSFET) having a channel length of the order of tens of nanometers] in which the overall device geometry, including the doping profiles and the injection of charge from the source, gate, and drain contacts, are approximated as being two-dimensional. The model and software constitute a computational framework for quantitatively exploring such device-physics issues as those of source-drain and gate leakage currents, drain-induced barrier lowering, and threshold voltage shift due to quantization. The model and software can also be used as means of studying the accuracy of quantum corrections to other semiclassical models.

The present model accounts for two quantum effects that become increasingly important as channel length decreases toward the nanometer range: quantization of the inversion layer and ballistic transport of electrons across the channel. Heretofore, some quantum effects in nanotransistors have been analyzed qualitatively by use of simple one-dimensional ballistic models, but two-dimensional models are necessary for obtaining quantitative results. Central to any quantum-mechanical approach to modeling of charge transport is the self-consistent solution of a wave equation to describe the quantum-mechanical aspect of the transport, Poisson's equation, and equations for statistics of the particle ensemble.



Drain Current Versus Gate Potential in a conceptual 25-nm-gate-length MOSFET commonly used as an example for testing MOSFET-simulating software was calculated by means of a three-band and a one-band version of the present quantum-based model. For comparison, the plot also shows results from a classical diffusion-drift model and a quantum-corrected model embodied in a commercial MOSFET-simulation computer program. A drain bias of 1 V and a gate oxide thickness of 1.5 nm were used in the simulations.

Non-equilibrium Green's function (NEGF) formalisms have been successful in modeling steady-state transport in a variety of one-dimensional semiconductor structures. The present model for the two-dimensional case includes the NEGF equations, which are solved self-consistently with Poisson's equation. At the time of this work, this was the most accurate full quantum model yet applied to simulation of two-dimensional semiconductor devices. Open boundary conditions (in which the nar-

row channel region opens into broad source, gate, and drain regions) and tunneling through oxide are treated on an equal footing. Interactions between electrons and phonons are taken into account, causing the modeled transport to deviate from ballistic in a realistic manner. Electrons in the wave-vector-space ellipsoids of the conduction band are treated within the anisotropic-effective-mass approximation.

Self-consistent solution of the Poisson and NEGF equations is computa-

tion-intensive because of the number of spatial and energy coordinates involved. Therefore, parallel distributed computing is imperative: the software that implements the model distributes the computations, energy-wise, to the

various processors. Initial simulations were performed using, variously, between 16 and 64 processors of an SGI Origin multiprocessor computer. The figure presents an example of results of one set of simulations.

This work was done by T. R. Govindan and B. Biegel of Ames Research Center and A. Svizhenko and M. P. Anantram of Computer Science Corp. Further information is contained in a TSP (see page 1). ARC-15471-1

Scanning Miniature Microscopes Without Lenses

Polarization-sensitive and multicolor versions should also be possible.

NASA's Jet Propulsion Laboratory, Pasadena, California

The figure schematically depicts some alternative designs of proposed compact, lightweight optoelectronic microscopes that would contain no lenses and would generate magnified video images of specimens. Microscopes of this type

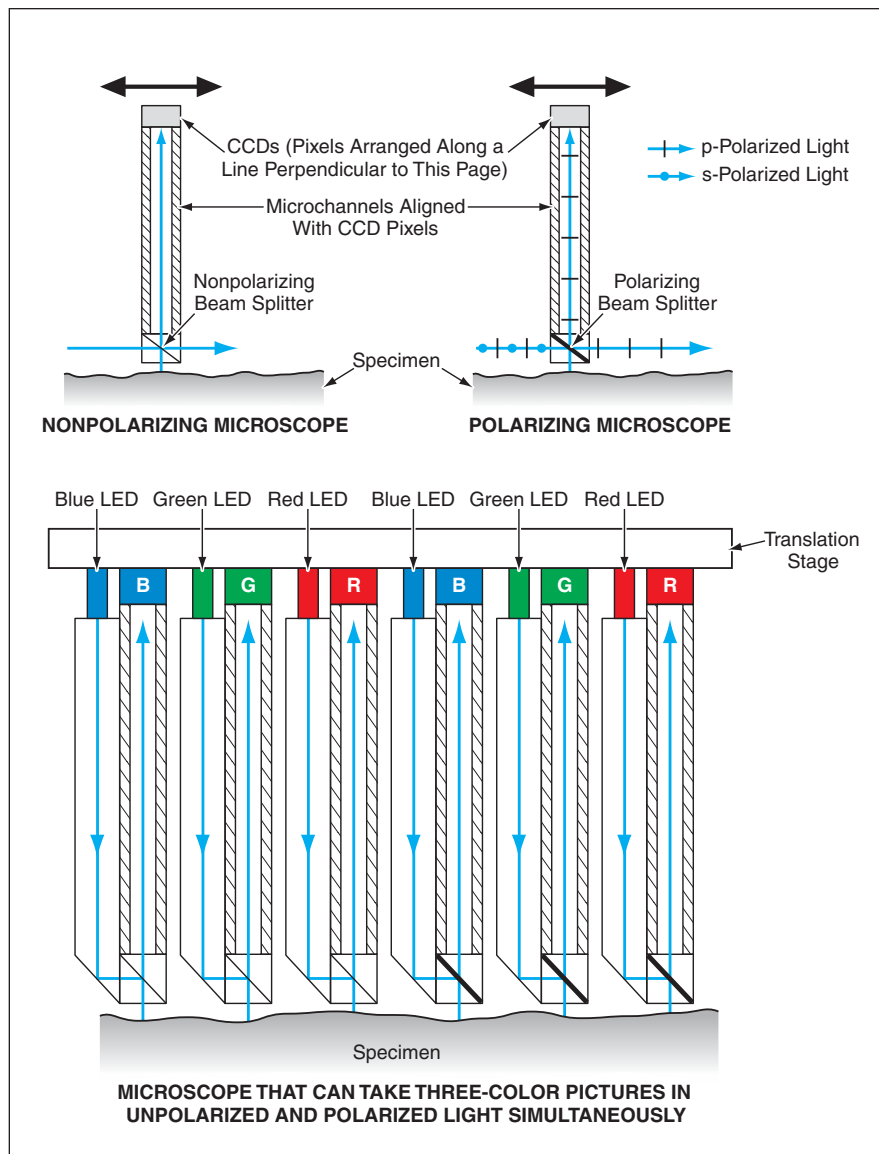
were described previously in "Miniature Microscope Without Lenses" (NPO-20218), *NASA Tech Briefs*, Vol. 22, No. 8 (August 1998), page 43 and "Reflective Variants of Miniature Microscope Without Lenses" (NPO20610), *NASA Tech*

Briefs, Vol. 26, No. 9 (September 1999), page 6a. To recapitulate: In the design and construction of a microscope of this type, the focusing optics of a conventional microscope are replaced by a combination of a microchannel filter and a charge-coupled-device (CCD) image detector. Elimination of focusing optics reduces the size and weight of the instrument and eliminates the need for the time-consuming focusing operation.

The microscopes described in the cited prior articles contained two-dimensional CCDs registered with two-dimensional arrays of microchannels and, as such, were designed to produce full two-dimensional images, without need for scanning. The microscopes of the present proposal would contain one-dimensional (line image) CCDs registered with linear arrays of microchannels. In the operation of such a microscope, one would scan a specimen along a line perpendicular to the array axis (in other words, one would scan in "pushbroom" fashion). One could then synthesize a full two-dimensional image of the specimen from the line-image data acquired at one-pixel increments of position along the scan.

In one of the proposed microscopes, a beam of unpolarized light for illuminating the specimen would enter from the side. This light would be reflected down onto the specimen by a nonpolarizing beam splitter attached to the microchannels at their lower ends. A portion of the light incident on the specimen would be reflected upward, through the beam splitter and along the microchannels, to form an image on the CCD.

If the nonpolarizing beam splitter were replaced by a polarizing one, then the specimen would be illuminated by s-polarized light. Upon reflection from the specimen, some of the s-polarized light would become p-polarized. Only the p-polarized light would contribute to the image on



Scanning Lensless Microscopes of various degrees of complexity and capability would be made from line-imaging CCDs, the pixels of which would be aligned with microchannels.

the CCD; in other words, the image would contain information on the polarization-rotating characteristic of the specimen.

The scanning microscopes described above could be used as building blocks for a multicolor, multipolarization microscope. In the example shown in the figure, six scanning microscopes would be

assembled on a single translation stage. The microchannels would be interspersed with light sources that would comprise light-emitting diodes (LEDs) coupled to the beam splitters via prismlike light guides.

This work was done by Yu Wang of Caltech for NASA's Jet Propulsion Laboratory.

Further information is contained in a TSP (see page 1).

This invention is owned by NASA, and a patent application has been filed. Inquiries concerning nonexclusive or exclusive license for its commercial development should be addressed to the Patent Counsel, NASA Management Office-JPL. Refer to NPO-20821.

Manipulating Neutral Atoms in Chip-Based Magnetic Traps

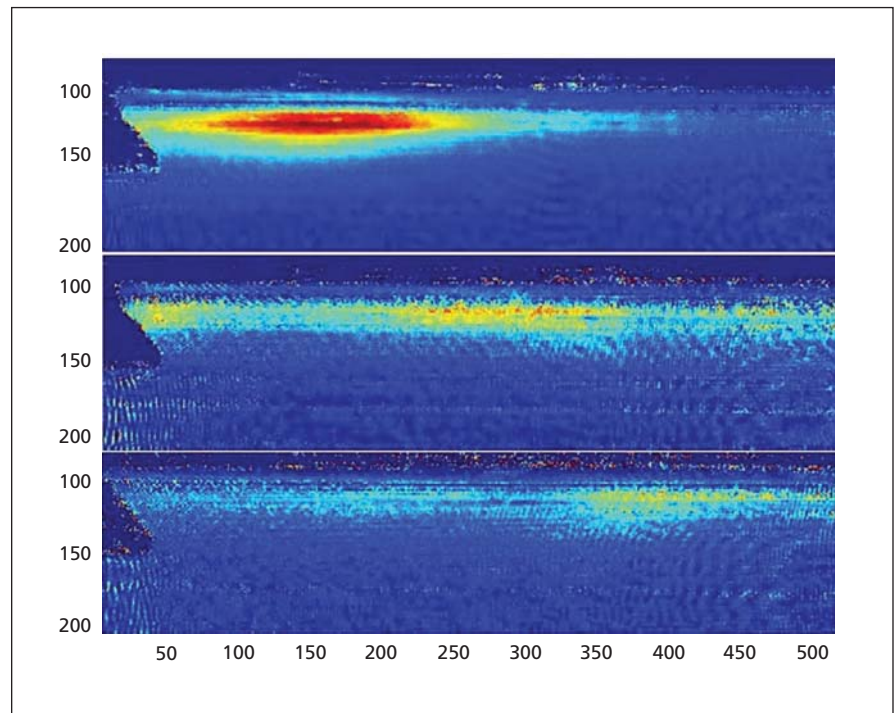
Magnetic-field gradients are used to accelerate and decelerate atoms.

NASA's Jet Propulsion Laboratory, Pasadena, California

Several techniques for manipulating neutral atoms (more precisely, ultracold clouds of neutral atoms) in chip-based magnetic traps and atomic waveguides have been demonstrated. Such traps and waveguides are promising components of future quantum sensors that would offer sensitivities much greater than those of conventional sensors. Potential applications include gyroscopy and basic research in physical phenomena that involve gravitational and/or electromagnetic fields. The developed techniques make it possible to control atoms with greater versatility and dexterity than were previously possible and, hence, can be expected to contribute to the value of chip-based magnetic traps and atomic waveguides.

The basic principle of these techniques is to control gradient magnetic fields with suitable timing so as to alter a trap to exert position-, velocity-, and/or time-dependent forces on atoms in the trap to obtain desired effects (see figure). The trap magnetic fields are generated by controlled electric currents flowing in both macroscopic off-chip electromagnet coils and microscopic wires on the surface of the chip.

The methods are best explained in terms of examples. Rather than simply allowing atoms to expand freely into an atomic waveguide, one can give them a controllable push by switching on an externally generated or a chip-based gradient magnetic field. This push can increase the speed of the atoms, typically from about 5 to about 20 cm/s. Applying a non-linear magnetic-field gradient exerts different forces on atoms in different positions — a phenomenon that one can exploit by introducing a delay between releasing atoms into the waveguide and turning on the magnetic field.



A Cold Cloud of ^{87}Rb Atoms is manipulated in an atomic waveguide by use of controlled gradient magnetic fields. This sequence of images shows the cloud moving rightward toward a potential barrier, then splitting into a part that passes through the barrier and a part reflected leftward from the barrier. The numbers on the axes are coordinates in units of $8\text{-}\mu\text{m}$ pixels.

Before the magnetic field is turned on, the fastest atoms move away from the region where the gradient will be the strongest, while the slower atoms lag behind, remaining in that region for a while. Hence, once the magnetic field is turned on, it can be expected to push the slower atoms harder than it will push the faster atoms. By controlling the amplitude and delay of the gradient, one can tailor the push so as to cause the slower atoms to catch up with the faster ones at a chosen location along the waveguide, thereby effectively focusing the atoms (in other words, greatly increasing the density of the cloud of atoms) at that location. Of course, in ad-

dition, the acceleration of the slower atoms effectively raises the temperature of the cloud of atoms. In a proposed variant of this accelerating-and-focusing technique, the gradient would be suitably repositioned along the waveguide and its amplitude and timing suitably altered, so as to preferentially decelerate the faster atoms, thereby effectively cooling the cloud of atoms.

This work was done by David Aveline, Robert Thompson, Nathan Lundblad, Lute Maleki, Nan Yu, and James Kohel of Caltech for NASA's Jet Propulsion Laboratory. Further information is contained in a TSP (see page 1). NPO-43015

Expansion Compression Contacts for Thermoelectric Legs

Ordinarily regarded as disadvantageous, thermal-expansion mismatch would be turned to advantage.

NASA's Jet Propulsion Laboratory, Pasadena, California

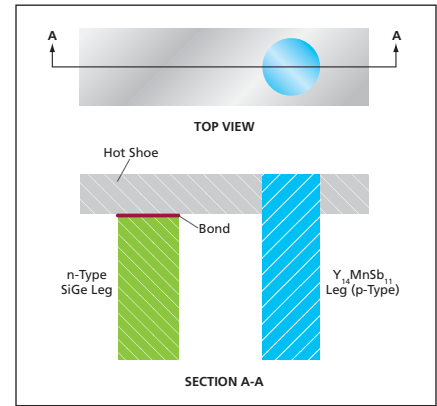
In a proposed alternative to previous approaches to making hot-shoe contacts to the legs of thermoelectric devices, one relies on differential thermal expansion to increase contact pressures for the purpose of reducing the electrical resistances of contacts as temperatures increase. The proposed approach is particularly applicable to thermoelectric devices containing p-type (positive-charge-carrier) legs made of a Zintl compound (specifically, $\text{Yb}_{14}\text{MnSb}_{11}$) and n-type (negative-charge-carrier) legs made of SiGe.

This combination of thermoelectric materials has been selected for further development, primarily on the basis of projected thermoelectric performance. However, it is problematic to integrate, into a practical thermoelectric device, legs made of these materials along with a metal or semiconductor hot shoe that is required to be in thermal and electrical contact with the legs. This is partly because of the thermal-expansion mismatch of these materials: The coefficient of thermal expansion (CTE) of SiGe is $4.5 \times 10^{-6} \text{ }^\circ\text{C}^{-1}$, while the CTE of $\text{Yb}_{14}\text{MnSb}_{11}$ is $20 \times 10^{-6} \text{ }^\circ\text{C}^{-1}$. Simply joining a $\text{Yb}_{14}\text{MnSb}_{11}$ and a SiGe leg to a common hot shoe could be expected to result in significant thermal stresses in either or both legs during operation.

Heretofore, such thermal stresses have been regarded as disadvantageous. In the proposed approach, stresses resulting from the CTE mismatch would be turned to advantage.

The figure depicts a thermoelectric unicouple according to the proposed approach. By use of established techniques, the n-type SiGe leg would be bonded to the hot shoe, which would be made of Si, Mo, or graphite. However, the $\text{Yb}_{14}\text{MnSb}_{11}$ leg would not be bonded to the hot shoe: instead, the $\text{Yb}_{14}\text{MnSb}_{11}$ leg would be inserted in a precisely fit hole in the hot shoe. The precision of the fit would be such that upon assembly at room temperature, the contact pressure between the hot shoe and the $\text{Yb}_{14}\text{MnSb}_{11}$ leg would be low. During heating up to a hot-shoe operating temperature of $1,000 \text{ }^\circ\text{C}$, the thermal expansion of the $\text{Yb}_{14}\text{MnSb}_{11}$ leg would exceed that of the hole by an amount that would increase the contact pressure to $>100 \text{ MPa}$. This pressure would suffice to keep the thermal and electrical contact resistances acceptably low.

Optionally, if the hot shoe were made of Si or Mo, the contact resistances could be made even lower by adding a thin, reactive layer of a metal at the in-



A Thermoelectric Unicouple as proposed would utilize thermal-expansion mismatch to obtain high contact pressure between the hot shoe and the $\text{Yb}_{14}\text{MnSb}_{11}$ leg.

terface between the $\text{Yb}_{14}\text{MnSb}_{11}$ leg and the hot shoe. Another option would be to taper the hole and the mating portion of the $\text{Yb}_{14}\text{MnSb}_{11}$ leg and to press-fit the leg and the hot shoe together at room temperature, thereby providing for maintenance of at least some pressure and prevention of separation during thermal cycling.

This work was done by Jeffrey Sakamoto of Caltech for NASA's Jet Propulsion Laboratory. Further information is contained in a TSP (see page 1). NPO-44896



Processing Electromyographic Signals To Recognize Words

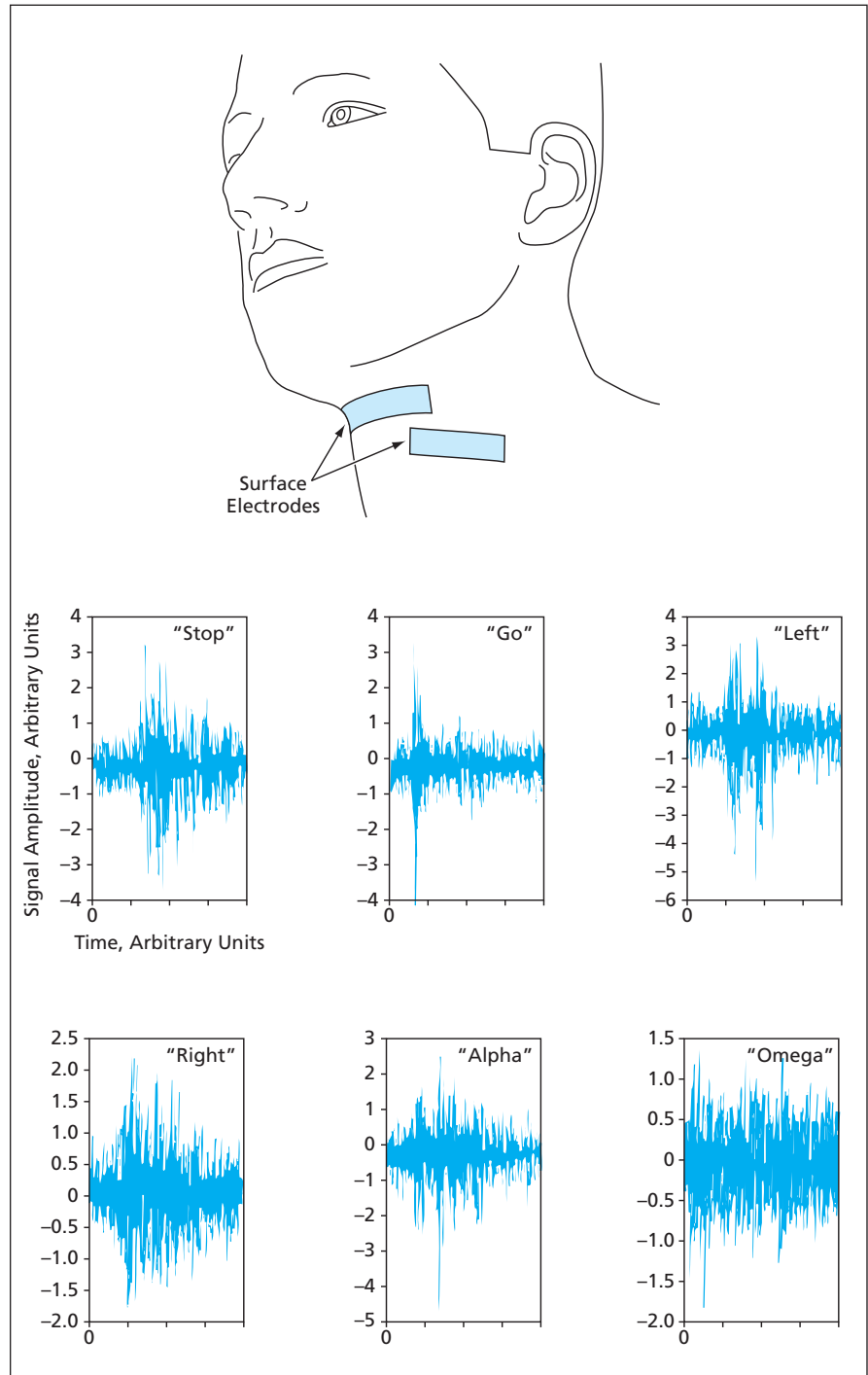
The speaker need not make any sound.

Ames Research Center, Moffett Field, California

A recently invented speech-recognition method applies to words that are articulated by means of the tongue and throat muscles but are otherwise not voiced or, at most, are spoken *sotto voce*. This method could satisfy a need for speech recognition under circumstances in which normal audible speech is difficult, poses a hazard, is disturbing to listeners, or compromises privacy. The method could also be used to augment traditional speech recognition by providing an additional source of information about articulator activity. The method can be characterized as intermediate between (1) conventional speech recognition through processing of voice sounds and (2) a method, not yet developed, of processing electroencephalographic signals to extract unspoken words directly from thoughts.

This method involves computational processing of digitized electromyographic (EMG) signals from muscle innervation acquired by surface electrodes under a subject's chin near the tongue and on the side of the subject's throat near the larynx (see figure). After preprocessing, digitization, and feature extraction, EMG signals are processed by a neural-network pattern classifier, implemented in software, that performs the bulk of the recognition task as described below.

Before processing signals representing words that one seeks to recognize, the neural network must be trained. During training, EMG signals representing known words and/or phrases are first sampled over specified time intervals (each typically about 2 seconds long). The portions of the signals recorded during each time interval are denoted sub-audible muscle patterns (SAMPs). Sequences of samples of SAMPs for overlapping time intervals are processed by a suitable signal-processing transform (SPT), which could be, for example, a Fourier, Hartley, or wavelet transform. The SPT outputs are entered into a matrix of coefficients, which is then decomposed into contiguous, non-overlapping two-dimensional cells of entries, each cell corresponding to a feature. Neural-network analysis is performed to esti-



Surface Electrodes Under and Near the Chin acquire signals indicative of tongue and throat muscle activity during articulation of words, even when the words are unvoiced. The signals are then processed to recognize the words. The six signal samples shown here correspond to the noted words.

mate reference sets of weight coefficients for weighted sums of the SAMP features that correspond to known words and/or phrases.

Once training has been done, a SAMP that includes an unknown word is sampled and processed by the SPT, the SPT outputs are used to construct a matrix, the matrix is decomposed into cells, and

neural-network analysis is performed, all in the same manner as that of training. The weight coefficients computed during training are used to determine whether there is a sufficiently close match between an unknown word in the SAMP and a known word in the training database. If such a match is found, the word is deemed to be recognized.

This work was done by C. C. Jorgensen and D. D. Lee of Ames Research Center. Further information is contained in a TSP (see page 1).

This invention is owned by NASA and a patent application has been filed. Inquiries concerning rights for the commercial use of this invention should be addressed to the Ames Technology Partnerships Division at (650) 604-2954. Refer to ARC-15040-1.

➤ Physical Principle for Generation of Randomness

NASA's Jet Propulsion Laboratory, Pasadena, California

A physical principle (more precisely, a principle that incorporates mathematical models used in physics) has been conceived as the basis of a method of generating randomness in Monte Carlo simulations. The principle eliminates the need for conventional random-number generators.

The Monte Carlo simulation method is among the most powerful computational methods for solving high-dimensional problems in physics, chemistry, economics, and information processing. The Monte Carlo simulation method is especially effective for solv-

ing problems in which computational complexity increases exponentially with dimensionality. The main advantage of the Monte Carlo simulation method over other methods is that the demand on computational resources becomes independent of dimensionality. As augmented by the present principle, the Monte Carlo simulation method becomes an even more powerful computational method that is especially useful for solving problems associated with dynamics of fluids, planning, scheduling, and combinatorial optimization.

The present principle is based on coupling of dynamical equations with the corresponding Liouville equation. The randomness is generated by non-Lipschitz instability of dynamics triggered and controlled by feedback from the Liouville equation. (In non-Lipschitz dynamics, the derivatives of solutions of the dynamical equations are not required to be bounded.)

This work was done by Michail Zak of Caltech for NASA's Jet Propulsion Laboratory. For further information, contact iaoffice@jpl.nasa.gov. NPO-43822

➤ DSN Beowulf Cluster-Based VLBI Correlator

Software architecture is scalable to meet faster processing needs for future data processing.

NASA's Jet Propulsion Laboratory, Pasadena, California

The NASA Deep Space Network (DSN) requires a broadband VLBI (very long baseline interferometry) correlator to process data routinely taken as part of the VLBI source Catalogue Maintenance and Enhancement task (CAT M&E) and the Time and Earth Motion Precision Observations task (TEMPO). The data provided by these measurements are a crucial ingredient in the formation of precision deep-space navigation models. In addition, a VLBI correlator is needed to provide support for other VLBI related activities for both internal and external customers.

The JPL VLBI Correlator (JVC) was designed, developed, and delivered to the DSN as a successor to the legacy Block II Correlator. The JVC is a full-capability VLBI correlator that uses software processes running on multiple computers to cross-correlate two-antenna broadband noise data. Components of this new system (see Figure 1)

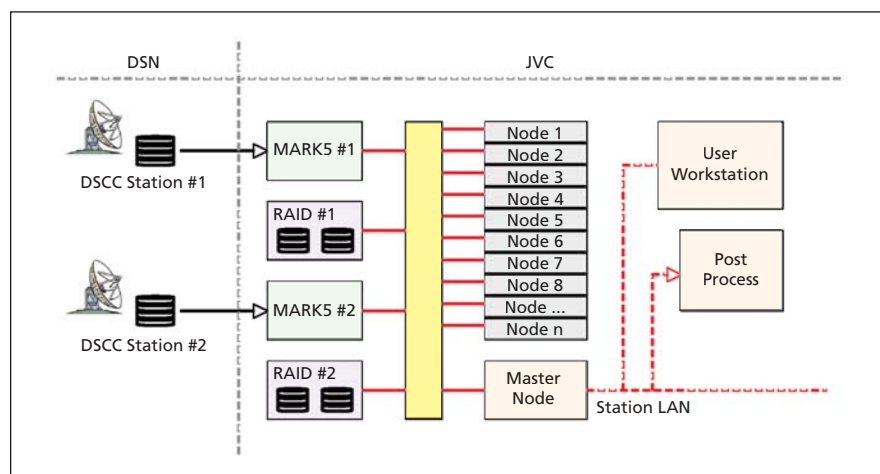


Figure 1. Components of the New Correlator are shown in this simplified block diagram.

consist of Linux PCs integrated into a Beowulf Cluster, an existing Mark5 data storage system, a RAID array, an existing software correlator package (SoftC) originally developed for Delta DOR

Navigation processing, and various custom-developed software processes and scripts.

Parallel processing on the JVC is achieved by assigning slave nodes of the

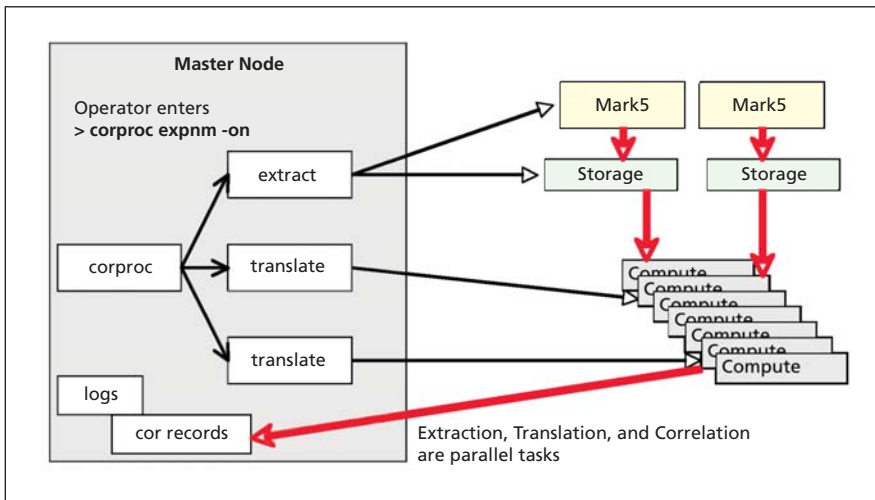


Figure 2. **Extraction, Translation, and Correlation** are run as parallel tasks.

Beowulf cluster to process separate scans in parallel until all scans have been processed. Due to the single-stream sequential playback of the Mark5 data, some ramp-up time is required before all nodes can have access to required scan data. Core functions of each processing step are accomplished using optimized C programs. The coordination and execution of these programs across the cluster is accomplished using Pearl scripts, PostgreSQL

commands, and a handful of miscellaneous system utilities.

Mark5 data modules are loaded on Mark5 Data systems playback units, one per station. Data processing is started when the operator scans the Mark5 systems and runs a script that reads various configuration files and then creates an experiment-dependent status database used to delegate parallel tasks between nodes and storage areas (see Figure 2). This script forks into three

processes: extract, translate, and correlate. Each of these processes iterates on available scan data and updates the status database as the work for each scan is completed.

The extract process coordinates and monitors the transfer of data from each of the Mark5s to the Beowulf RAID storage systems. The translate process monitors and executes the data conversion processes on available scan files, and writes the translated files to the slave nodes. The correlate process monitors the execution of SoftC correlation processes on the slave nodes for scans that have completed translation.

A comparison of the JVC and the legacy Block II correlator outputs reveals they are well within a formal error, and that the data are comparable with respect to their use in flight navigation. The processing speed of the JVC is improved over the Block II correlator by a factor of 4, largely due to the elimination of the reel-to-reel tape drives used in the Block II correlator.

This work was done by Stephen P. Rogstad, Andre P. Jongeling, Susan G. Finley, Leslie A. White, Gabor E. Lanyi, John E. Clark, and Charles E. Goodhart of Caltech for NASA's Jet Propulsion Laboratory. For more information, contact iaoffice@jpl.nasa.gov. NPO-46279

Hybrid NN/SVM Computational System for Optimizing Designs

The NN and the SVM help each other “learn” in an iterative process.

Ames Research Center, Moffett Field, California

A computational method and system based on a hybrid of an artificial neural network (NN) and a support vector machine (SVM) (see figure) has been conceived as a means of maximizing or minimizing an objective function, optionally subject to one or more constraints. Such maximization or minimization could be performed, for example, to optimize solve a data-regression or data-classification problem or to optimize a design associated with a response function. A response function can be considered as a subset of a response surface, which is a surface in a vector space of design and performance parameters. A typical example of a design problem that the method and system can be used to solve is that of an airfoil, for which a response function could be the spatial distribution of pressure over the airfoil. In this example, the response surface would describe the pressure distribu-

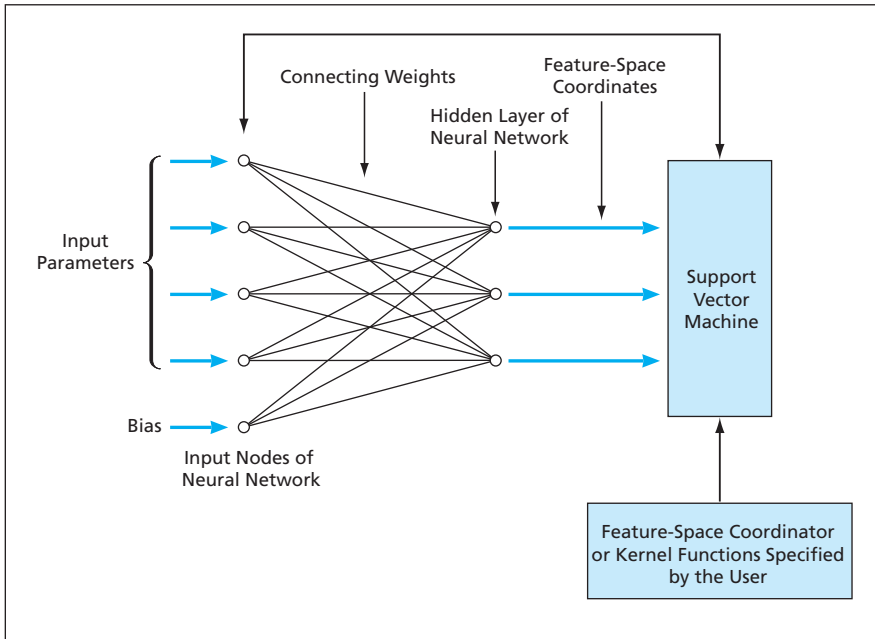
tion as a function of the operating conditions and the geometric parameters of the airfoil.

The use of NNs to analyze physical objects in order to optimize their responses under specified physical conditions is well known. NN analysis is suitable for multidimensional interpolation of data that lack structure and enables the representation and optimization of a succession of numerical solutions of increasing complexity or increasing fidelity to the real world. NN analysis is especially useful in helping to satisfy multiple design objectives. Feedforward NNs can be used to make estimates based on nonlinear mathematical models. One difficulty associated with use of a feedforward NN arises from the need for nonlinear optimization to determine connection weights among input, intermediate, and output variables. It can be very expensive to train an NN in

cases in which it is necessary to model large amounts of information.

Less widely known (in comparison with NNs) are support vector machines (SVMs), which were originally applied in statistical learning theory. In terms that are necessarily oversimplified to fit the scope of this article, an SVM can be characterized as an algorithm that (1) effects a nonlinear mapping of input vectors into a higher-dimensional feature space and (2) involves a dual formulation of governing equations and constraints. One advantageous feature of the SVM approach is that an objective function (which one seeks to minimize to obtain coefficients that define an SVM mathematical model) is convex, so that unlike in the cases of many NN models, any local minimum of an SVM model is also a global minimum.

In the SVM approach as practiced heretofore, underlying feature-space co-



A Hybrid NN/SVM System offers capabilities greater than those of an NN or a conventional SVM alone.

ordinates or functions must be specified. In the NN approach as practiced heretofore, resampling of data is needed to implement a process, known in the art as model hybridization, in which a superior neural network is generated from the synaptic-connection weight vectors of multiple neural networks that yield local minima with acceptably low errors. What is needed is a machine-learning algorithm that combines the desirable features of the NN and SVM approaches and does not require intimate *a priori* familiarity with operational details of the object to be optimized. Preferably, the algorithm should automatically provide a character-

ization of many or all of the aspects in feature space needed for the analysis.

A hybrid NN/SVM system (see figure) accepts inputs in the form of parameter values, which are regarded as independent coordinates in an input vector space. In the construction of the SVM, the input coordinates are mapped into a feature space of appropriately greater dimensionality, wherein the coordinates include computed combinations (e.g., powers and/or polynomials) of the input space coordinates. The NN is initially programmed with random synaptic-connection weights and used to construct inner

products for the SVM. The inner products are, in turn, used to compute Lagrange multipliers. A training error associated with the connection weights and Lagrange multipliers is calculated. If the training error is too large, one or more connection weights are changed and all of the foregoing (except the initial programming with random weights) steps are repeated. If the training error is not too large, the connection weights and the Lagrange multipliers are accepted as optimal.

An important advantage of this system over a conventional SVM is that the feature-space coordinates that must be specified *a priori* are determined by the NN subsystem. Moreover, the feature-space coordinates are generated by the NN subsystem to correspond to the data at hand; in other words, the feature space provided by the NN subsystem evolves to match or correspond to the data. A feature space that evolves in this manner is referred to as "data-adaptive." The feature-space coordinates generated by the NN subsystem can be easily augmented with additional feature-space coordinates (combinations of parameters) and kernel functions provided by the user.

This work was done by Man Mohan Rai of Ames Research Center. Further information is contained in a TSP (see page 1).

This invention has been patented by NASA (U.S. Patent No. 6,961,719). Inquiries concerning rights for the commercial use of this invention should be addressed to the Ames Technology Partnerships Division at (650) 604-2954. Refer to ARC-14586.



Books & Reports

Criteria for Modeling in LES of Multicomponent Fuel Flow

A report presents a study addressing the question of which large-eddy simulation (LES) equations are appropriate for modeling the flow of evaporating drops of a multicomponent liquid in a gas (e.g., a spray of kerosene or diesel fuel in air). The LES equations are obtained from the direct numerical simulation (DNS) equations in which the solution is computed at all flow length scales, by applying a spatial low-pass filter. Thus, in LES the small scales are removed and replaced by terms that cannot be computed from the LES solution and instead must be modeled to retain the effect of the small scales into the equations. The mathematical form of these models is a subject of contemporary research.

For a single-component liquid, there is only one LES formulation, but this study revealed that for a multicomponent liquid, there are two non-equivalent LES formulations for the conservation equations describing the composition of the vapor. Criteria were proposed for selecting the multicomponent LES formulation that gives the best accuracy and increased computational efficiency. These criteria were applied in examination of filtered DNS databases to compute the terms in the LES equations. The DNS databases are from mixing layers of diesel and kerosene fuels. The comparisons resulted in the selection of one of the multicomponent LES formulations as the most promising with respect to all criteria.

This work was done by Josette Bellan and Laurent Selle of Caltech for NASA's Jet Propulsion Laboratory. Further information is contained in a TSP (see page 1). NPO-45065

Computerized Machine for Cutting Space Shuttle Thermal Tiles

A report presents the concept of a machine aboard the space shuttle that would cut oversized thermal-tile blanks to precise sizes and shapes needed to replace tiles that were damaged or lost during ascent to orbit. The machine would include a computer-controlled jigsaw enclosed in a clear acrylic shell that would prevent escape of cutting debris. A vacuum motor would collect the debris into a reservoir

and would hold a tile blank securely in place. A database stored in the computer would contain the unique shape and dimensions of every tile.

Once a broken or missing tile was identified, its identification number would be entered into the computer, wherein the cutting pattern associated with that number would be retrieved from the database. A tile blank would be locked into a crib in the machine, the shell would be closed (proximity sensors would prevent activation of the machine while the shell was open), and a "cut" command would be sent from the computer. A blade would be moved around the crib like a plotter, cutting the tile to the required size and shape. Once the tile was cut, an astronaut would take a space walk for installation.

This work was done by Luis E. Ramirez and Lisa A. Reuter of The Boeing Co. for Johnson Space Center. For further information, contact the JSC Innovation Partnerships Office at (281) 483-3809. MSC-24140-1

Orbiting Depot and Reusable Lander for Lunar Transportation

A document describes a conceptual transportation system that would support exploratory visits by humans to locations dispersed across the surface of the Moon and provide transport of humans and cargo to sustain one or more permanent Lunar outpost. The system architecture reflects requirements to (1) minimize the amount of vehicle hardware that must be expended while maintaining high performance margins and (2) take advantage of emerging capabilities to produce propellants on the Moon while also enabling efficient operation using propellants transported from Earth.

The system would include reusable single-stage lander spacecraft and a depot in a low orbit around the Moon. Each lander would have descent, landing, and ascent capabilities. A crew-taxi version of the lander would carry a pressurized crew module; a cargo version could carry a variety of cargo containers. The depot would serve as a facility for storage and for refueling with propellants delivered from Earth or propellants produced on the Moon. The depot could receive propellants and cargo sent from Earth on a variety of spacecraft. The depot could provide power and orbit

maintenance for crew vehicles from Earth and could serve as a safe haven for lunar crews pending transport back to Earth.

This work was done by Andrew Petro of Johnson Space Center. Further information is contained in a TSP (see page 1). MSC-24231-1

FPGA-Based Networked Phasemeter for a Heterodyne Interferometer

A document discusses a component of a laser metrology system designed to measure displacements along the line of sight with precision on the order of a tenth the diameter of an atom. This component, the phasemeter, measures the relative phase of two electrical signals and transfers that information to a computer.

Because the metrology system measures the differences between two optical paths, the phasemeter has two inputs, called measure and reference. The reference signal is nominally a perfect square wave with a 50-percent duty cycle (though only rising edges are used). As the metrology system detects motion, the difference between the reference and measure signal phases is proportional to the displacement of the motion. The phasemeter, therefore, counts the elapsed time between rising edges in the two signals, and converts the time into an estimate of phase delay.

The hardware consists of a circuit board that plugs into a COTS (commercial, off-the-shelf) Spartan-III FPGA (field-programmable gate array) evaluation board. It has two BNC inputs, (reference and measure), a CMOS logic chip to buffer the inputs, and an Ethernet jack for transmitting reduced data to a PC. Two extra BNC connectors can be attached for future expandability, such as external synchronization. Each phasemeter handles one metrology channel. A bank of six phasemeters (and two zero-crossing detector cards) with an Ethernet switch can monitor the rigid body motion of an object.

This device is smaller and cheaper than existing zero-crossing phasemeters. Also, because it uses Ethernet for communication with a computer, instead of a VME bridge, it is much easier to use. The phasemeter is a key part of the Precision Deployable Apertures and Structures strategic R&D effort to design large, deployable, segmented space telescopes.

This work was done by Shanti Rao of Caltech for NASA's Jet Propulsion Laboratory. Further information is contained in a TSP (see page 1). NPO-45504

Aquarius Digital Processing Unit

Three documents provide information on a digital processing unit (DPU) for the planned Aquarius mission, in which a radiometer aboard a spacecraft orbiting Earth is to measure radiometric temperatures from which data on sea-surface salinity are to be deduced. The DPU is the interface between the radiometer

and an instrument-command-and-data system aboard the spacecraft. The DPU cycles the radiometer through a programmable sequence of states, collects and processes all radiometric data, and collects all housekeeping data pertaining to operation of the radiometer. The documents summarize the DPU design, with emphasis on innovative aspects that include mainly the following:

- In the radiometer and the DPU, conversion from analog voltages to digital data is effected by means of asynchronous voltage-to-frequency converters in combination with a frequency-measurement scheme implemented in field-programmable gate arrays (FPGAs).

- A scheme to compensate for aging and changes in the temperature of the DPU in order to provide an overall temperature-measurement accuracy within 0.01 K includes a high-precision, inexpensive DC temperature-measurement scheme and a drift-compensation scheme that was used on the Cassini radar system.
- An interface among multiple FPGAs in the DPU guarantees setup and hold times.

This work was done by Joshua Forgione, George Winkert, and Norman Dobson of Goddard Space Flight Center. Further information is contained in a TSP (see page 1). GSC-15413-1



Three-Dimensional Optical Coherence Tomography

Advantages over prior OCT systems include less bulk and greater speed.

John H. Glenn Research Center, Cleveland, Ohio

Three-dimensional (3D) optical coherence tomography (OCT) is an advanced method of noninvasive infrared imaging of tissues in depth. Heretofore, commercial OCT systems for 3D imaging have been designed principally for external

ophthalmological examination. As explained below, such systems have been based on a one-dimensional OCT principle, and in the operation of such a system, 3D imaging is accomplished partly by means of a combination of electronic

scanning along the optical (Z) axis and mechanical scanning along the two axes (X and Y) orthogonal to the optical axis.

In 3D OCT, 3D imaging involves a form of electronic scanning (without mechanical scanning) along all three axes. Consequently, the need for mechanical adjustment is minimal and the mechanism used to position the OCT probe can be correspondingly more compact. A 3D OCT system also includes a probe of improved design and utilizes advanced signal-processing techniques. Improvements in performance over prior OCT systems include finer resolution, greater speed, and greater depth of field.

Figure 1 includes a simplified schematic representation of the optical subsystem of a typical prior OCT system. In this system, near-infrared light from an incandescent lamp or other low-coherence source is sent through optical fibers and a fiber-optic coupler to a reference mirror. Some of the light is also sent through the fiber optics to a lens that, in turn, focuses the light to a point that lies at or near the depth of interest in a specimen. In the fiber-optic coupler, light reflected from the reference mirror is combined with light scattered from a focal point in the specimen and is then sent along another optical fiber to a photodetector. When the length of the optical path from the light source to the mirror equals or nearly equals the corresponding length to the focal point in the specimen, the photodetector puts out a

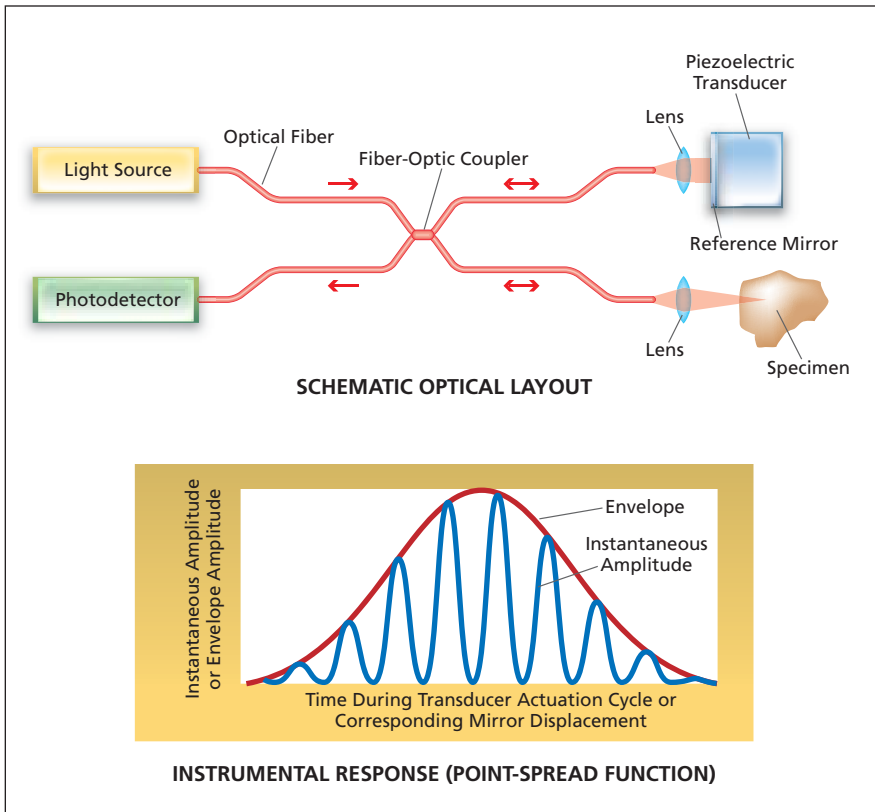


Figure 1. In a Typical Prior OCT System, scanning in Z involves piezoelectric actuation of the reference mirror, and scanning in X and Y is involves mechanical motion of the probe.

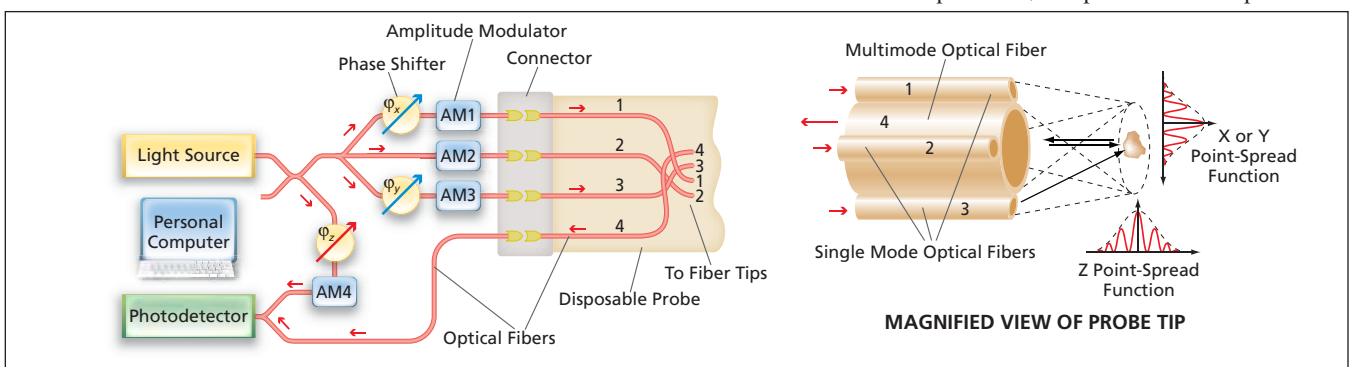


Figure 2. In a 3D OCT System, scanning in all three dimensions involves a combination of amplitude modulation, nonlinear detection, and advanced signal processing.

signal representing a pixel at the focal point in the specimen. Scanning along the depth (Z) axis is accomplished by using the piezoelectric transducer to move the reference mirror closer to, or farther from, the light source. Scanning along the X and Y axes is accomplished by mechanical motion of the probe along X and Y.

The lower part of Figure 1 depicts a typical instrumental response (point-spread function) in the photodetector output obtained in scanning along the Z axis. The response includes oscillations attributable to interference between the light scattered from a point in the specimen and light scattered from the mirror. As the Z displacement increases, the contrast of the interference pattern is reduced by the loss of coherence. Usually, the envelope of the oscillations (in contradistinction to the oscillations themselves) is what is measured. In such a case, the width of the envelope and, thus, the depth resolution, is comparable to the coherence length of the light source.

Figure 2 includes a simplified schematic representation of the optical subsystem of a 3D OCT system. This system is based partly on the same principles as those of the prior system. However, there are several important differences:

- Light from the source is fed through a more-complex fiber-optic subsystem, not only to a photodiode but to three single-mode optical fibers on a probe. Light emerging from the tips of these three fibers illuminates the specimen and creates a 3D interference pattern in the specimen.
- Light scattered from the specimen is collected and sent to the photodetector by a wider, multimode optical fiber. The probe containing the illuminating single-mode fibers and the light-collecting multimode optical fibers is significantly smaller and more rugged, relative to a lens-containing probe in a prior OCT system.
- Instead of utilizing lenses and a piezoelectric actuation of a reference mirror to effect scanning in Z and focusing in conjunction with mechanical

scanning in X and Y, the system utilizes a combination of (1) amplitude modulation of the light in the three illuminating optical fibers and of a portion of the source light sent directly to the photodetector, (2) nonlinear detection, and (3) an advanced signal-processing technique that, among other things, exploits the 3D nature of the interference pattern in order to obtain (4) a 3D point-spread function that affords localization in X, Y, and Z. In principle, because mechanical scanning is no longer necessary, it is possible to achieve scanning at a video frame rate.

This work was done by Mikhail Gutin, Xu-Ming Wang, and Olga Gutin of Applied Science Innovations, Inc. for Glenn Research Center. Further information is contained in a TSP (see page 1).

Inquiries concerning rights for the commercial use of this invention should be addressed to NASA Glenn Research Center, Innovative Partnerships Office, Attn: Steve Fedor, Mail Stop 4-8, 21000 Brookpark Road, Cleveland, Ohio 44135. Refer to LEW-18352-1.

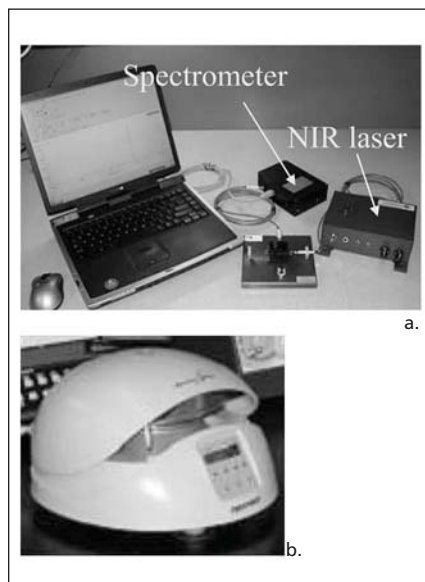
Benchtop Antigen Detection Technique Using Nanofiltration and Fluorescent Dyes

This technique can help to monitor the quality of water by testing for contamination at restaurants, water treatment plants, and food processing plants.

John H. Glenn Research Center, Cleveland, Ohio

The designed benchtop technique is primed to detect bacteria and viruses from antigenic surface marker proteins in solutions, initially water. This inclusive bio-immunoassay uniquely combines nanofiltration and near infrared (NIR) dyes conjugated to antibodies to isolate and distinguish microbial antigens, using laser excitation and spectrometric analysis. The project goals include detecting microorganisms aboard the International Space Station, space shuttle, Crew Exploration Vehicle (CEV), and human habitats on future Moon and Mars missions, ensuring astronaut safety. The technique is intended to improve and advance water contamination testing both commercially and environmentally as well. Lastly, this streamlined technique poses to greatly simplify and expedite testing of pathogens in complex matrices, such as blood, in hospital and laboratory clinics.

The approach relies on NIR fluorescent dyes derivatized to specific anti-



The Benchtop Analysis System (a) consists of a medium-power, class IV laser, a four-port cuvette sampler holder, a spectrometer, laptop and software, and fiber-optic cables. (b) The microcentrifuge used in nanofiltration of the complexes.

body sets that are selected to bind and differentiate microbial surface proteins, termed antigens. In a solution containing an antigenic slurry, NIR conjugated antibodies are added to the mixture, and will bind to the respective antigens if present. To eliminate any false positives, excess antibodies, i.e., those antibodies not bound to an antigenic protein or those with no respective antigen present, are removed via the nanofiltration process using a portable, table-top centrifuge. The remaining NIR dye/antibody and antigenic protein pairs left on the nanofilter are transferred to cuvette, excited by an NIR laser, and detected by spectrometer. Using simple computer software, the results are easily interpreted as intensity peaks at the appropriate NIR offset wavelength emission.

Initial data reveal the assay sensitively identified antigens at intensity counts of 100 IC or higher (or roughly 36 pW) with an accuracy of 85 percent for 2-

hour incubations and 75 percent for 3-hour incubations. Interestingly, samples incubated for less time (2 hours vs 3 hours) produced an increased percentage of antigen detection. Further testing at incubation times such as 1 hour or lower could potentially increase positive predictability based on

the study's results. Also encouraging were negative control experiments with nonspecific antigens, beta galactosidase and thyroglobulin, which showed results of 100 percent accuracy, with no false positive detection.

This work was done by Maximilian C. Scardelletti and Vanessa Varaljay of Glenn Re-

search Center. Further information is contained in a TSP (see page 1).

Inquiries concerning rights for the commercial use of this invention should be addressed to NASA Glenn Research Center, Innovative Partnerships Office, Attn: Steve Fedor, Mail Stop 4-8, 21000 Brookpark Road, Cleveland, Ohio 44135. Refer to LEW-18387-1.

Isolation of Precursor Cells From Waste Solid Fat Tissue

Lyndon B. Johnson Space Center, Houston, Texas

A process for isolating tissue-specific progenitor cells exploits solid fat tissue obtained as waste from such elective surgical procedures as abdominoplasties ("tummy tucks") and breast reductions. Until now, a painful and risky process of aspiration of bone marrow has been used to obtain a limited number of tissue-specific progenitor cells.

The present process yields more tissue-specific progenitor cells and involves

much less pain and risk for the patient. This process includes separation of fat from skin, mincing of the fat into small pieces, and forcing a fat saline mixture through a sieve. The mixture is then digested with collagenase type I in an incubator. After centrifugation tissue-specific progenitor cells are recovered and placed in a tissue-culture medium in flasks or Petri dishes. The tissue-specific progenitor cells can be used for such purposes as

(1) generating three-dimensional tissue equivalent models for studying bone loss and muscle atrophy (among other deficiencies) and, ultimately, (2) generating replacements for tissues lost by the fat donor because of injury or disease.

This work was done by Diane Byerly of Johnson Space Center and Marguerite A. Sognier of Universities Space Research Association. Further information is contained in a TSP (see page 1). MSC-23775-1

Identification of Bacteria and Determination of Biological Indicators

Identifying mechanisms of micro-organisms can prevent forward contamination in space missions and can help in developing new antibiotics and amino acids.

NASA's Jet Propulsion Laboratory, Pasadena, California

The ultimate goal of planetary protection research is to develop superior strategies for inactivating resistance-bearing micro-organisms like *Rummelibacillus stabekisii*. By first identifying the particular physiologic pathway and/or structural component of the cell/spore that affords it such elevated tolerance, eradication regimes can then be designed to target these resistance-conferring moieties without jeopardizing the structural integrity of spacecraft hardware. Furthermore, hospitals and government agencies frequently use biological indicators to ensure the efficacy of a wide range of sterilization processes. The spores of *Rummelibacillus stabekisii*, which are far more resistant to many of such perturbations, could likely serve as a more significant biological indicator for potential survival than those being used currently.

Numerous surveys of the contaminant microbial diversity housed within spacecraft assembly facilities over the past six years have resulted

in the recurrent isolation of spore-forming bacteria belonging to the *Bacillus* genus. As *Bacillus* species are capable of existing as metabolically inactive, extremely hardy spores, many lineages exhibit remarkable resilience to varying modes of bioreduction/sterilization aimed at their eradication (UV and gamma radiation, oxidizing disinfectants, etc.). The microorganism *Rummelibacillus stabekisii* *sp. nov.* was isolated from the surfaces of the cleanroom facility in which the Mars Exploration Rovers (MER) underwent assembly. This bacterium has not been previously reported, and shows no close relation to any previously described species (as is assessed via 16S rRNA gene sequence comparison). This unique isolate, and the *Bacillus* species most genetically similar to it, were subjected to a multitude of biochemical tests in order to thoroughly characterize its taxonomic position based on physiological and phylogenetic ev-

idence. The results clearly show that this bacterium is significantly different from its nearest relatives.

The microbial colonization of spacecraft and cleanroom assembly facility surfaces is of major concern to NASA and others commissioning modern-day space exploration. The search for life elsewhere in the solar system will rely heavily on validated cleaning and sterility methods. It would be devastating to the integrity of a mission directed at pristine environments such as the Europa's subsurface ocean or the Martian polar caps to be compromised as a result of terrestrial microbial contamination. To this end, planetary protection policies are in place to ensure the cleanliness and sterility of mission-critical spacecraft components in order to prevent forward or backward contamination.

Spores of *Bacillus subtilis*, a model spore-forming laboratory strain that demonstrates higher susceptibility to ultraviolet and gamma radiation than

other wild type spore formers, have nevertheless been shown to survive up to six years under interstellar space conditions. Previously undescribed spore-forming species, such as *Rumelibacillus stabekisii*, may exhibit even

greater resilience. It is in the best interests of NASA to thoroughly understand the physiological capabilities of each and every novel micro-organism isolated from these spacecraft-associated cleanrooms.

This work was done by Kasthuri Venkateswaran, Myron T. La Duc, and Parag A. Vaishampayan of Caltech for NASA's Jet Propulsion Laboratory. For more information, contact iaoffice@jpl.nasa.gov. NPO-46221.

Further Development of Scaffolds for Regeneration of Nerves

Scale-up toward clinically significant dimensions has been partially completed.

NASA's Jet Propulsion Laboratory, Pasadena, California

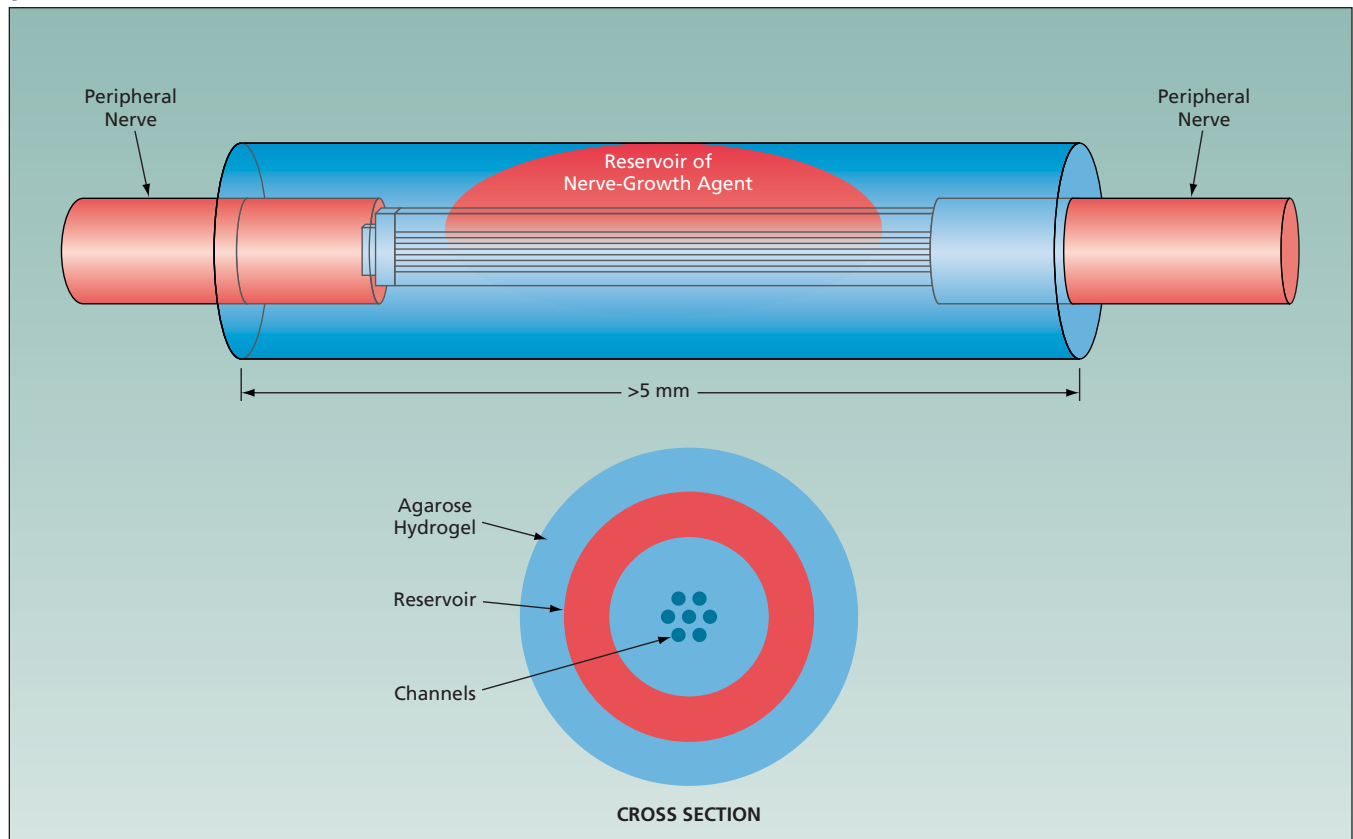
Progress has been made in continuing research on scaffolds for the guided growth of nerves to replace damaged ones. The scaffolds contain pores that are approximately cylindrical and parallel, with nearly uniform widths ranging from tens to hundreds of microns. At the earlier stage of development, experimental scaffolds had been made from agarose hydrogel. Such a scaffold was made in a multistep process in which poly(methyl methacrylate) [PMMA] fibers were used as templates for the pores. The process included placement of a bundle of the PMMA fibers in a tube, filling the interstices in the tube with a hot agarose solution, cooling to turn the solution into a gel, and then immersion in acetone to

dissolve the PMMA fibers. The scaffolds were typically limited to about 25 pores per scaffold, square cross sections of no more than about 1.5 by 1.5 mm, and lengths of no more than about 2 mm.

To be clinically relevant, the scaffolds must be scaled up: They are required to have typical cross-sectional dimensions of the order of 1 cm and to have lengths in the approximate range of 2 to 2.5 cm. For repairs of the central nervous system, there is an additional requirement that each scaffold contain between about 100 and about 1,000 pores; for repairs of peripheral nerves, there is a requirement for sustained or timed release of brain-derived neurotrophic factor (BDNF) or another suitable

nerve-growth agent to enable growth to continue to the required lengths.

The work performed since the earlier stage has been oriented toward satisfying these and other requirements. The work has included development of a more-complex version of the prior multistep process that has made it possible to partly satisfy the scaling-up requirements in that scaffolds having cross sections exceeding 1 cm² in area and lengths up to 1 cm have been fabricated. One notable feature of the present version of the process is a multistep subprocess in which a template of polystyrene (PS) fibers is made from a composite of polystyrene fibers surrounded by a continuous PMMA matrix. Another notable fea-



A Nerve-Growth Scaffold containing a reservoir of a nerve-growth agent would be attached to severed ends of a peripheral nerve.

ture of the present version of the process is the use of centrifugation to ensure complete permeation of the template by the hot agarose solution.

To satisfy the requirement for sustained or timed release of nerve-growth agents, it has been proposed to incorporate, into scaffolds, reservoirs containing such agents. In cases in which the agent is BDNF, the proposal encompasses an alternative approach in which the reservoirs would be filled with genetically engineered cells that secrete BDNF. The figure illustrates the proposal as it might be implemented in a scaffold that would

be attached to the severed ends of a peripheral nerve. Attached to the scaffold would be open-ended sleeves that would enable attachment to the severed nerve ends. The pores in the scaffold would serve as channels to guide the growth of the nerve ends toward each other. The reservoir containing the nerve-growth agent would be integrated into the outer wall of the scaffold. The nerve-growth agent would be delivered from the reservoir to the channels by diffusion through the agarose hydrogel matrix.

This work was done by Jeffrey Sakamoto of Caltech and Mark Tuszynski of UC

San Diego for NASA's Jet Propulsion Laboratory.

In accordance with Public Law 96-517, the contractor has elected to retain title to this invention. Inquiries concerning rights for its commercial use should be addressed to:

*Innovative Technology Assets Management
JPL*

Mail Stop 202-233

4800 Oak Grove Drive

Pasadena, CA 91109-8099

E-mail: iaoffice@jpl.nasa.gov

Refer to NPO-45303, volume and number of this NASA Tech Briefs issue, and the page number.

Chemically Assisted Photocatalytic Oxidation System

Lyndon B. Johnson Space Center, Houston, Texas

The chemically assisted photocatalytic oxidation system (CAPOS) has been proposed for destroying microorganisms and organic chemicals that may be suspended in the air or present on surfaces of an air-handling system that ventilates an indoor environment. The CAPOS would comprise an upstream and a downstream stage that would implement a tandem combination of two partly redundant treatments. In the upstream stage, the air stream and, optionally, surfaces of the air-handling system would be treated with ozone, which would be generated from oxygen in the air by means of an

electrical discharge or ultraviolet light. In the second stage, the air laden with ozone and oxidation products from the first stage would be made to flow in contact with a silica-titania photocatalyst exposed to ultraviolet light in the presence of water vapor. Hydroxyl radicals generated by the photocatalytic action would react with both carbon-containing chemicals and microorganisms to eventually produce water and carbon dioxide, and ozone from the first stage would be photocatalytically degraded to O₂. The net products of the two-stage treatment would be H₂O, CO₂, and O₂.

This work was done by Jean Andino, Chang-Yu Wu, David Mazyck, and Arthur A. Teixeira of the University of Florida for Johnson Space Center. Further information is contained in a TSP (see page 1).

In accordance with Public Law 96-517, the contractor has elected to retain title to this invention. Inquiries concerning rights for its commercial use should be addressed to:

University of Florida

Environmental Engineering

Weil Hall

Gainesville, FL 32611

Refer to MSC-23828-1, volume and number of this NASA Tech Briefs issue, and the page number.

Use of Atomic Oxygen for Increased Water Contact Angles of Various Polymers for Biomedical Applications

Improved polymer hydrophilicity is beneficial for cell culturing and implant growth.

John H. Glenn Research Center, Cleveland, Ohio

The purpose of this study was to determine the effect of atomic oxygen (AO) exposure on the hydrophilicity of nine different polymers for biomedical applications. Atomic oxygen treatment can alter the chemistry and morphology of polymer surfaces, which may increase the adhesion and spreading of cells on Petri dishes and enhance implant growth. Therefore, nine different polymers were exposed to atomic oxygen and water-contact angle, or hydrophilicity, was measured after exposure. To determine whether hydrophilicity remains static after initial atomic oxygen exposure, or changes with higher fluence ex-

posures, the contact angles between the polymer and water droplet placed on the polymer's surface were measured versus AO fluence. The polymers were exposed to atomic oxygen in a 100-W, 13.56-MHz radio frequency (RF) plasma asher, and the treatment was found to significantly alter the hydrophilicity of non-fluorinated polymers.

Pristine samples were compared with samples that had been exposed to AO at various fluence levels. Minimum and maximum fluences for the ashing trials were set based on the effective AO erosion of a Kapton witness coupon in the asher. The time intervals for ashing

were determined by finding the logarithmic values of the minimum and maximum fluences. The difference of these two values was divided by the desired number of intervals (ideally 10). The initial desired fluence was then multiplied by this result (2.37), as was each subsequent desired fluence. The flux in the asher was determined to be approximately 3.0×10^{15} atoms/cm² sec, and each polymer was exposed to a maximum fluence of 5.16×10^{20} atoms/cm².

It was determined that after the shortest atomic oxygen exposure (fluence of 2.07×10^{18} atoms/cm²), non-

Abbreviation	Polymer Name	Trade Name	Thickness
PE	Polyethylene	Alathon; Lupolen	2 mil
PET	Polyethylene terephthalate	Mylar A	2 mil
POM	Polyoxymethylene	Delrin; Celcon	4 mil
PS	Polystyrene	Lustrex; Polystyrol	2 mil
PP	Polypropylene	Profax; Propathene	20 mil
PMMA	Polymethylmethacrylate	Plexiglas; Lucite	2 mil
FEP	Fluorinated ethylene propylene	Teflon FEP	2 mil
PTFE	Polytetrafluoroethylene	Fluon; Teflon	2 mil
PCTFE	Polychlorotrifluoroethylene	Neoflon CTFE M-300	5 mil

Polymers Tested for atomic oxygen-altered hydrophilicity.

fluorinated polymer samples became significantly more hydrophilic than their pristine counterparts. This may be due to either surface texture changes or oxidation functionality surface changes. Despite long-term exposure (fluence of 5.16×10^{20} atoms/cm²), the water contact angles

remained relatively unchanged after the initial exposure. This implies that increasing the atomic oxygen fluence after an initial short exposure did not further affect the hydrophilicity of the polymers. Rather, polymers were affected by a very short exposure ($<1 \times 10^{19}$ atoms/cm²). This indicates that

oxidation functionality is more likely the contributor to increased hydrophilicity than texture, as texture continues to develop with fluence. The water contact angles of fluorinated polymers were found to change significantly less than non-fluorinated polymers for equivalent atomic oxygen exposures, and two of the fluorinated polymers became more hydrophobic.

Significant decreases in the post-exposure water contact angle were measured for non-fluorinated polymers. The majority of change in water contact angle was found to occur with very low fluence exposures, indicating potential cell culturing and other biomedical benefits with very short treatment time.

This work was done by Kim de Groh of Glenn Research Center; Lauren Berger and Lily Roberts of Hathaway Brown School; and Bruce Further information is contained in a TSP (see page 1). Inquiries concerning rights for the commercial use of this invention should be addressed to NASA Glenn Research Center, Innovative Partnerships Office, Attn: Steve Fedor, Mail Stop 4-8, 21000 Brookpark Road, Cleveland, Ohio 44135. Refer to LEW-18386-1.

Crashworthy Seats Would Afford Superior Protection

Adjustments enable optimization of support for different body sizes and shapes.

Lyndon B. Johnson Space Center, Houston, Texas

Seats to prevent or limit crash injuries to astronauts aboard the crew vehicle of the Orion spacecraft are undergoing development. The design of these seats incorporates and goes beyond crash-protection concepts embodied in prior spacecraft and racing-car seats to afford superior protection against impacts. Although the seats are designed to support astronauts in a recumbent, quasi-fetal posture that would likely not be suitable for non-spacecraft applications, parts of the design could be adapted to military and some civilian aircraft seats and to racing-car seats to increase levels of protection.

The main problem in designing any crashworthy seat is to provide full support of the occupant against anticipated crash and emergency-landing loads so as to safely limit motion, along any axis, of any part of the occupant's body relative to (1) any other part of the occupant's body, (2) the spacecraft or other vehicle,

and (3) the seat itself. In the original Orion spacecraft application and in other applications that could easily be envisioned, the problem is complicated by severe limits on space available for the seat, a requirement to enable rapid egress by the occupant after a crash, and a requirement to provide for fitting of the seat to a wide range of sizes and shapes of a human body covered by a crash suit, space suit, or other protective garment. The problem is further complicated by other Orion-application-specific requirements that must be omitted here for the sake of brevity.

To accommodate the wide range of crewmember body lengths within the limits on available space in the original Orion application, the design provides for taller crewmembers to pull their legs back closer toward their chests, while shorter crewmembers can allow their legs to stretch out further. The range of

hip-support seat adjustments needed to effect this accommodation, as derived from NASA's Human Systems Integration Standard, was found to define a parabolic path along which the knees must be positioned. For a given occupant, the specific position along the path depends on the distance from the heel to the back of the knee.

The application of the concept of parabolic adjustment of the hip-support structure caused the seat pan to also take on a parabolic shape, yielding the unanticipated additional benefit that the seat pan fits the occupant's buttocks and thighs more nearly conformally than do seat pans of prior design. This more nearly conformal fit effectively eliminates a void between the occupant's body and the seat pan, thereby helping to prevent what, in prior seat designs, was shifting of the occupant's body into that void during an impact.

The seat includes a thigh-support structure and a lower-leg support structure that can be adjusted for various heel-to-back-of-knee lengths. The occupant's heels are supported by a heel support pan and could be affixed to the pan by clips similar to those of mountain biking shoes and pedals or by straps over the tops of the feet. At the pivot between the thigh and lower-leg support structures there is a flat panel that provides for strength in adjustment and provides lateral support of the knees. The combination of lateral support of the knees and support and restraint of the feet is intended to prevent flailing or other movement of the legs while the occupant is seated.

The seat includes lateral supports at the hips that serve the dual purpose of

restraining the occupant from shifting laterally and providing structural support to the rest of the seat by acting as a gusset. To accommodate all hip sizes, the seat pan is designed to fit the largest hip breadth allowable. For a smaller occupant, spacer pads can be installed to fill the voids. Shoulder supports, which cover the shoulder joints and extend short distances down the arms, are also sized for occupants having shoulders of maximum breadth and to be fitted to smaller occupants by use of spacer pads. The seat supports bony protrusions of the torso at the shoulders and hips only, leaving the mid-torso area free of supports to enable the occupant to leave the seat by rolling through the clear space.

The seat includes a head support. However, head support on the prototype differs from the envisioned Orion head support: In Orion, the occupant would wear a space helmet and the head support would extend along the right and left sides of the helmet to prevent lateral motion of the head.

Another prominent design feature is a load-distributing seven-point harness similar to harnesses worn in off-road automobile racing. The seven-point harness includes straps over the tops of the shoulders that act, in effect, as wrap-around extensions of the lateral shoulder supports.

This work was done by Dustin Gohmert of Johnson Space Center. Further information is contained in a TSP (see page 1). MSC-24485-1

Open-Access, Low-Magnetic-Field MRI System for Lung Research

Lyndon B. Johnson Space Center, Houston, Texas

An open-access magnetic resonance imaging (MRI) system is being developed for use in research on orientational/gravitational effects on lung physiology and function. The open-access geometry enables study of human subjects in diverse orientations. This system operates at a magnetic flux density, considerably smaller than the flux densities of typical other MRI systems, that can be generated by resistive electromagnet coils (instead of the more-expensive superconducting coils of the other systems).

The human subject inhales air containing ^3He or ^{129}Xe atoms, the nuclear spins of which have been polarized by use of a laser beam to obtain a mag-

netic resonance that enables high-resolution gas space imaging at the low applied magnetic field. The system includes a bi-planar, constant-current, four-coil electromagnet assembly and associated electronic circuitry to apply a static magnetic field of 6.5 mT throughout the lung volume; planar coils and associated circuitry to apply a pulsed magnetic-field-gradient for each spatial dimension; a single, detachable radio-frequency coil and associated circuitry for inducing and detecting MRI signals; a table for supporting a horizontal subject; and electromagnetic shielding surrounding the electromagnet coils.

This work was done by Ross W. Mair, Matthew S. Rosen, Leo L. Tsai, and Ronald L. Walsworth of the Harvard-Smithsonian Center for Astrophysics; Mirko I. Hrovat of Mirtech, Inc.; Samuel Patz of Brigham and Women's Hospital; and Iullian C. Ruset and F. William Hersman of the University of New Hampshire for Johnson Space Center.

In accordance with Public Law 96-517, the contractor has elected to retain title to this invention. Inquiries concerning rights for its commercial use should be addressed to:

*Harvard-Smithsonian Center for Astrophysics
Cambridge, MA 02138*

Refer to MSC-24182-1/3-1, volume and number of this NASA Tech Briefs issue, and the page number.

Microfluidic Mixing Technology for a Universal Health Sensor

John H. Glenn Research Center, Cleveland, Ohio

A highly efficient means of microfluidic mixing has been created for use with the rHEALTH sensor — an elliptical mixer and passive curvilinear mixing patterns. The rHEALTH sensor provides rapid, handheld, complete blood count, cell differential counts, electrolyte measurements, and other lab tests based on a reusable, flow-based microfluidic platform.

These geometries allow for cleaning in a reusable manner, and also allow for

complete mixing of fluid streams. The microfluidic mixing is performed by flowing two streams of fluid into an elliptical or curvilinear design that allows the combination of the flows into one channel. The mixing is accomplished by either chaotic advection around microfluidic loops.

All components of the microfluidic chip are flow-through, meaning that cleaning solution can be introduced into the chip to flush out cells, plasma

proteins, and dye. Tests were performed on multiple chip geometries to show that cleaning is efficient in any flow-through design. The conclusion from these experiments is that the chip can indeed be flushed out with microliter volumes of solution and biological samples are cleaned readily from the chip with minimal effort.

The technology can be applied in real-time health monitoring at patient's bedside or in a doctor's office, and real-

time clinical intervention in acute situations. It also can be used for daily measurement of hematocrit for patients on anticoagulant drugs, or to detect acute myocardial damage outside a hospital.

This work was done by Eugene Y Chan and Candice Bae of DNA Medicine Institute for Glenn Research Center.

Inquiries concerning rights for the commercial use of this invention should be ad-

ressed to NASA Glenn Research Center, Innovative Partnerships Office, Attn: Steve Fedor, Mail Stop 4-8, 21000 Brookpark Road, Cleveland, Ohio 44135. Refer to LEW-18391-1.

Microfluidic Extraction of Biomarkers Using Water as Solvent

Terahertz modulation of permittivity of water would enable solvation of molecules of interest.

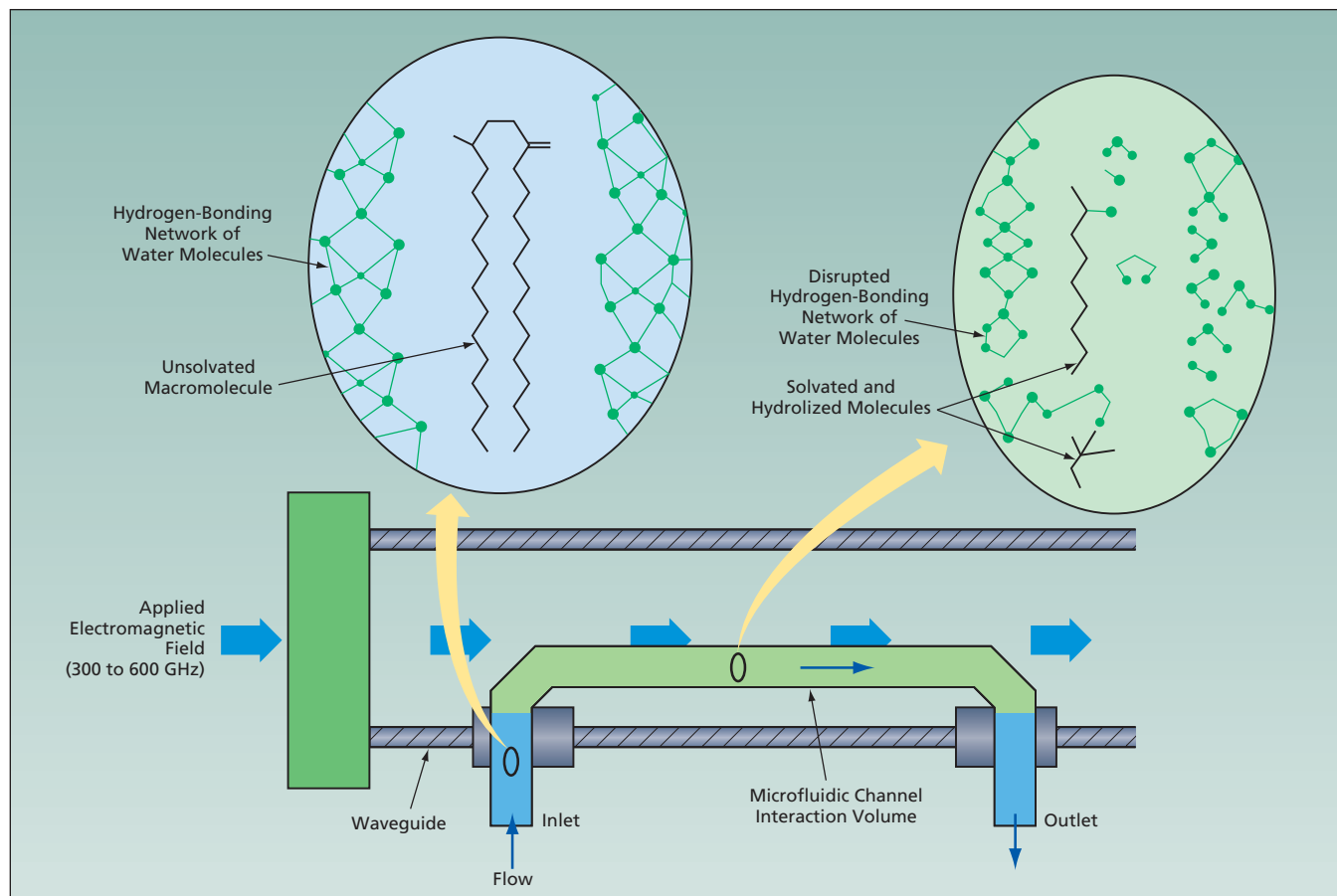
NASA's Jet Propulsion Laboratory, Pasadena, California

A proposed device, denoted a miniature microfluidic biomarker extractor (μ -EX), would extract trace amounts of chemicals of interest from samples, such as soils and rocks. Traditionally, such extractions are performed on a large scale with hazardous organic solvents; each solvent capable of dissolving only those molecules lying within narrow ranges of specific chemical and physical characteristics that notably include volatility, electric charge, and polarity. In contrast, in the μ -EX, extractions could be performed by use of small amounts (typically between 0.1 and 100 μ L) of water as a universal solvent.

As a rule of thumb, in order to enable solvation and extraction of molecules, it is necessary to use solvents that have polarity sufficiently close to the polarity of the target molecules. The μ -EX would make selection of specific organic solvents unnecessary, because μ -EX would exploit a unique property of liquid water: the possibility of tuning its polarity to match the polarity of organic solvents appropriate for extraction of molecules of interest. The change of the permittivity of water would be achieved by exploiting interactions between the translational states of water molecules and an imposed electromagnetic field in the frequency range of

300 to 600 GHz. On a molecular level, these interactions would result in disruption of the three-dimensional hydrogen-bonding network among liquid-water molecules and subsequent solvation and hydrolysis of target molecules. The μ -EX is expected to be an efficient means of hydrolyzing chemical bonds in complex macromolecules as well and, thus, enabling analysis of the building blocks of these complex chemical systems.

The μ -EX device would include a microfluidic channel, part of which would lie within a waveguide coupled to an electronically tuned source of broadband electromagnetic radiation in the fre-



Water Flowing in a Microfluidic Channel would be exposed to electromagnetic radiation, causing the solvation of biomarker macromolecules that would otherwise be insufficiently soluble in water.

quency range from 300 to 600 GHz (see figure). The part of the microfluidic channel lying in the waveguide would constitute an interaction volume. The dimensions of the interaction volume would be chosen in accordance with the anticipated amount of solid sample material needed to ensure extraction of suffi-

cient amount of target molecules for detection and analysis. By means that were not specified at the time of reporting the information for this article, the solid sample material would be placed in the interaction volume. Then the electromagnetic field would be imposed within the waveguide and water would be pumped

through the interaction volume to effect the extraction.

This work was done by Xenia Amashukeli, Harish Manohara, Goutam Chattopadhyay, and Imran Mehdi of Caltech for NASA's Jet Propulsion Laboratory. For more information, contact iaoffice@jpl.nasa.gov. NPO-46150

Microwell Arrays for Studying Many Individual Cells

Lyndon B. Johnson Space Center, Houston, Texas

“Laboratory-on-a-chip” devices that enable the simultaneous culturing and interrogation of many individual living cells have been invented. Each such device includes a silicon nitride-coated silicon chip containing an array of micro-machined wells sized so that each well can contain one cell in contact or proximity with a patch clamp or other suitable single-cell-interrogating device. At the bottom of each well is a hole, typically $\approx 0.5 \mu\text{m}$ wide, that connects the well with one of many channels in a mi-

crofluidic network formed in a layer of poly(dimethylsiloxane) on the underside of the chip. The microfluidic network makes it possible to address wells (and, thus, cells) individually to supply them with selected biochemicals. The microfluidic channels also provide electrical contact to the bottoms of the wells.

This work was done by Albert Folch and Turgut Fettah Kosar of the University of Washington for Johnson Space Center. For further information, contact the JSC Innovation Partnerships Office at (281) 483-3809.

In accordance with Public Law 96-517, the contractor has elected to retain title to this invention. Inquiries concerning rights for its commercial use should be addressed to:

*ROI Coordinator
Office of Technology Licensing
University of Washington
1107 NE 45th Street, Suite 200
Seattle, WA 98105*

Refer to MSC-24046-1, volume and number of this NASA Tech Briefs issue, and the page number.

Droplet-Based Production of Liposomes

Lyndon B. Johnson Space Center, Houston, Texas

A process for making monodisperse liposomes having lipid bilayer membranes involves fewer, simpler process steps than do related prior methods. First, a microfluidic, cross-junction droplet generator is used to produce vesicles comprising aqueous-solution droplets contained in single-layer lipid membranes. The vesicles are collected in a lipid-solvent mix that is at most partially soluble in water and is less dense than is water. A layer of water is dispensed on top of the solvent. By virtue of the difference in densities, the water sinks to the bottom and the solvent floats to

the top. The vesicles, which have almost the same density as that of water, become exchanged into the water instead of floating to the top. As there are excess lipids in the solvent solution, in order for the vesicles to remain in the water, the addition of a second lipid layer to each vesicle is energetically favored.

The resulting lipid bilayers present the hydrophilic ends of the lipid molecules to both the inner and outer membrane surfaces. If lipids of a second kind are dissolved in the solvent in sufficient excess before use, then asymmetric liposomes may be formed.

This work was done by Donald E. Ackley and Anita Forster of Nanotrope, Inc. for Johnson Space Center. For further information, contact the JSC Innovation Partnerships Office at (281) 483-3809.

In accordance with Public Law 96-517, the contractor has elected to retain title to this invention. Inquiries concerning rights for its commercial use should be addressed to:

*Nanotrope Inc.
3030 Bunker Hill St
San Diego, CA 92109
Phone No.: (858) 270-7992*

Refer to MSC-24302-1, volume and number of this NASA Tech Briefs issue, and the page number.

Identifying and Inactivating Bacterial Spores

NASA's Jet Propulsion Laboratory, Pasadena, California

Problems associated with, and new strategies for, inactivating resistant organisms like *Bacillus canaveralius* (found at Kennedy Space Center during a survey of three NASA clean-rooms) have been defined. Identifying

the particular component of the spore that allows its heightened resistance can guide the development of sterilization procedures that are targeted to the specific molecules responsible for resistance, while avoiding using un-

duly harsh methods that jeopardize equipment.

The key element of spore resistance is a multilayered protein shell that encases the spore called the spore coat. The coat of the best-studied spore-forming mi-

crobe, *B. subtilis*, consists of at least 45 proteins, most of which are poorly characterized. Several protective roles for the coat are well characterized including resistance to desiccation, large toxic molecules, ortho-phthalaldehyde, and ultraviolet (UV) radiation.

One important long-term specific goal is an improved sterilization procedure that will enable NASA to meet planetary protection requirements without a terminal heat sterilization step. This would support

the implementation of planetary protection policies for life-detection missions. Typically, hospitals and government agencies use biological indicators to ensure the quality control of sterilization processes. The spores of *B. canaveralius* that are more resistant to osmotic stress would serve as a better biological indicator for potential survival than those in use currently.

This work was done by David Newcombe, Anne Dekas, and Kasthuri Venkateswaran of Caltech for NASA's Jet Propulsion Laboratory.

In accordance with Public Law 96-517, the contractor has elected to retain title to this invention. Inquiries concerning rights for its commercial use should be addressed to:

*Innovative Technology Assets Management
JPL*

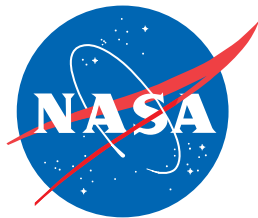
Mail Stop 202-233

4800 Oak Grove Drive

Pasadena, CA 91109-8099

E-mail: iaoffice@jpl.nasa.gov

Refer to NPO-45182, volume and number of this NASA Tech Briefs issue, and the page number.



National Aeronautics and
Space Administration